Use of poly(L-lactide-co-ε-caprolactone) based biomaterials in urological and gynaecological tissue engineering applications

Alma Kurki

Master's thesis

Faculty of Medicine and Health Technology

Tampere University

April 2019

Pro Gradu –tutkielma

Paikka: Tampereen yliopisto
BioMediTech (BMT), Lääketieteen ja terveysteknologian tiedekunta
Tekijä: KURKI, ALMA HENRIIKKA AMANDA

Otsikko: Poly(L-laktidi-ko-ε-kaprolaktoni) -pohjaisten biomateriaalien hyödyntäminen gynekologian ja urologian kudosteknologisissa sovelluksissa

Sivumäärä: 102

Ohjaaja: LT, DI Reetta Sartoneva ja apulaisprofessori Susanna Miettinen
Tarkastajat: Professori Heli Skottman ja LT, DI Reetta Sartoneva

Päiväys: huhtikuu 2019

Tiivistelmä

Tutkimuksen tausta ja tavoitteet: Lantionpohjan ja virtsaputken kudosvaurioiden korjaamiseen ei ole vielä olemassa täysin optimaalista korjausmenetelmää tai -materiaalia. Lantionpohjan laskeuma on hyvin yleinen ongelma naisilla. Ensisijaisesti laskeumat korjataan potilaan omilla kudoksilla, mutta näihin korjausmenetelmiin liittyy jopa 30 %:n riski laskeuman uusiutumiseen. Osa uusiutuneista laskeumista korjataan tavallisimmin sulamattomalla polypropyleeni -verkolla, johon liittyy komplikaatioita, kuten verkon eroosiota ja lantion alueen kipuja. Myös virtsaputken rakenteellisten poikkeamien, kuten kuroumien ja hypospadian, korjaamiseen nykyisillä menetelmillä liittyy useita komplikaatioita, kuten uusien kuroumien ja fistelien muodostuminen. Tässä työssä tutkittiin urologisiin ja gynekologisiin sovellutuksiin uutta korjausmateriaalia poly(L-laktidi-ko-ε-kaprolaktoni) -tukirakennetta, johon on lisätty tiettyä askorbiinihapon johdannaista (PLCLas). Tavoitteena oli määrittää askorbiinihapon johdannaisen (AAD) vaikutus ihmisen vaginan stroomasoluihin, rasvan kantasoluihin sekä uroteelisoluihin yksisoluviljelmissä sekä rasvan kantasolujen ja uroteelisolujen yhteisviljelmässä.

Tutkimusmenetelmät: Vaginan stroomasoluja viljeltiin yksisoluviljelmässä PLCL kalvoilla, ja rasvan kantasoluja ja uroteelisoluja ylikriittisellä hiilidioksidilla huokoistetuilla PLCL tukirakenteilla yksisolu- sekä yhteisviljelmissä 1, 7, ja/tai 14 päivän ajan. Solujen elinkyky ja morfologia määritettiin Live/Dead® analyysillä sekä pyyhkäisyelektronimikroskoopilla. Solujen jakaantuminen määritettiin kvantitatiivisesti CyQUANT® analyysillä, ja tuotetun kollageenin kokonaismäärä Sircol™ analyysillä. Tiettyjen proteiinien ilmentymistä tutkittiin immunovärjäyksillä, ja valikoitujen geenien ilmenemistä reaaliaikaisella kvantitatiivisella polymeraasiketjureaktiolla.

Tutkimustulokset: Kaikki solutyypit pysyivät elinkykyisinä tutkituilla biomateriaaleilla. Stroomasolut säilyttivät myofibroblasti -fenotyypinsä ja rasvan kantasolut kykynsä erilaistua lihassolujen suuntaan sekä PLCLas että PLCL tukirakenteilla, myöskin uroteelisolujen fenotyyppi säilyi molemmilla biomateriaaleilla. AAD lisäsi merkitsevästi vaginan stroomasolujen ja rasvan kantasolujen jakaantumista sekä kollageenin tuotantoa. Uroteelisoluissa vaste oli puolestaan vastakkainen, ja solumäärä ja kollageenin tuotanto vähenivät. AAD paransi rasvan kantasolujen elinkykyä yhteisviljelmässä. Lisäksi sekä rasvan kantasolut että uroteelisolut säilyttivät fenotyyppinsä yhteisviljelmässä.

Johtopäätökset: AAD lisää stroomasolujen ja rasvan kantasolujen kollageenin tuotantoa ja jakaantumista, mutta uroteelisoluissa vastaavaa vaikutusta ei nähty. Uroteelisolut ja rasvan kantasolut säilyivät elinkykyisinä yhteisviljelmässä, mutta yhteisviljelmän medium vaatii vielä optimointia. Saatujen tulosten perusteella PLCLas tukirakenne vaikuttaa potentiaaliselta materiaalilta urologisiin ja gynekologisiin sovelluksiin.

Master's Thesis

Place: Tampere University
BioMediTech (BMT), Faculty of Medicine and Health Technology
Author: KURKI, ALMA HENRIIKKA AMANDA

Title: Use of poly(L-lactide-co-ε-caprolactone) based biomaterials in urological and gynaecological tissue engineering applications

Pages: 102
Supervisor: MD PhD, MSc Tech Reetta Sartoneva and associate professor Susanna Miettinen
Reviewers: Professor Heli Skottman and MD PhD, MSc Tech Reetta Sartoneva
Date: April 2019

Abstract

Background and aims: Repair of pelvic floor and urethral defects both currently lack the ideal repair methods and materials. Pelvic organ prolapse (POP) is a very common disorder affecting numerous women. Current repair methods for POP are insufficient and 30 % of primary repair surgeries lead to relapse and ultimately may need repair with nonabsorbable polypropylene surgical mesh with substantially high risk of complications as mesh erosion and pelvic pain. Repair of urethral defects, such as strictures and hypospadia, are also prone to complications with the currently available methods and often lead to formation of strictures or fistulas, for example. Aim of this study was to determine the cellular effect of ascorbic acid derivate (AAD) embedded in biodegradable poly(L-lactide-co-ε-caprolactone) PLCL scaffolds, when compared to plain PLCL scaffolds in human vaginal stromal cell (hVSC), adipose derived stem cell (hASC) and urothelial cell (hUC) monocultures and hUC/hASC co-culture.

Methods: PLCL membranes with or without embedded AAD were studied with hVSCs for pelvic floor fascia regeneration. For regeneration of urothelial defects, hUC and hASC monocultures and hUC/hASC co-culture were performed on plain or AAD embedded 3D scPLCL scaffolds. Cellular effect of AAD in PLCL scaffolds was analyzed with variety of analyses in time points of d1, d7 and d14; Cell viability and morphology was determined with Live/Dead® assay and scanning electron microscope imaging. Cell proliferation was quantified with CyQUANT® assay and collagen production with Sircol™ assay. Expression of specific markers was visualized with immunocytochemistry, and gene expression of specific genes was quantified with real-time polymerase chain reaction.

Results: Cells remained viable on all biomaterials. AAD significantly increased the collagen production and cell proliferation of hVSCs and hASCs, whereas decreased them in hUCs. Human VSCs synthetized collagen more rapidly on PLCL membrane with AAD and maintained myofibroblastic phenotype on membranous PLCL with or without AAD. In hASC monoculture on 3D PLCL with AAD, the cells proliferated rapidly, covering the scaffold with dense cell sheet. On plain PLCL scaffolds both hVSCs and hASCs formed cell clusters, not spreading on the material surface. Human ASCs maintained their myogenic potential and hUCs their phenotype in 3D PLCL scaffolds with and without AAD. Further, AAD seemed to enhance the viability of hASC in hUC/hASC co-culture.

Conclusion: AAD in PLCL scaffolds enhance hVSC and hASC proliferation, whereas such benefit in hUCs was not seen. Increased collagen production and hVSC proliferation would enhance regeneration of neofascia and thus be very beneficial for pelvic floor applications. Cells in hUC/hASC co-culture remained viable with added AAD, and thus this design could be optimized in further studies to be used in regenerating functional urothelium and smooth muscle layers in urethral tissue. In all, PLCL scaffolds with embedded AAD seem promising for urological and gynaecological tissue engineering applications.

Acknowledgements

This study was conducted in the Adult stem cell research group, BioMediTech, Faculty of Medicine and Health Technology, Tampere University. Foremost, I want to sincerely thank our group leader Associate professor Susanna Miettinen. I am most grateful for the opportunity to pursue my thesis in the field of tissue engineering, which has been my passion throughout my studies. I truly enjoyed researching the topic of my thesis. I am grateful to my excellent hard-working supervisor MD PhD, MSc (Tech) Reetta Sartoneva for her guidance and for always being promptly available for help, advice and support. Thank you.

I want to especially thank DSc Kaarlo Paakinaho for providing me with the biomaterials central for my thesis. Further, I highly appreciate all the technical support and practical guidance received from Anna-Maija Honkala and Sari Kalliokoski. Moreover, I highly value all the help and advices given to me by Laura Hyväri, Miia Juntunen and Kaisa Vuornos. Thank you for the rest of the "Mese"-group for providing such an inspiring work environment. Also, thank you, Inari Lyyra, for your help and support.

Lastly, thank you for my family and friends for support and being there for me during my studies in general and during this pro gradu project, in which I became totally immersed in. Thank you for my late grandmother Helena for always being so proud and supportive of my studies. I wish you could have been here this day.

13.4.2019 Tampere

Alma Kurki

Table of Contents

Abbreviations

3D	Three-dimensional
αMEM	Minimum Essential Medium Eagle-Alpha Modification
αSMA	Alpha-smooth muscle actin
AA	Ascorbic acid
AAD	Ascorbic acid derivate
AUM	Asymmetric unit membrane
BAMG	Bladder acellular matrix graft
BSA	Bovine serum albumin
cDNA	Complementary DNA
CK7	Cytokeratin 7
CK8	Cytokeratin 8
CK19	Cytokeratin 19
CD	Cluster of differentiation
COL I	Collagen type I
COL III	Collagen type III
DAPI	4',6-diamidino-2-phenylindole
DHA	Dehydroascorbate
DPBS	Dulbecco's Phosphate-buffered saline
ECM	Extra cellular matrix
EDTA	Ethylenediaminetetraacetic acid
EMT	Epithelial-mesenchymal transition
ER	Endoplasmic reticulum
EthD-1	Ethidium homodimer-1
EtOH	Ethanol
FBS	Fetal bovine serum
FDA	The U.S. Food and Drug Administration
GLO	L-gulono-lactone oxidase
hAM	Human amniotic membrane
hASC	Human adipose-derived stem cell
HBSS	Hanks' balanced salt solution
HEPES	N′-2-hydroxyethylpiperazine-N′-2-ethanesulphonic acid
HMDS	Hexamethyldisilane
hPLCL	Holed poly-L-lactide-co-ε-caprolactone membrane
hPLCLas	Holed poly-L-lactide-co-ε-caprolactone membrane with added ascorbic acid derivate
HS	Human serum
hUC	Human urothelial cell
hVEC	Human vaginal epithelial cell
hVSC	Human vaginal stromal cell
ICC	Immunocytochemistry
mRNA	Messenger RNA
MSC	Mesenchymal stem cell
OF	Oral buccal mucosa fibroblast
PFA	Paraformaldehyde
PLGA	Poly(lactic-co-glycolic acid)
PGA	Poly(glycolic acid)
PLCL	Poly-L-lactide-co-ε-caprolactone
PLCLas	Poly-L-lactide-co-ε-caprolactone membrane with added ascorbic acid derivate

POP	Pelvic Organ Prolapse
ROX	6-carboxy-x-rhodamine
P/S	Penicillin and Streptomycin
qRT-PCR	Real-Time Quantitative Polymerase Chain Reaction
ROS	Reactive Oxygen Species
RPLP0	Large Ribosomal Protein P0
RT	Room temperature
$scCO_2$	supercritical carbon dioxide
scPLCLas	Super critical carbon dioxide foamed poly-L-lactide-co-ε-caprolactone with added ascorbic acid derivate
scPLCL	Super critical carbon dioxide foamed poly-L-lactide-co-ε-caprolactone
SEM	Scanning Electron Microscope
SIS	Small intestine submucosa
SMC	Smooth muscle cell
SVF	Stromal vascular fraction
TGF-β1	Transforming growth factor beta 1
UI	Urinary incontinence
UP	Uroplakin

1 INTRODUCTION

Tissue engineering has become a promising novel method for treating urological and gynaecological defects. Urethral defects are rather common and mainly caused by traumas, infections, iatrogenic causes or due to congenital disorders such as hypospadias (Yamzon et al., 2008). The reconstruction of urological defects is highly challenging. Typically, small urethral defects are repaired with patients' own genital tissue, yet this is insufficient for larger defects. Reconstruction of larger urethral defects requires additional autologous or allogenic non-urologic grafts, which brings the challenges to even greater level. Further, the autologous donor sites are very limited. The most frequently used nonurologic tissue is oral buccal mucosa. Additionally, bladder acellular matrix (BAMG) and small intestinal submucosa (SIS) have been studied for urethral reconstruction. Yet, the nonurologic grafts lack the proper functional properties of urethra and often lead to complications such as strictures or formation of fistulas. (de Kemp et al., 2015; Garriboli et al., 2014; Maya et al., 2010; C. Zhang et al., 2014) Due to major difficulties and challenges of urethral repair, developing a new treatment method, such as tissue engineering based approach, is important. Cell-seeded scaffolds such as poly-lactic acid (PLA), poly(lactic-co-glycolic acid) (PLGA) and poly(L-lactide-co-caprolactone (PLCL) have been studied for urethral and bladder reconstruction with potential results (Atala et al., 2006; de Kemp et al., 2015; Garriboli et al., 2014).

In addition to urethral defects, developing new treatment methods for pelvic organ prolapse (POP) was the other focus of this study. POP is a highly common problem affecting a large number, even up to 50 % (FDA, 2011), of women. It is defined as descent of the anterior and/or posterior vaginal wall, the uterus and/or the vaginal apex, due to weakened support of the fascia and pelvic muscle floor. The POP is primarily repaired with patient's own fascia (Osborn et al., 2013) yet the recurrence level is up to 30 % (Barber & Maher, 2013; Osborn et al., 2013). If the primary surgery fails and need reoperation, the recurrent prolapse is usually treated with synthetic non-absorbable polypropylene mesh. However, these mesh operations are susceptible to complications such as pain, mesh erosion or contraction and sexual dysfunction. (Osborn et al., 2013; Roman et al., 2015) In fact, in 2011 the U.S. Food and Drug Administration (FDA) has classified the surgical mesh to have a risk classification of Class III: the highest possible risk class (FDA, 2011). Therefore, as current methods are insufficient, developing novel repairing methods is crucial. Again, tissue engineered scaffold could be a one possible answer for this challenge.

This masters project studies specific ascorbic acid derivate (AAD) embedded in poly(L-lactide-co-ε-caprolactone) (PLCL) membranes and three-dimensional (3D) scaffolds for urological and gynaecological applications. PLCL scaffolds have shown promising results in soft tissue applications such as urothelial, vascular and neural tissue engineering (Laurent et al., 2018; Prabhakaran et al., 2009; Sartoneva et al., 2011; Shafiq et al., 2015). The aim of this study was to determine the effect of added specific salt to cell function in human vaginal stromal cells (hVSCs), human urothelial cells (hUCs) and human adipose derived stem cells (hASC). The induced cellular effect of added specific ascorbic acid derivate was compared to cells cultured on plain PLCL scaffolds. AAD is hypothesized to enhance formation of extra cellular matrix and collagen, and thus contribute to repair of soft tissue and guide the differentiation of hASC towards smooth muscle cells (SMCs). The 3D PLCL-scaffold could provide applicable tissue engineered graft for urethral defects to regenerate defected urothelium, smooth muscle and soft tissue. Membranous PLCL-scaffold in turn could provide support and regenerate the natural pelvic fascia support system in defected pelvic floor.

2 REVIEW OF THE LITERATURE

2.1 Anatomy and histology of urinary tract

The urinary tract conveys urine outside of the body and consists of kidneys, ureters, urinary bladder and urethra. Renal pelvis collects urine from kidney to be carried to urinary bladder along ureter. Urine is stored in urinary bladder and excreted from the body through urethra. (Drake et al., 2015) Organs in urinary system are presented in Figure 1.

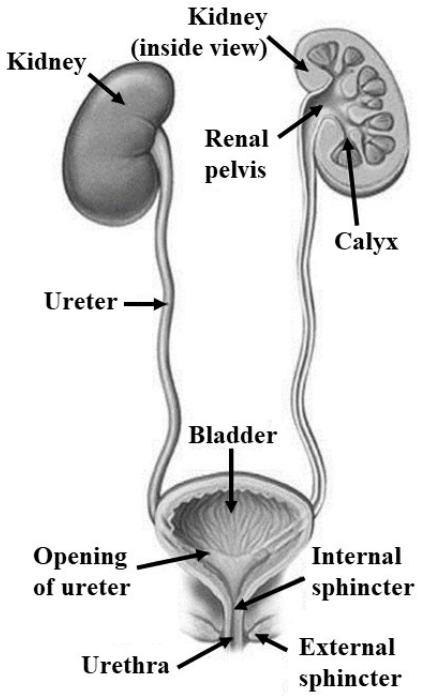

Figure 1 Organs in urinary tract. Urinary tract consists of kidneys, ureters, bladder and urethra. Urine flows from kidneys to bladder through ureters and is excreted via urethra. Modified from https://oncologypro.esmo.org/Education-Library/Essentials-for-Clinicians/Genitourinary-Tract-Tumours/Tumours-of-the-Urinary-System, 14.12.2019.

Ureters are about 22 – 30 cm long fibromuscular tubes draining urine from renal pelvis to bladder. Urinary bladder is a muscular organ that stores urine until controlled urination. It expands or shrinks its volume according to the filling state. Muscles of urethral sphincter control the urine flow out of the bladder. When bladder squeezes and urethral sphincter is relaxed, urine is discharged through urethra. The tube walls of ureters and urethra are exposed to repetitive fluid shear stress and pressure; therefore, they need to be tough but elastic (Singh et al., 2018). In males, urethra functions also as a passage for semen. The structure of urethra differs between males and females by its length and segments. The male urethra is about 20 cm long and divided into three different segments called prostatic, membranous and spongy urethra.

The most proximal prostatic urethra, and following membranous urethra, that passes the pelvic floor, are lined with pseudostratified columnar epithelium. The most distal segment, spongy urethra, is lined with squamous epithelium. (Drake et al., 2015; Hickling et al., 2015; Ross & Pawlina, 2011) Female urethra is about 4 cm long, lined with transitional epithelium, called uroepithelium, proximally and with squamous epithelium at the distal end (Faiena et al., 2016; Ross & Pawlina, 2011). Histologically, the urinary tract, similarly to other excretory canals, consists of epithelium, lamina propria, muscularis and adventitia/serosa (Figure 2) (Ross & Pawlina, 2011).

The specialized epithelium called uroepithelium, or transitional epithelium, lines the urinary tract from minor calyces of kidney to proximal part of urethra. The bottom cell layer of urothelium, called basal cell layer, is attached to dense collagenous lamina propria. Connective tissue underneath lamina propria is mainly formed from collagen type I and type III and elastin. (Hickling et al., 2015; Orabi et al., 2013; Ross & Pawlina, 2011) The muscularis layer beneath the connective tissue is formed from two smooth muscle layers: inner longitudal layer and outer circular layer. The muscle layers in urinary tract are mixed with connective tissue and regulate the urine flow through the tract. (Ross & Pawlina, 2011; Singh et al., 2018)

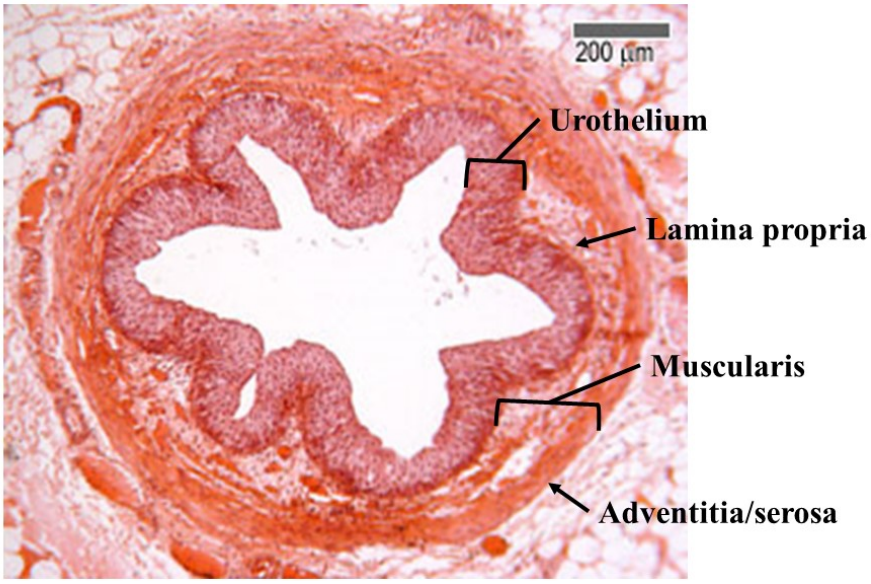

Figure 2 Layers of ureter. Cross section of ureter with its histological layers. Modified from http://www.histology.leeds.ac.uk/urinary/assets/Ureter_60_6-3x.jpg, 12.12.2018.

2.2 Uroepithelium and urothelial cells

Urothelium has a very important role in preventing toxic substances to permeate from urea to blood circulation (Hickling et al., 2015; Ross & Pawlina, 2011). The barrier properties of urothelium are one of the highest in human body, even higher than human epidermis (Wu et al., 2009) and it is highly impermeable to macromolecules and pathogens. Urothelium also participates in system homeostasis by transporting ions, creatinine, water and urea out of urine, changing the composition of urine along its passage (Khandelwal et al., 2009).

Urothelium is composed of three cell layers: luminal umbrella cells, intermediate layer and basal cell layer (Figure 3). The number of layers in urothelium change in different regions and depending on the filling state. Urothelium is able to expand and contract while keeping its tight barrier properties intact. Especially in case of bladder, the change can be quite large shifting from six intermediate cell layers of empty bladder to just three cell layers in full bladder. (Hickling et al., 2015; Ross & Pawlina, 2011) In minor calyces, the urothelium has two cell layers, four to five in ureter and up to six in urinary bladder (Ross & Pawlina, 2011). The urothelium is in close contact with the surrounding smooth muscle layer, as it regulates the expansion and contraction of the uroepithelium tissue (Singh et al., 2018).

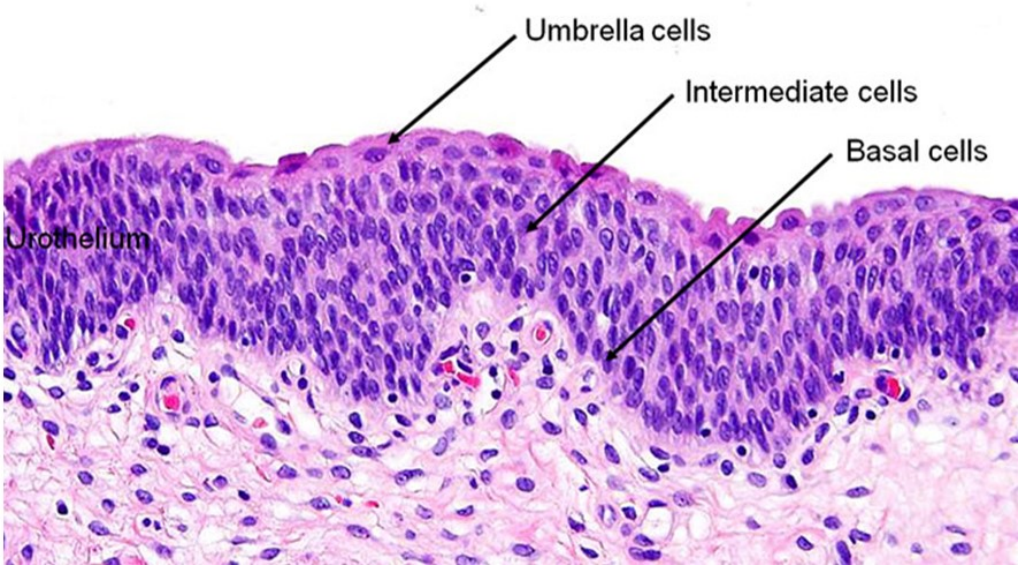

Figure 3 Histological structure of the uroepithelium presenting the luminal umbrella cell monolayer, intermediate cell layer and basal cell layer attached to lamina propria. Modified from https://www.auanet.org/images/education/pathology/normalhistology/normal_urothelium-figureA_Big.jpg, 10.12.2018.

The superficial or luminal cell layer consists of monolayer of terminally differentiated umbrella cells (also called facet cells or superficial cells). These cells are 25-250 µm in size, often multinucleated, concaved cells covering the intermediate cell layer (Khandelwal et al., 2009; Ross & Pawlina, 2011). Specialized umbrella cells form strong tight junctions, have specific apical layer protein and lipid composition. Umbrella cells can also regulate their surface area by endo- and exocytosis. (Khandelwal et al., 2009; Singh et al., 2018) This special umbrella cell surface structure is composed of asymmetric unit membranes (AUMs), formed from uroplakin plaques, that can also be found in intracellular fusiform vesicles (Southgate et al., 1999; Wu et al., 2009). The shape of the umbrella cells changes according to the state of the urine passage. If the bladder is full, the umbrella cells are squamous and flat, whereas with empty bladder they are roughly cuboidal and more dome-shaped. (Khandelwal et al., 2009; Ross & Pawlina, 2011) Umbrella cell borders are distinct with ridge visible in scanning electron microscope (SEM) -imaging. The ridges are result of interlocked apical cell membranes of neighbouring cells that strengthen the tight junctions between the cells, increasing the barrier function of the urothelium. (Khandelwal et al., 2009; Ross & Pawlina, 2011) The cells in intermediate cell layer are connected to neighbouring cells by desmosomes. The intermediate cells of urothelium are single-nucleated pyriform shaped cells and a lot smaller than umbrella cells, about 10-15 µm in diameter. (Khandelwal et al., 2009; Ross & Pawlina, 2011) Intermediate layer can have five layers, but the number varies by the state of urine passage through the urinary tract. When the tissue expands, the layers slide past each other increasing the area. (Khandelwal et al., 2009; Southgate et al., 1999) The intermediate cells in the uppermost layer are partially differentiated with some observed uroplakins and those cells are able to rapidly differentiate into umbrella cells if the umbrella cell layer is damaged (Khandelwal et al., 2009; Ross & Pawlina, 2011). The basal layer cells are small, approximately 10 µm, single nucleated, and are attached to the lamina propria by hemidesmosomes and to intermediate layer by desmosomes (Khandelwal et al., 2009).

Urothelium has relatively slow turnover, up to 6 months (Khandelwal et al., 2009; Lee, 2011; Wu et al., 2009). However, when damaged, the urothelial cells proliferate quickly to regenerate the breach (Kreft et al., 2005; Singh et al., 2018), which is critical in order to protect the surrounding tissues from acidic urine. When the urothelium is damaged, the damaged cells are destroyed and underlying basal cells proliferate rapidly. The stem cell-like cells are among basal cells, and allow the rapid regeneration of damaged urothelium (Hickling et al., 2015; Ho et al., 2012; Ross & Pawlina, 2011) The cells of intermediate cell layer below the umbrella cells are

capable to rapidly differentiate to form new terminally differentiated umbrella cells. (Kreft et al., 2005; Lee, 2011)

2.2.1 Cytokeratins

Cytokeratins (CKs) are a group of polypeptides which form intermediate filament matrix in most of the epithelial cell types. Currently there are twenty identified human cytokeratins that are named CK1-CK20 in decreasing molecular weight order. Each epithelial cell type has their own characteristic set of cytokeratins and their expression can be used to assess the differentiation or maturation stages of specific epithelial cell type. (Southgate et al., 1999)

Urothelial cells have extensive cytokeratin network. The expressed cytokeratins vary between the urothelium cell layers and can therefore be used as an indication of the cell differentiation rate. All urothelial cell layers express cytokeratins CK7, CK8, CK18 and CK19. Cytokeratins CK5 and CK17 can only be found in basal cells, whereas, CK13 and CK14 are expressed in intermediate and basal cells but not in the umbrella cells. (de Graaf et al., 2017; Khandelwal et al., 2009; Southgate et al., 1999) The CK20 is mainly present in differentiated umbrella cells, however, some cells in intermediate layer can also express the CK20 (Southgate et al., 1999). In immunological characterizations, anti-pan-cytokeratin [AE1/AE3] marker can be used to assess the overall cytokeratin expression identifying urothelial cells. AE1 contains CK10, CK13-16 and CK19, and AE3 contains CK1-8 (Denstedt & Atala, 2009). Further, neoplastic transformation of urothelium, called transitional cell carcinoma, changes the CK expression of urothelial cells. Therefore, changes in urothelial cytokeratin patterns can be used as tool for cancer diagnostics. (Southgate et al., 1999)

2.2.2 Asymmetric unit membrane and uroplakins

The terminally matured and differentiated umbrella cells of urothelium have apical membranes composed of differentiated urothelial plaques. These plaques form the AUMs on the apical side of the umbrella cells. (Khandelwal et al., 2009; Olsburgh et al., 2003; Singh et al., 2018; Wu et al., 2009) Majority of the urothelial apical surface, up to 90 %, is covered with AUMs. AUMs can also be found in fusiform vesicles, controlled by cytokeratin network, inside the umbrella cells (Khandelwal et al., 2009; Lee, 2011; Southgate et al., 1999; Wu et al., 2009). These AUM plagues are formed by glycoproteins called uroplakins (UP) that are highly conserved in mammals. They are expressed only in terminally differentiated superficial urothelial cells and are therefore used as a major urothelial cell differentiation marker. (Lee, 2011) UCs are

characterized with expression of UPs in superficial cell layer, and characteristic CK profiles of different layers of urothelium (de Graaf et al., 2017; Khandelwal et al., 2009; Southgate et al., 1999). Some intermediate cells connected to umbrella cells do express some UPs, as they are readily able to differentiate into new umbrella cells if needed (Khandelwal et al., 2009). Uroplakins have five different forms (UPIa, UPIb, UPII, UPIIIa and UPIIIb), each having their own role in forming plaques. (Kątnik-Prastowska et al., 2014; Khandelwal et al., 2009) Tight gap, called the hinge-region, between AUMs is occupied with urohingin and non-plague proteins such as ion channels (Khandelwal et al., 2009). One AUM plaque is formed from six UP-tetramers, where UPIa/UPII heterodimers form the inner ring and UPIb/UPIII the outer ring of the structure (Figure 4) (Kątnik-Prastowska et al., 2014; Khandelwal et al., 2009).

UPs are critical in forming the barrier properties of the urothelium by forming the AUM plagues (Wu et al., 2009). Additionally, UPs trigger immune response leading to apoptosis, when umbrella cells become infected (Hickling et al., 2015; Khandelwal et al., 2009). Further, abnormal expression of UPs leads to leakage of urothelium and increase the risk of *E. coli* infections. (Hickling et al., 2015; Kątnik-Prastowska et al., 2014; Khandelwal et al., 2009)

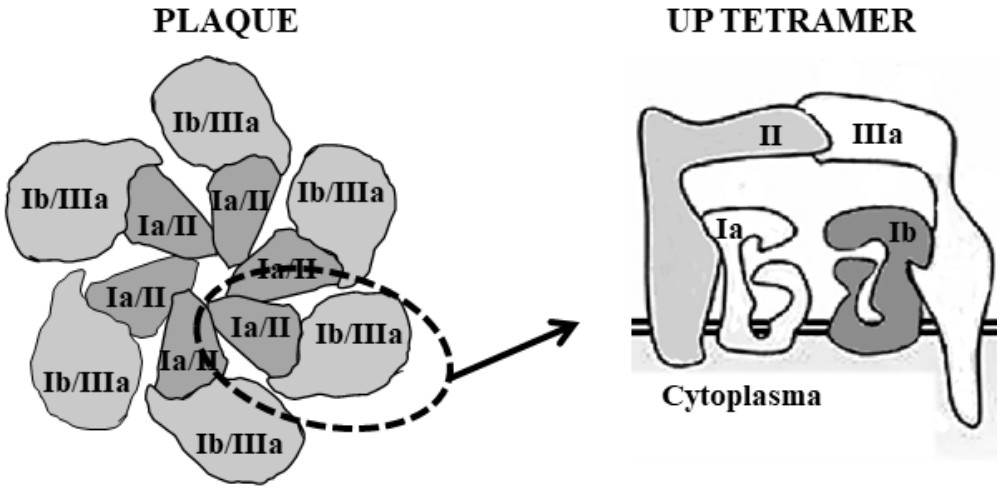

Figure 4 Structure of AUM plaques present in apical umbrella cells. Plagues are formed from six transmembrane UP tetramers with UPIA/UPII -dimer in the inner ring and UPIB/UPIIIA -dimer in the outer ring. Modified from Kątnik-Prastowska et al., 2014.

2.3 Female pelvic floor

The bony pelvis consists of two hip bones connected to pubic symphysis at front and to sacrum at back. The pelvic cavity can be divided to two areas: upper major pelvis and lower minor pelvis. Abdominal organs are positioned in the major pelvis, whereas the organs situated in the inferior pelvic area are the lower urinary tract organs (bladder and urethra), genital organs (vagina, uterus) and colorectal organs (anus and rectum). (Drake et al., 2015; Herschorn, 2004)

The inferior pelvic opening is covered with pelvic floor, or pelvic diaphragm, that keeps the organs in place. The fibromuscular pelvic floor has openings for urethra, vagina and anus, but otherwise it covers the opening. Pelvic diaphragm is composed of important collaboration of muscles and connective tissue (Figure 5). (De Lancey, 2016; Drake et al., 2015) The connective tissue component of pelvic floor is most importantly composed of endopelvic fascia and tendinous arch. The role of the connective tissue in pelvic floor is to suspend the organs in their positions. The organs of minor pelvis are all attached to the endopelvic fascia that is bound to pelvic walls. (Ashton-Miller & DeLancey, 2007; Herschorn, 2004) The fascia support system is divided into three levels. In level one, the cervix and upper proportion of vagina are suspended to pelvic walls by ligaments. In level two, the middle segment of vagina is attached to tendinous arch. In level three, the most distal segment of vagina is connected to muscles of pelvic floor and perineal body. (De Lancey, 2016) The muscular component of the pelvic support is primarily formed by levator ani and coccygeus muscles spreading over the pelvic opening from both sides, meeting at the middle. These muscles continuously work to keep the openings of pelvic floor closed and carry the weight of the organs resting above. Thus, the muscles cancel out the stress subjected to the pelvic floor connective tissue, preventing the overworked stretching of the pelvic fascia. (Ashton-Miller & DeLancey, 2007; De Lancey, 2016)

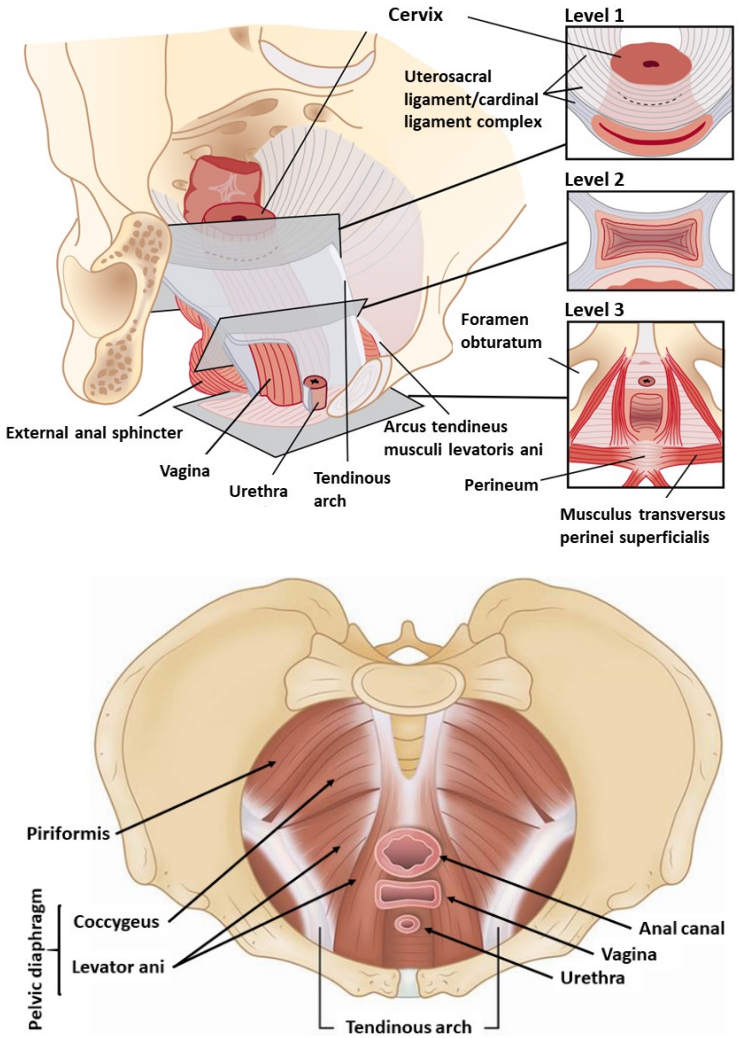

Figure 5 Connective tissue and muscles of female pelvic floor. Pelvic floor is supported by levels of the connective tissue support and the large layers of pelvic floor muscles forming the pelvic diaphragm. Modified from (Kiilholma & Nieminen, 2009) and (Greenwell & Cutner, 2018).

Histologically, the pelvic floor support system is composed of smooth muscle cells (SMCs), fibroblasts, myofibroblasts and supportive extra cellular matrix (ECM). ECM surrounds the cells and is composed of complex cross-linked network of collagens, elastin, proteins, proteoglycans, fibronectin, growth factors and glycosaminoglycans. (Alperin & Moalli, 2006; Chapple et al., 2015; Singh et al., 2018). The pelvic ECM consists of collagens, mainly types I and III, and elastin, and is produced by fibroblasts and myofibroblasts. Fibroblastic cells produce and constantly regulate ECM composition. The support of fascia is dependent on the ratio of fibroblastic cells' anabolic and catabolic functions. With dysfunctional balance, the composition of fascia is altered, leading to disrupt of the pelvic fascia support system. (Ruiz-Zapata et al., 2016)

The collagen fibres are the main factors determining the tissue strength. Collagen is a fibrillar protein formed from three α-polypeptide chains. The types of α-polypeptides vary between different collagen types and are thus used for their characterization. (Alperin & Moalli, 2006) Collagen type I forms large fibres with high tensile strength, the force it withstands before breaking. It is the predominant collagen type in tissues under a lot of strength such as ligaments, tendon and bone. Collagen type III forms smaller fibres and have lower tensile strength and is the main collagen type in tissues with high flexibility and periodic stress, such as blood vessels, but also in vagina and pelvic floor. (Alperin & Moalli, 2006; Zhou et al., 2012) Collagen types I and III form copolymers and their ratio is important for the normal functionality of the connective tissue. The altered collagen ratios may have a role in weakened support of the pelvic floor (Alperin & Moalli, 2006; Zhou et al., 2012).

Another important protein in connective tissue is elastin, an insoluble polymer that gives the tissue elastic properties. It enables the tissue to be stretched, bent or compressed and revert to its original state; important for functions of both vagina and male urethra. Along with collagen, it is a central factor in maintaining pelvic floor support. (Alperin & Moalli, 2006; Chapple et al., 2015; Ribeiro-Filho & Sievert, 2015) Elastin is stable in adults with low turnover (Klutke et al., 2008; Ribeiro-Filho & Sievert, 2015). During pregnancy however, elastin metabolism increases to compensate the structural changes occurring in the pelvic area. (Alperin & Moalli, 2006; Klutke et al., 2008) It has been shown that abnormal elastin metabolism is associated with pelvic organ prolapse (POP) and stress urinary incontinence (UI) in women. (Alperin & Moalli, 2006; Chapple et al., 2015; Chen et al., 2008)

2.4 Defects

2.4.1 Urethral defects

Urethral defects are common and often result of traumas, infections, iatrogenic causes or congenital disorders such as hypospadias (Horiguchi, 2017; Yamzon et al., 2008).

Urethral strictures are common and caused by diverse causes such as blunt trauma or other injury, lichen sclerosus, sexually transmitted diseases or urinary tract infections. Prevalence of urethral stricture disease in UK is 40 per 100 000 in men by age 65 years and increases to over 100 per 100 000 in men older than 65 years (Spilotros et al., 2018). In stricture, the urethra is narrowed due to excessive fibrosis, disrupting the flow of urine. Minor defects may be repaired surgically with dilation or incision of the narrowed stricture, but larger scale and recurrent

defects need surgical repair with urethroplasty, the reconstruction of urethra. Even though the reconstructive surgery of small and large strictures are common, they both have high relapse rates and often require reoperations (Chapple et al., 2015). If non-urological tissue is required for reconstruction, the harvested oral buccal mucosa graft is the most commonly used urethral graft material for urethroplasty (Atala et al., 2017; Chapple et al., 2015; Horiguchi, 2017)

Other common urethral defect is the congenital disorder hypospadia. Hypospadias are quite frequent congenital disorders and their occurrence is about 1 in 300 male infants (Abbas et al., 2018; Versteegden et al., 2017). In hypospadia, the urinary meatus is misplaced ventral to penis with abnormal penis curvature due to the unsuccessful closure of the urethral folds during fetal development (Abbas et al., 2018; Keays & Dave, 2017). Large hypospadias are extremely challenging to repair with existing methods. The reconstructive surgery is challenging with high risk for complications leading to reoperations. Typical complications include fistulas, urethral strictures and reopening of the operation site. Further, failed hypospadia surgery is one of the common reasons for the urethral stricture disease. (Abbas et al., 2018; Keays & Dave, 2017; Spilotros et al., 2018) Variety of tissue grafts such as skin grafts, buccal mucosa or bladder mucosa have been used for hypospadia repair (de Kemp et al., 2015). At present, clinicians are successfully utilizing oral buccal mucosa to repair complex urethral strictures and hypospadias and it is considered as the best urethral substitute in urethroplasty surgery (Atala et al., 2017; Horiguchi, 2017). Oral tissue can be harvested quite safely, and its histological structure resembles that of urothelium. It is also sturdy enough for surgical utilization. However, the donor site availability is very limited and thus another solution is needed for larger defect repairs. (Chapple et al., 2015; Horiguchi, 2017; Singh et al., 2018). Further, the currently used repair grafts may also fail over time since most of the hypospadia repair surgeries are executed during the early childhood and the grafts may not keep up with the pubertal development leading to stricture or secondary chordee. (Abbas et al., 2018; Keays & Dave, 2017; Spilotros et al., 2018)

2.4.2 Pelvic floor defects

UI and POP are common pelvic floor defects in women, and they often co-exist together (Chapple et al., 2015). However, in this text the focus is in the introduction of POP.

POP, or urogenital prolapse, is a common condition affecting large number of women. In POP, the normal support of pelvic floor is weakened, leading to prolapse of lower pelvic organs to the vaginal opening. It is defined as descent of the anterior and/or posterior vaginal wall, the uterus and/or the vaginal apex. (Jelovsek et al., 2007; Lobo et al., 2017; Osborn et al., 2013) Anterior vaginal wall is the most common segment to prolapse leading to descent of bladder. Prolapse of vaginal apex leads to prolapse of uterus or after hysterectomy (removal of uterus) to descent of small intestine, bladder or colon. Rectum can be descended in case of posterior vaginal wall prolapse. The herniation of intestines through vaginal wall is called enterocele. (Jelovsek et al., 2007) Types of POP are presented in Figure 6.

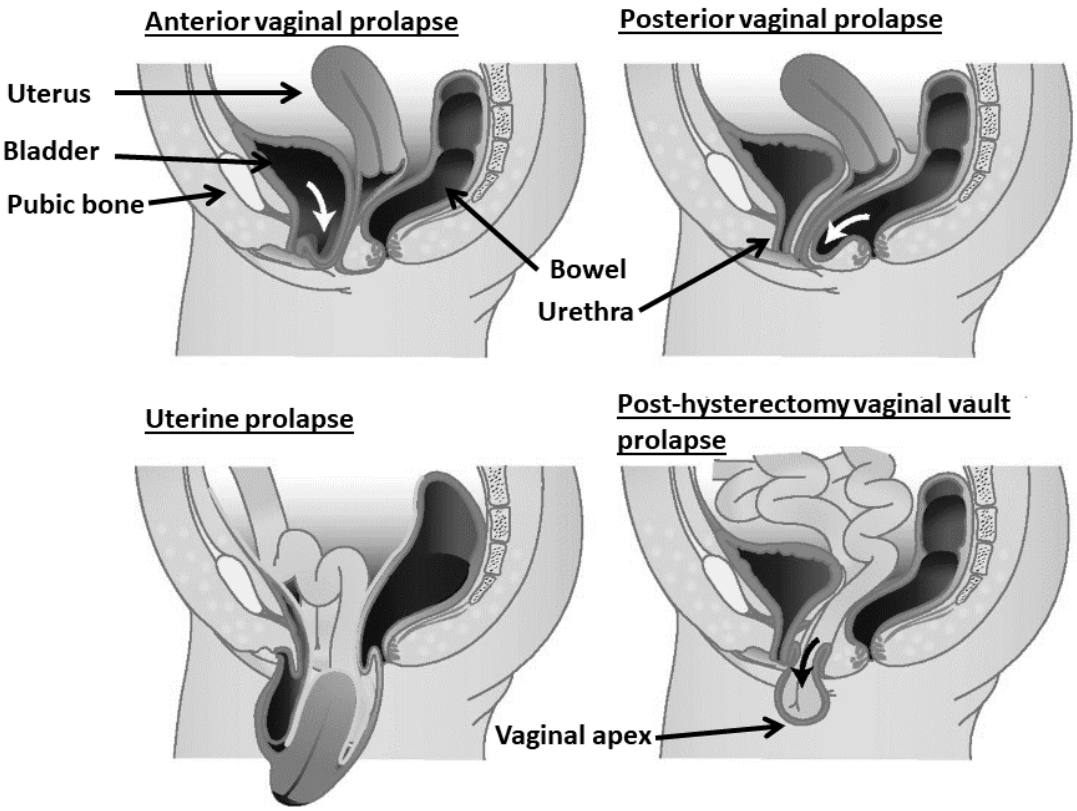

Figure 6 Types of pelvic organ prolapse. Depending on the weakened support wall, different organs can be prolapsed into the vaginal opening. Anterior vaginal prolapse is the most common type of POP. Hysterectomy gives rise to possibility of bowel prolapse. Modified from Barber, 2016.

POP is likely a multifactorial condition. The weakened support of pelvic floor has been associated for instance with pregnancy, vaginal delivery, higher age, obesity, genetic factors and hysterectomy (Chapple et al., 2015; Lobo et al., 2017; Norton & Brubaker, 2006; Vergeldt et al., 2015). Even though one single cause cannot be stated, the injuries caused by vaginal delivery, especially instrumental vaginal delivery, appears to be the most common cause associated to prevalence of POP. The injuries to pelvic floor levator ani muscles significantly weaken the pelvic support capability, also leading to weakening of the connective tissue support through over stretching the fascia. (Ashton-Miller & DeLancey, 2007; De Lancey, 2016; Herschorn, 2004; Jelovsek et al., 2007) Additionally, POP may be associated with dysfunctional fibroblastic metabolism and weakened muscle control (Ruiz-Zapata et al., 2016). The altered fibroblastic metabolism leads to disturbances in collagen and elastin synthesis in connective tissue. Patients suffering from POP have decreased quantities of collagen and elastin. Further, it has been shown, that the collagen and elastin fibres are disorganized, and their content is altered, leading to increased stiffness. (Alperin & Moalli, 2006; Chapple et al., 2015; Klutke et al., 2008; Ruiz-Zapata et al., 2016)

The prevalence of POP in routine gynaecological examination of postmenopausal women is approximately 43-76 % but only small portion of women, approximately 3-6 % develop symptoms. The women often become symptomatic when the prolapsed organ descents beyond the hymen. The symptoms include vaginal bulging, pelvic pressure, low back pain, bleeding or discharge. (Jelovsek et al., 2007; Lobo et al., 2017; Vergeldt et al., 2015) The lifetime risk for women to undergo surgery due to POP is 11-19 %. However, after primary surgery, even up to 30 % of patients will need at least one reoperation. (Alperin & Moalli, 2006; Hung et al., 2010; Medel et al., 2015; Osborn et al., 2013) In the reconstruction, the primary approach is to use patients' own tissue. However, if it fails and needs reoperation, the recurrent prolapse is usually reconstructed with nonabsorbable synthetic polypropylene mesh. Yet, the synthetic meshes are prone to complications such as pain, bleeding, sexual dysfunction, mesh erosion, formation of fistulas and infection. (Medel et al., 2015; Osborn et al., 2013; Roman et al., 2015) Due to these adverse effects, the U.S. Food and Drug Administration (FDA) has announced that use of mesh can lead to serious complications and if possible, the use of surgical synthetic mesh should be avoided (FDA, 2011). Currently, extensive research is conducted to develop replacing methods. Tissue engineering provides possible resolution for the use of synthetic mesh. Using biodegradable materials and cells, the support capability of pelvic fascia could be regenerated without using permanent synthetic materials.

2.5 Cells in urological and gynaecological tissue engineering

Ideally, the cells used in tissue engineering would be autologous harvested cells expressing the desired tissue specific attributes able to regenerate the damaged tissue, for example vaginal stromal cells for vaginal stroma, and urothelial cells for urothelium. However, harvest of specific desired primary cells can be challenging, and limited, and thus also different cell types have been tested to be used as substitutes.

Urothelial cells (UCs) can be fairly easily isolated and expanded *in vitro*, further, the UCs are studied for urethral reconstruction with promising results (Elsawy & de Mel, 2017; Fraser et al., 2004; Southgate et al., 2002), however also other cell types, for instance buccal mucosa keratinocytes and fibroblasts (Bhargava et al., 2004; Zhou et al., 2017), epidermal cells (Fu et al., 2007) and mesenchymal stem cells of different origins (Li et al., 2013; Li et al., 2014; Tian et al., 2018; Wu et al., 2011) have been tested for urological applications. In a rabbit study by Fu *et al*., foreskin epidermal cells were seeded on acellular bladder matrix. The cells were able to form layered cell structure and regenerate urethral structure. (Fu et al., 2007) Regeneration of smooth muscle layer is highly important in urethral tissue engineering since it could prevent the development of strictures in urethral grafts (Maya et al., 2010). Co-culturing SMCs with UCs has given promising results for urethral regeneration (De Filippo et al., 2002; Raya-Rivera et al., 2011; Zhang et al., 2017). However, *in vitro* cultured SMCs rapidly lose their phenotype and cannot be cultured extended periods of time (Denstedt & Atala, 2009). To overcome the muscle cell senescence *in vitro*, mesenchymal stem cells (MSCs) have been studied in co-cultures with easily harvestable adipose derived stem cells (ASCs), for example (Wu et al., 2011; Zhao et al., 2012).

The vaginal fascia is mainly composed of fibroblastic cells, and their harvest requires surgical invasion. More easily harvestable oral buccal mucosa fibroblasts (OF) have been studied for use in pelvic floor applications and urethral repair. (Mangera et al., 2013) To overcome the need for surgical cell harvest, MSCs have also been studied for fascia tissue engineering applications (Lee et al., 2006; Roman et al., 2015).

2.5.1 Human uroepithelial cells

hUCs have been used widely in urological tissue engineering, since their isolation and culture are well established in literature (Elsawy & de Mel, 2017; Fraser et al., 2004; Southgate et al., 2002). Primary autologous hUCs can be isolated from tissue biopsies (Southgate et al., 2002)

or bladder washing (Fossum et al., 2003). They grow adherently *in vitro* and have typical epithelial cobblestone-like morphology as presented in Figure 7.

Human UCs are widely used in urethral tissue engineering both *in vitro* and *in vivo* (de Kemp et al., 2015; Fossum et al., 2007; Raya-Rivera et al., 2011; Zhang et al., 2017). Autologous *in vitro*-expanded hUCs have been successfully used for repairing defected urethra in clinical studies (Fossum et al., 2007; Raya-Rivera et al., 2011). Human UCs have also been used to regenerate functional bladder (Atala et al., 2006). However, the hUCs implanted *in vivo* often need layer of SMCs in order to effectively regenerate the functional uroepithelium (Atala et al., 2006; de Kemp et al., 2015; Raya-Rivera et al., 2011).

Unfortunately, functional urothelium barrier has been difficult to sustain in *in vitro* conditions. The isolated fully matured hUCs gradually lose their differentiated phenotype *in vitro* and expression of UPIII decreases (Xu et al., 2015). The *in vitro* cultured hUCs lack some key properties of urothelium: the mature expression of uroplakins forming AUMs and proper tight junctions (Singh et al., 2018). The *in vitro* cultured hUCs are able to synthesize UPs in their endoplasmic reticulum (ER), but the UPs do not form necessary dimers for their functionality (Lee, 2011). Additionally, the *in vitro* expansion of hUCs has been insufficient in many studies and the ultimate uroepithelium maturation is not fully achieved *in vitro*. It is still not sufficiently known how the urothelial cells differentiate and what exactly the actual origin of different uroepithelium cell types is. (Singh et al., 2018)

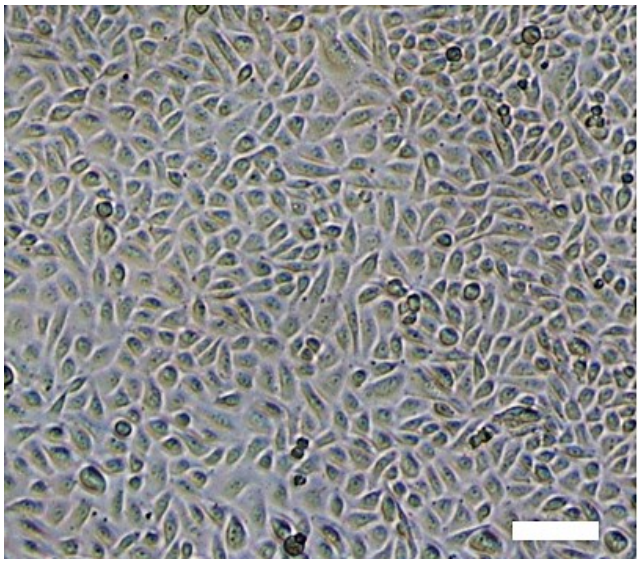

Figure 7 Light microscopy image of hUCs. Confluent layer of cultured hUCs *in vitro* in a culturing flask. Scale bar 100 µm.

2.5.2 Human adipose derived stem cells

MSCs have been studied for tissue engineering applications, as they can differentiate towards several different cell types. Further, the isolation of MSCs is straightforward, and they do not face the ethical problems of embryonal stem cells. MSCs also secrete cytokines and growth factors and thus regulate their surrounding cell and tissue growth. (Elsawy & de Mel, 2017; Ferraro et al., 2016; Singh et al., 2018; Tian et al., 2018). MSCs can be isolated from various sources for example from bone marrow, adipose tissue, dental tissue, amniotic membrane and skin. The bone marrow derived mesenchymal stem cells (BMSCs) are thought as the standard MSCs that other MSCs are compared to. (Elsawy & de Mel, 2017; Sterodimas et al., 2010; Ullah et al., 2015)

Many of the MSC harvest sites are limited, excluding the adipose tissue that is readily available. The MSCs isolated from adipose tissue are named adipose derived stem cells (ASCs). ASCs display stable growth and proliferation kinetics and multipotency to differentiate into variety of cell lineages, such as bone, fat, muscle, neural, epithelial and cartilage cells (Li et al., 2014; Rodriguez et al., 2006; Shi et al., 2012; Sterodimas et al., 2010; Ullah et al., 2015). The differentiation can be directed by using conditioned culture medium or culturing in co-cultures (de Graaf et al., 2017; Li et al., 2013). ASCs are easily harvested from excess adipose tissue resulting from liposuctions or surgical procedures. They perform well in long-time culture, remaining stable with low level of senescence (Rodriguez et al., 2006). They grow adherently when cultured *in vitro* and have spindle-like morphology (Figure 8). Due to their abundance and easy isolation, hASCs could be potential stem cell type for urological tissue engineering (Elsawy & de Mel, 2017) ASCs are isolated from heterogeneous stromal vascular fraction (SVF) cells of the adipose tissue. The SVF is composed of stromal cells, ASCs and microvascular cells (Ferraro et al., 2016; Lindroos et al., 2011). The stem cells are identified amongst the SVF cells by their specific cell surface markers called clusters of differentiation (CD) (Ferraro et al., 2016; Ullah et al., 2015). The ASCs have been shown to express 90 % identical CD profile with BMSCs as are thus thought to be good alternative for BMSCs (Ferraro et al., 2016).

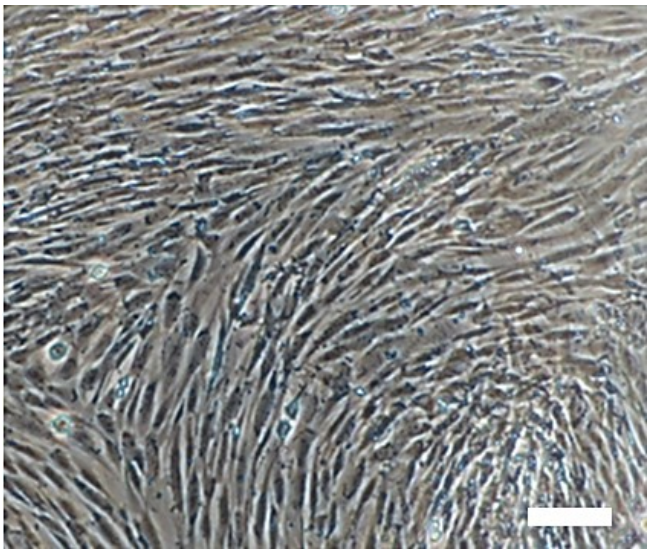

Figure 8 Confluent hASCs. Layer of cultured hASCs *in vitro*. Scale bar 100 µm.

ASCs can differentiate into SMCs, which are important in urothelium regeneration (Garriboli et al., 2014; Li et al., 2014; Shi et al., 2012) and the SMCs contribute to the contractility of uroepithelium. MSCs co-cultured with urothelial cells aim to induce the formation of urethral stroma and angiogenesis, which has been a major challenge in urethral tissue engineering (Pangesty et al., 2017). There are studies, which indicate that the hASCs can differentiate towards urothelial cell type, however, these cells do not sufficiently express the key markers crucial for urothelium barrier properties, such as the UPs and tight junctions (Shi et al., 2012; Singh et al., 2018). In urethral tissue engineering, hASCs have been used both to differentiate into SMCs (Rodríguez et al., 2009; Zhao et al., 2012) and UCs (Liu et al., 2009; Shi et al., 2012; Zhang et al., 2013). Human ASCs were selected for this study for studying smooth muscle regeneration for urethral tissue engineering, since they are readily available and able to differentiate towards SMCs (Ferraro et al., 2016; Garriboli et al., 2014; Maya et al., 2010).

2.5.3 Human vaginal stromal cells

Human vaginal stromal cells (hVSCs) are the cells of vaginal connective tissue, consisting of fibroblasts and myofibroblasts (Alperin & Moalli, 2006; Chapple et al., 2015). These fibroblastic cells produce the ECM and regulate its composition continuously (Alperin & Moalli, 2006; Ruiz-Zapata et al., 2016). They are adherent cells and appear elongated when cultured *in vitro* (Figure 9).

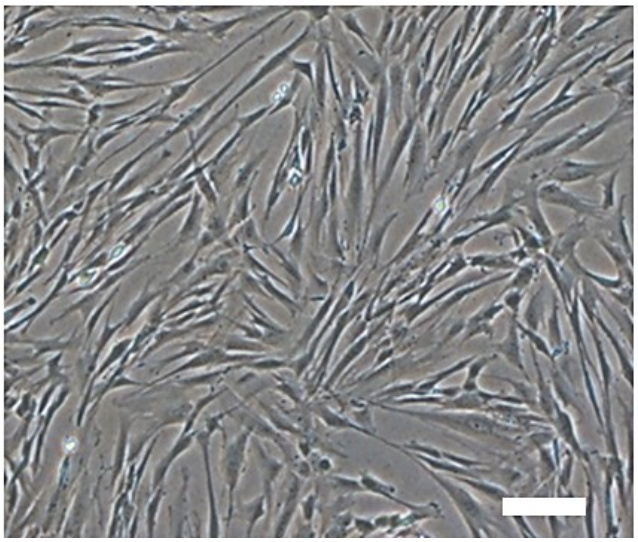

Figure 9 Layer of hVSCs. Human VSCs cultured in culture flask. Scale bar 100 µm.

Fibroblasts are activated to differentiate into myofibroblasts. Extracellular signal molecule transforming growth factor beta 1 (TGF-β1) recruits fibroblasts and regulates their transdifferentiation to myofibroblasts (Hinz et al., 2001; Ruiz-Zapata et al., 2016; Sun et al., 2016). Myofibroblasts are contractile fibroblasts that combine features of SMCs and fibroblasts. They are characterized by expression of alpha-smooth muscle actin (αSMA). (Denstedt & Atala, 2009; Jones & Ehrlich, 2011) Alpha-SMA gives myofibroblasts their contractile capability, and it is similar to actins in SMCs (Hinz et al., 2001). Myofibroblasts are the main fibroblastic cell type in pelvic floor fascia and connective tissue (Chapple et al., 2015; Ruiz-Zapata et al., 2016). Human VSCs have been successfully expanded *in* vitro and implanted *in vivo* to regenerate natural-like fascia (Hung et al., 2010).

2.6 Biomaterials in urological and gynaecological tissue engineering

Tissue engineering can be used for developing more suitable grafts for urethral and pelvic defects, but the best biomaterial for these applications has not yet been established. Biomaterials can be classified to natural and synthetic biomaterials. The natural biomaterials include natural polymers, such as collagen, and acellular tissue matrixes, whereas the synthetic biomaterials contain synthetic polymers. (Kim et al., 2000) The biomaterials in tissue engineering function as an artificial ECM and needs to be carefully selected for desired application to resemble the mechanical properties of the natural tissue. Many different approaches with natural and synthetic materials have been studied, yet still the materials lack the sufficient mechanical design and functionality to regenerate the biological functions. (Chapple et al., 2015; Nair & Laurencin, 2007; Singh et al., 2018)

Generally, the materials in tissue engineering have few essential requirements. The scaffold materials need to be immunologically inert, biocompatible and bioactive. Scaffold should be biodegradable and enhance the cell ingrowth to sustain the reconstruction of natural tissue. If the biocompatibility and bioactivity are not suitable for the target tissue, the site may face serious fibrosis and other complications. The scaffold guides the regeneration of the tissue and thus enhances the integration of the surrounding tissue. In this, the material physical properties, porosity, fabrication, degradation rate and degradation product fate are important. (Abbas et al., 2018; Chapple et al., 2015; Kim et al., 2000; Nair & Laurencin, 2007; Singh et al., 2018) Also, the material should have adequate self-life to be used in clinical applications (Nair & Laurencin, 2007).

Scaffolds can be used with or without seeded cells, but without pre-seeded cells the scaffold needs to promote cell migration on site into the degrading scaffold. However, the *in situ* regenerating capacity might not be enough, and there is a risk of graft shrinkage, fibrosis and poor tissue replacement (Chapple et al., 2015; Singh et al., 2018).

2.6.1 Natural biomaterials

Many kinds of autologous, allogeneic and xenogeneic natural materials have been studied for their suitability in urological and gynaecological tissue engineering. Natural biomaterial availability is limited, as they are harvested from animals or humans, and batch-to-batch variations are high. Natural biomaterials used for tissue engineering include acellular matrices, collagen and silk, for example. Existing problems with natural biomaterials are the shrinkage of the scaffold and risk for acute inflammatory response at implantation site leading to fibrosis. (Chapple et al., 2015; Horiguchi, 2017; Kim & Mooney, 1998)

Acellular matrices, such as human dermis, porcine small intestine submucosa (SIS) and porcine bladder acellular matrix graft (BAMG), are common natural biomaterials used in tissue engineering (Davis et al., 2018; de Kemp et al., 2015; Herschorn, 2004; Singh et al., 2018). Use of acellular matrices is based on the utilization of the natural collagen-rich ECM construct after the removal of all cellular components. In acellular matrices, the ECM stays very similar to ECM in natural tissue and has specific collagen matrix with bioactive molecules and growth factors. These bioactive molecules enhance specific cell interactions and maturation and are efficient in supporting cell growth and migration. However, the ECM composition does alter between tissues, so the desired properties need to be considered when selecting source of used

ECM. (Kim et al., 2000; Kim & Mooney, 1998; Ribeiro-Filho & Sievert, 2015; Singh et al., 2018)

Prepared acellular matrices can be applied unseeded or seeded with selected cell types. In unseeded approach, the ECM construct is implanted *in vivo*, and cells from surrounding tissue are then migrating into the scaffold. However, in urethral repair, the unseeded scaffolds are appropriate only for smaller defects as their regenerating ability is sufficient only in short distances of about 1 cm (Davis et al., 2018; Dorin et al., 2008). Seeded scaffolds can be used for larger defect repairs, *in vivo* studies indicate, that they benefit from the paracrine function of the pre-formed cell layer further promoting tissue regeneration. (Davis et al., 2018) Using cell-seeded scaffolds in urethral applications has been shown to be more favourable since it may decrease the risk of the development of fibrosis and strictures (De Filippo et al., 2015; Singh et al., 2018).

Even though acellular matrices have been successfully utilized and have advantages in cell signalling and attachment, numerous complications arise from using natural acellular biomaterials. The natural materials degrade rapidly and pose a thread of immune-rejection and disease transmission. The most common complications emerging are graft shrinkage, urethral strictures, especially in longer defects, infections, stenosis and major scarring. All these lead to dysfunction of the organ, which causes great distress for the patient. (de Kemp et al., 2015; Elsawy & de Mel, 2017; Garriboli et al., 2014; Maya et al., 2010; Zhang et al., 2014)

Collagen is in the key role when using acellular matrices, as it is the major component of the natural ECM. It can be easily isolated, causes minimal inflammatory response and enhances the cell attachment. (Kim et al., 2000) Collagen's mechanical properties can be altered with crosslinking and it can be processed into several structures to be used as scaffolds (Fu et al., 2007; Pinnagoda et al., 2016; Yao et al., 2017). Pinnagoda *et al*. manufactured an acellular tubular collagen scaffold for urethral regeneration and achieved natural-like urethral tissue even in 2 cm defect (Pinnagoda et al., 2016). Possibility of using acellular grafts also for larger repairs would bypass the cell harvesting and culturing step and thus decrease the time and money consumption. Increasing knowledge on biomaterials and their fabrication may expand the capacities of unseeded matrices for larger scale repairs also.

2.6.2 Synthetic biomaterials

In general, natural biomaterials are insufficient for larger scale repairs, and thus artificial biomaterials are needed. The synthetic nonabsorbable polypropylene mesh used for repair of hernias and POP also needs a safer substitute (Chapple et al., 2015). Synthetic biodegradable polymer scaffolds are the most promising materials for scaffold design, as the scaffold is purposed to degrade as the tissue regenerates. Their molecular composition is well-known, and their function is predictable and modifiable. Material properties can be designed and altered by combining different synthetic polymers. (Denstedt & Atala, 2009; Dorati et al., 2014) Synthetic polymeric materials vary by their chemistry, solubility, hydrophilicity and hydrophobicity, surface energy, water absorption and degradation mechanisms, for example (Nair & Laurencin, 2007). By careful design, the material can be adapted for the functional and structural requirements of desired cells and tissues in planned applications (Denstedt & Atala, 2009; Dorati et al., 2014). The research for the best synthetic biomaterial for urological and gynaecological tissue engineering is still ongoing. The typical problems with synthetic materials are that they are lacking the natural cell recognition sites, are less bioactive and more hydrophobic compared to natural biomaterials which leads to weaker cell attachment (Kim & Mooney, 1998; Maya et al., 2010). The synthetic biomaterials have different mechanical properties compared to natural tissue, the synthetic materials tend to have too high mechanical strength and stiffness. However, their mechanical properties can be changed and controlled, and the large-scale manufacturing is relatively easy with lower batch-to-batch variations compared to natural biomaterials. (Elsawy & de Mel, 2017; Kim & Mooney, 1998)

The most investigated polymers for urological and gynaecological applications are biodegradable polymers of poly-L-lactide (PLLA), polycaprolactone (PCL), and poly(lactic-co-glycolic acid) (PLGA) (Abbas et al., 2018; Dorati et al., 2014; Hung et al., 2010; Mangera et al., 2013; Roman et al., 2015). They belong into a group of thermoplastic poly(α-ester)s, which are the most extensively studied class of biodegradable polymers. Additionally, they are generally used polymers for other biomedical applications, such as absorbable sutures. (Nair & Laurencin, 2007)

The properties of poly(α-ester)s are easily tailored for desired applications by forming copolymers and altering their monomer ratios (Abbas et al., 2018; Nair & Laurencin, 2007). Poly(α-ester)s are aliphatic polymers whose ester bonds degrade by hydrolysis. Their degradation products are natural metabolites that are secreted from the body as water and carbon dioxide. They can be fabricated with various techniques to achieve variety of shapes and forms.

(Kim & Mooney, 1998; Nair & Laurencin, 2007) However, their molecular structure lacks functional groups, which cuts back ability for covalent modifications (Kim & Mooney, 1998).

PLLA belongs into group of poly(α-hydroxy acid)s (Kim & Mooney, 1998). It is a semi crystalline polymer, with crystallinity of 37 % and tensile modulus of 4.8 GPa. It is hydrophobic and thus its degradation time is not very rapid; two to 5.6 years for total absorption *in vivo.* The degradation rate is dependent on the porosity of the matrix controlling the water diffusion into the scaffold. The slow degradation time of PLLA is being compensated by combining it to co-polymers with more rapidly degrading polymers. (Nair & Laurencin, 2007)

PCL is a polyester formed from monomers of ε-caprolactone. It is a versatile material, as it is soluble into a variety of organic solvents and easily blended with numerous other polymers. PCL has low melting point of 55-60℃ and glass transition at -60℃. PCL degrades through hydrolysis, but rather slowly, taking two to three years. Therefore, PCL is often copolymerized for more rapid degradation time. (Nair & Laurencin, 2007; Shakhssalim et al., 2017) PCL has low tensile modulus, about 23 MPa, but can be stretched to over 700 % before breakage. PCL has been studied for use in drug delivery devices due to its relatively slow rate and high permeability for various drugs. Further, PCL is also an interesting material for tissue engineering applications. PCL is flexible and has good load-bearing capacity, and has therefore been studied in tissue engineering applications for bone, cartilage and muscle regeneration. (Garkhal et al., 2007; Nair & Laurencin, 2007)

2.6.3 Poly(L-lactide-co-ε-caprolactone)

Poly(L-lactide-co-ε-caprolactone) (PLCL) is a copolymer of PLLA and PCL. The copolymerization decreases the degradation time compared to plain PCL, and it can be altered for specific applications by changing monomer ratios. Due to the properties of PCL, PLCL is also very elastic material. (Laurent et al., 2018; Nair & Laurencin, 2007) Because being flexible, elastic and having controllable degradation properties, PLCL is especially interesting biomaterial for soft tissue applications in tissue engineering (Wu et al., 2016). However, PLCL is hydrophobic, like many of the synthetic polymers, which limits the attachment of cells in tissue engineering applications (Fu et al., 2014). Altering PLA and PCL ratios also adjusts the stiffness and elasticity of PLCL. PLA as itself is brittle in nature whereas PCL is elastic. In PLCL, PLA forms the stiff domains in soft PCL matrix. (Jeong et al., 2004; Laurent et al., 2018) PLCL can be processed into many different scaffold shapes like foams, tubular, electro spun fibres and sheets. PLCL has been successfully studied in many tissue engineering applications,

including cartilage (Kim et al., 2013), neural (Prabhakaran et al., 2009), ocular (Yao et al., 2017), gynaecological (Sartoneva et al., 2018; Wu et al., 2016), urological (Sartoneva et al., 2012) and vascular (Pangesty et al., 2017; Shafiq et al., 2015) applications. PLCL is also observed to have shape-memory, which could have benefits in some applications. PLCL can also be embedded with growth factors, heparin or other factors to improve cellular responses (Laurent et al., 2018). Because of this feature, the PLCL scaffolds in this study were embedded with specific ascorbic acid derivate.

2.6.4 Ascorbic acid

Ascorbic acid (AA), or vitamin C, is a small carbohydrate functioning as an important reducing agent and essential enzymatic cofactor in numerous intracellular pathways (Arrigoni & De Tullio, 2002; D'Aniello et al., 2017). Humans obtain their daily intake from nutrients, as humans are unable to synthetize AA due to the mutation in L-gulono-lactone oxidase (GLO) enzyme needed for AA biosynthesis (Arrigoni & De Tullio, 2002; D'Aniello et al., 2017). However, AA is unstable and easily breaks down by oxidation, and forms dehydroascorbate (DHA), which can also be reduced back to AA (D'Aniello et al., 2017; Du et al., 2012; Saitoh et al., 2013). More stable ascorbic acid derivates (AADs) have been used for cell culture with comparable results to AA (Boyera et al., 1998; Du et al., 2012; Mangir et al., 2016; Saitoh et al., 2013). AA functions as an antioxidant by reducing reactive oxygen species (ROS) and free radicals, and inhibits them from causing tissue damage (Arrigoni & De Tullio, 2002; Saitoh et al., 2013). The reducing capability of AA is due to its easy oxidation (Du et al., 2012). AA also has a role in epigenetics, as increased AA intake leads to increased histone acetylation (D'Aniello et al., 2017; Du et al., 2012). Presence of AA *in vitro* leads to increased cell proliferation rate compared to absence of AA, which causes the cell proliferation to be impaired (Fernandes et al., 2009). This can be seen as impaired wound healing in absence of AA as no matured collagen can be formed (Kishimoto et al., 2012). The AA thus shows mitogenic effect on cells and is essential in cell culture mediums.

In addition to numerous metabolism processes, AA has an essential role in collagen synthesis. It is necessary cofactor for enzymes prolyl hydroxylase and lysyl hydroxylase in post-translational procollagen modifications in ER prior to extracellular excretion. Without AA, no collagen is being modified and secreted, as it needs to be in its native form. (Fernandes et al., 2009; Piersma et al., 2017; Pozzer et al., 2017) The wrongly modified collagens are degraded inside the cells before excretion (Pinnell, 1985). AA is also regulating collagen synthesis by

activating collagen gene expression (Mangir et al., 2016). AA has also been shown to affect messenger RNA (mRNA) stability; stabilizing collagen mRNA and destabilizing elastin mRNA (Arrigoni & De Tullio, 2002).

AA is associated with mesenchymal stem cell osteogenesis and chondrogenesis (D'Aniello et al., 2017; Fernandes et al., 2009). Osteogenesis and chondrogenesis are increased with presence of AA through increased collagen synthesis, whereas in absence of AA other differentiation lineages are upregulated (Fernandes et al., 2009). However, many studies have shown that AA also enhances adipogenesis of MSCs (Cuaranta-Monroy et al., 2014; Weiser et al., 2009), and also enhances the generation of induced pluripotent stem cells (Esteban et al., 2010).

2.6.5 Supercritical carbon dioxide processing

After scaffold material selection, the scaffold design and fabrication are very important. The fabrication method and scaffold design could have an effect on cell attachment and tissue regeneration, so developing an optimal fabrication method and design is highly important (Kim & Mooney, 1998; Nair & Laurencin, 2007). In tissue engineering, the porous scaffolds structure is favourable in most applications. The pore size and overall interconnected material porosity have an important role in cell migration and viability. The pores work as pathways for nutrient, signalling molecules and oxygen diffusion through the scaffold, enhancing cell viability across the material. (Elsawy & de Mel, 2017)

The 3D porous scaffolds used in this study were fabricated with supercritical carbon dioxide ($scCO_2$) foaming to avoid any harmful substances used in other common fabrication methods. Supercritical fluid processing for pore formation is an appealing alternative for solvent casting, a common fabrication method for forming porous 3D scaffolds. Solvent casting requires toxic organic solvents, such as chloroform, leaving cytotoxic residues on the scaffold. Solvent casting is also very time consuming. (Kim et al., 2013; Salerno et al., 2015) $ScCO_2$ is the most appealing supercritical fluid for medical applications. $ScCO_2$ is non-toxic, inexpensive and non-flammable supercritical fluid and it is readily available (Kim et al., 2013; Salerno et al., 2015). In superficial fluid processing, the supercritical fluid is solubilized inside the polymer matrix, and pore formation is controlled with temperature and pressure changes, and thus no toxic substances are present. In constant pressure and higher temperatures, the formed pores will be larger and more interconnected, as the $scCO_2$ is better able to penetrate between the polymer chains in the matrix. In turn, with constant temperatures, the foaming results in many smaller

pores. (Kim et al., 2013) This method can also be used to fabricate polymer matrix with bioactive compounds (Salerno et al., 2015).

2.7 Tissue engineering in urethral repair

Variety of urethral tissue engineering research is ongoing both *in vitro* and *in vivo*. The studies focus on finding the optimal cell source and material combination to be used in urethral repair, as the functional tissue engineered graft has many requirements to be successful. Most importantly, the biomaterial needs to contribute to the barrier function of urothelium, provide nutrients to cells and enhance smooth muscle generation important for functional urethra. The material must be elastic and stabile under pressure, since it will be susceptible for strong fluid forces and stress from erectile functions. (Abbas et al., 2018; Elsawy & de Mel, 2017; Singh et al., 2018) The current challenges in the present urethral tissue engineering research include establishing sufficient barrier properties, maintaining differentiation of the UCs, regeneration of urethral smooth muscle layers and vascularization and maintaining contractility with available materials (Elsawy & de Mel, 2017; Singh et al., 2018).

2.7.1 *In vitro* tissue engineering

In vitro studies enable the close monitoring of cellular functions and cell-biomaterial interactions under controlled study environment. Specific cellular functions are studied in easily established cell cultures, before moving on to complex *in vivo* studies in physiological environment in animal or human studies.

Previously, Wünch *et al*. compared the adhesion on morphology of the formed urothelium on six different commercially available biomaterials. Two of these materials were PLA-based synthetic materials, and rest four were derived from porcine or bovine donors and based on collagen frameworks. Natural biomaterials did mostly achieve adequate results compared to synthetic materials, so they seem to be suitable for urothelial cell culture. However, as the tested natural biomaterials are xenogeneic, their usage needs careful consideration. (Wünsch et al., 2005) The viability and proliferation of hUCs on natural acellular matrices of porcine SIS and BAMG were compared by Davis *et al*. Human UCs remained viable on both matrices, but on BAMG the proliferation rate was fourfold higher. They expanded their study by culturing hUCs on BAMG in urine. However, the cell proliferation and viability were significantly higher in the control group cultured in growth media. (Davis et al., 2011) Generally, SIS isolated in laboratory has had better results compared to commercial SIS products. This might be because

of the needed safety protocols in manufacturing the commercial products, such as freeze-drying and sterilization that alter the commercial SIS properties. (Ribeiro-Filho & Sievert, 2015) However, overall SIS seems not to be ideal for UC culture (Davis et al., 2011; Maya et al., 2010). As the gastro intestinal tract and urinary tract are different in structure, using SIS has a high risk for serious complications. The epithelium of SIS has inherent absorptive and secretory properties as the urothelium has barrier properties, thus using SIS in urethral repair can lead to urine leakage and serious infections. (Singh et al., 2018)

Xu *et al*. produced electrospun scaffolds from ureter ECM/PLLA blend and porcine SIS/PLLA blend, to benefit from both natural ECM composition and mouldable synthetic biopolymers. Scaffolds were seeded with hUCs. Ureter ECM/PLLA scaffold successfully promoted hUC viability and proliferation, but also maintained differentiated hUC phenotype. The expression of UPIII was significantly higher on ECM/PLLA than in control materials SIS/PLLA and plain PLLA. (Xu et al., 2015) Further, Sartoneva *et al*. compared human amniotic membrane (hAM) and PLCL membranes for hUC culture. Human UCs were successfully cultured on plain PLCL membranes, which they preferred over hAM. The hUC proliferation was higher, and the viability was significantly better on PLCL than on hAM. The hUCs maintained their phenotype and proliferated significantly more efficiently than on control materials. (Sartoneva et al., 2011)

As seen from these example studies, the hUCs have maintained their phenotype, remained viable and proliferative *in vitro* on tissue engineered scaffolds. *In vitro* studies continue to give detailed valuable information on cellular functions when testing new materials and cells for urethral tissue engineering. The urethral reconstructive research, however, is already in point where *in vivo* and even clinical studies are done in increasing numbers.

2.7.2 *In vivo* tissue engineering and clinical pilot studies

Urological tissue engineering has already been extended to *in vivo* studies both with animals and clinical studies with humans; many patients have been treated with acellular constructs or cell-seeded grafts (Davis et al., 2018). *In vivo* studies enable the monitoring of the tissue engineered construct under physiological conditions that cannot be simulated *in vitro*. Different approaches have been implemented *in vivo* with promising results.

In previous *in vivo* studies, urethral regeneration in dogs was performed by Orabi *et al.* in their study where they seeded tubular BAMG with SMCs and UCs isolated from bladder biopsies. The control group with acellular BAMG all formed severe strictures and urine leakage, whereas

animals with cell seeded scaffold regenerated functional urethra. (Orabi et al., 2013) Other scaffold approach in *in* vivo study by Tian *et al*. utilized silk fibroin scaffold. They seeded silk fibroin with hASCs and implanted the construct to rabbit urethra. Six weeks post-surgery, normal-like urothelium was formed, with underlying SMCs and blood vessels. (Tian et al., 2018) Further, Zhang *et al*. bioprinted tubular 3D urethra from polymer blend of PCL/PLCL as a matrix. Fibrin hydrogel seeded with UCs and SMCs was simultaneously bioprinted around it. SMCs were printed to the outer side of the PCL/PLCL matrix and UCs to the inner side, to achieve the natural like layering of the urethra. Graft was then implanted in rabbits. Cells remained viable and expressed normal phenotype at least to day seven post-implantation. The results were really promising for future of urethral tissue engineering. (Zhang et al., 2017)

In addition to animal studies, few clinical pilot studies on urethral regeneration have been published. Fossum *et al*. performed a clinical study repairing hypospadia with a graft of acellular dermis seeded with autologous hUCs isolated with bladder wash procedure. Six patients were treated, out of which four developed complications, and only three expressed hUCs on the transplant during the follow-up period. After complications were treated, repaired urethras remained functional and patients were satisfied. (Fossum et al., 2007) Further, autologous buccal mucosa keratinocytes and fibroblasts were seeded on de-epidermized dermis in a pilot study by Bhargava *et al*. and used for treating urethral strictures in five human patients suffering from lichen sclerosus. Two patients needed reoperation of the procedure due to formation of fibrosis while the other three needed assisting operations. However, in the end of their follow-up periods, no recurrence was reported in any of the patients. (Bhargava et al., 2008) In addition, Raya-Rivera *et al*. experimentally treated urethral defects in five boys aged 10 – 15 years with tubular poly(glycolic acid) (PGA) matrix scaffold, seeded with hUCs and SMCs. At the 36-month follow-up, all regenerated urethras were functional, and the tissue engineered PGA graft had formed and retained normal urethral architecture. (Raya-Rivera et al., 2011)

Animal studies are essential for studying novel biomaterial and cell combinations to understand the host responses and degradation profile after implantation, prior to conducting studies with human patients. New novel structures are emerging in attempt to find the clinically optimal tissue engineered construct for urethral regeneration. These example studies show that tissue engineered constructs have already been used in clinical applications with potential results, however, the number of treated patients is small and more evidence on the tissue engineering based reconstruction is required.

2.8 Tissue engineering in pelvic floor applications

As the current use of polypropylene mesh for POP correction is prone for complications, numerous *in vitro* studies are ongoing to find the safer compensatory repair material. The biomaterials for pelvic floor applications should regenerate and strengthen the natural collagen framework of the pelvic support (Chapple et al., 2015). Tissue engineered cell seeded scaffold could regenerate the natural supporting fascia by recruiting ECM producing cells to produce supportive connective tissue on site. (Aboushwareb et al., 2011; Medel et al., 2015; Roman et al., 2015)

In previous *in vitro* study, Roman *et al*. aimed to mimic natural ECM alignment in human fascia for treating POP with hASCs cultured on electrospun PLA scaffolds with different degrees of fibre alignment. Cells produced more collagen on aligned scaffolds compared to controls, growing oriented along the fibre alignment. Their test suggested that the alignment of fibres and cells are important for fascial tensile strength and thus supporting the pelvic floor. (Roman et al., 2015) Further, Mangera *et al*. studied seven different scaffold materials *in vitro* for SUI and POP with OFs. These seven materials included AlloDerm® (acellular cadaveric dermis), cadaveric dermis, porcine dermis, polypropylene mesh, porcine SIS, sheep stomach and electrospun PLA. Out of the seven candidates, SIS and PLA achieved the best cell attachment, ECM production and mechanical properties fit for pelvic floor application. (Mangera et al., 2013) Wu *et al.* manufactured electrospun PLCL/fibrinogen mesh and studied its potential in POP repair. They implanted PLCL/fibrinogen mesh into abdominal wall of dogs but also conducted small clinical trial on POP patients. In both studies, the PLCL/fibrinogen mesh performed better than nonabsorbable polypropylene mesh with faster vascularization and tissue regeneration. PLCL mesh therefore appears to be a promising repair option for POP. (Wu et al., 2016)

In addition, tissue engineered fascia graft consisting of hVSCs and biodegradable PLGA mesh was tested *in vivo* in mice by Hung *et al*. In their study, hVSCs were mixed within collagen solution and then seeded onto PLGA mesh. The seeded hVSCs were labelled with fluorescent marker on their cell membranes before implantation. Fabricated PLGA mesh was then inserted subcutaneously in mice. In their study, they achieved formation of new fascia of human origin in the test mice, seen as abundance of the pre-labelled hVSCs in the newly-formed fascial tissue. (Hung et al., 2010) Roman *et al*. studied *in vitro* for the possibility to use hASCs or OFs as alternatives for vaginal cells. The cells were seeded on electrospun PLA meshes, which were strained or unstrained in cell culture holders. After 14 days in culture, they determined the cell

collagen production and expression of ECM collagen type I and III and elastin. Both cell types performed well and produced good amounts of collagen. On unstrained mesh, hASCs produced increased amount and denser collagen than OFs. However, on strained mesh, no superiority over other was seen in their analyses. Further, elastin production of both cell types was increased compared to unstrained conditions. They conclude that both hASCs and OFs can be used for pelvic floor tissue engineering. (Roman et al., 2014)

As pelvic floor support system is very complex structure, its regeneration is not that straight forward. Current studies aim for regenerating the connective tissue in pelvic floor, and thus studies focus on increasing and improving cell collagen production. Promising results for fascia development have been acquired with different approaches, and effects of material properties to cellular functions have been unravelled.

3 AIMS OF THE STUDY

This project studies the effect of PLCL scaffolds embedded with AAD on hVSCs, hUCs and hASCs. The effect on cell viability, cell proliferation, cell maturation and gene expression are determined to evaluate the suitability of the novel PLCL based scaffolds for use in urological and gynaecological tissue engineering applications. The study is divided into two phases:

I. Determining the effect of AAD embedded in PLCL membrane on hVSC viability, collagen production and cell maturation and expression of specific genes.

II. Determining the effect of supercritical carbon dioxide foamed PLCL scaffold embedded with AAD (scPLCLas) on hUC and hASC viability, collagen production, cell maturation and expression of specific genes compared to plain scPLCL. Further, the effect of co-culture of hUCs and hASCs is studied on scPLCLas and scPLCL by determining the cell viability and phenotype maintenance. Prior to hUC/hASC co-culture study, different medium compositions are studied in order to optimize the co-culture medium.

4 MATERIALS AND METHODS

This study was carried out in two consecutive phases: *Phase I* hVSC seeded PLCL membranes and *Phase II* hUC and hASC monoculture on 3D scPLCL –scaffolds, co-culture medium optimization and hUC/hASC co-culture. Below are described the methods used in this study.

4.1 Biomaterials

The scaffolds used in this thesis project were manufactured at former Tampere University of Technology, Department of Biomedical Sciences and Engineering. In Phase I, three different types of PLCL membranes were used: holed PLCL with added ascorbic acid derivate (hPLCLas) and unholed PLCL membrane with added ascorbic acid derivate (PLCLas) and plain holed PLCL membrane (hPLCL) (Figure 10). Membranes were manufactured from 70/30 PLCL copolymer granules with inherent viscosity of 1.6 dl/g (Corbion, Gorinchem, The Netherlands). Granules, with or without added known amount of AAD, were compression moulded with Nike Hydraulics press (Type ZB110 NIKE Hydraulics Ab, Eskilstuna, Sweden) into 0.3 mm thick membrane sheet. Twelve mm diameter samples were cut out with laser cutting, using Epilog Laser Fusion 75W (Golden, CO, USA) laser cutter, along with the holes for holed membranes. Samples were then washed with ethanol, vacuum dried and sterilized by minimum of 25 kGy gamma irradiation before cell culture. For the experiment, membranes were put in place in wells with CELLCROWN™ (Scaffdex Oy, Tampere, Finland).

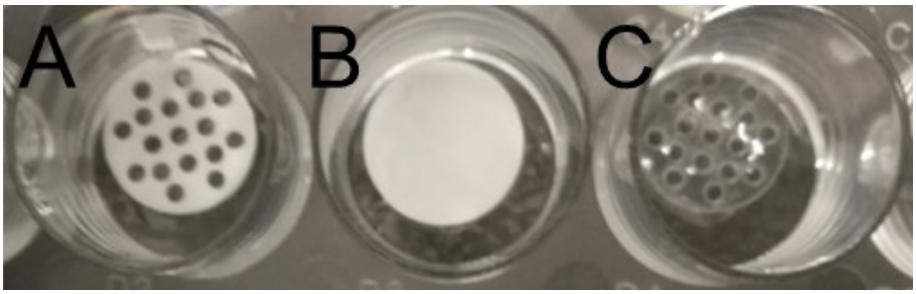

Figure 10 PLCL membranes used in Phase I. Three different membranes were studied with hVSCs: A) hPLCLas B) PLCLas C) hPLCL.

In Phase II, two kinds of 3D scaffolds were studied: scPLCLas and plain scPLCL 3D-scaffolds (Figure 11). The protocol for scPLCL scaffold manufacturing and characterization was similar to as described earlier (Sartoneva et al., 2018). Briefly, 70/30 PLCL copolymer granules with inherent viscosity of 1.6 dl/g (Corbion) were used to manufacture the scaffolds. The porous interconnected scPLCL scaffolds were produced by transforming PLCL granules into rods by

melt-extrusion and then fabricated by custom-fitted $scCO_2$ reactor system (Waters Operating Corporation, Milford, MA, USA). Samples were then cut into scaffolds with diameter of 5 mm and thickness of 2 - 2.5 mm. The scPLCLas scaffolds were prepared similarly but were embedded with known amount of AAD. Scaffolds were washed with ethanol and sterilized by gamma irradiation, min 25 kGy, before cell culture.

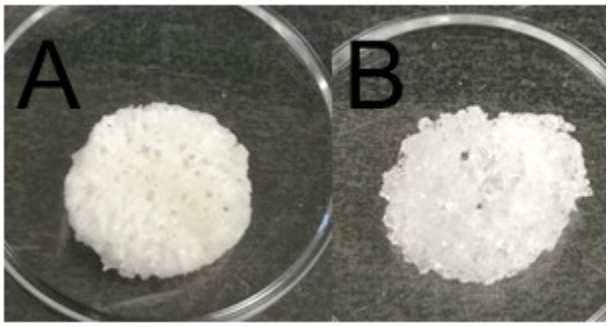

Figure 11 3D scaffolds used in Phase II. Two different 3D PLCL scaffolds were studied with hUCs and hASCs: A) scPLCLas, B) plain scPLCL.

All scaffolds were prewetted in growth medium in +37 °C for 24 hours prior to plating the cells for the experiment.

4.2 Isolation of cells and cell culture

4.2.1 Human vaginal stromal cells

Human VSCs were isolated as described by (Sartoneva et al., 2018) from vaginal tissue pieces from patients undergoing vaginectomy. Briefly, the donated tissues were cut to small pieces and digested for 60 min at +37 °C water bath with shaker in a solution containing 1.5 mg/ml collagenase type I (Life Technologies, Thermo Fisher Scientific, Waltham, MA, USA) and 4 mg/ml dispase (Invitrogen, Thermo Fisher Scientific) in Hanks' balanced salt solution (HBSS, Life Technologies). Digested tissue pieces were filtered through 100 cell strainer (BD Biosciences, San Jose, CA, USA) and centrifuged. The tissue pieces and cell pellet were then cultured in separate T75 CellBind flasks (Sigma-Aldrich, St Louis, MO, USA) in EpiLife medium containing 1 % EpiLife Defined Growth Supplement (EDGS) (Gibco by Life Technologies, Thermo Fisher Scientific), 0.1 % calcium chloride ($CaCl_2$) (Gibco by Life Technologies), 0.35 % antibiotics 100 U/ml penicillin and 0.1 mg/ml streptomycin (P/S; Lonza, BioWhittaker, Verviers, Belgium) in EpiLife® basal medium (Gibco by Life Technologies). To isolate the hVSCs, the primary culture was treated with TrypLE Select (Gibco by Life Technologies) for 2 min and cells passaged to T75 Nunc flasks (Nunc, Thermo Fisher

Scientific) in DMEM/F12 medium (Thermo Fisher Scientific) with 5 % human serum (HS) (Biowest, Nuaille´, France), 1% GlutaMAX (Life Technologies) and 1% of P/S (Lonza). Donor information is described in Table 1.

Table 1 Donor information for hVSC cells used in Phase I of this study.

Donor	Study	Passage	Age	Sex
1	I	3	28	Female
2	I	3	38	Female
3	I	4	23	Female

Prior the experiments, hVSCs were thawed and expanded on polystyrene T75 cm^2 flasks (Nunc™ EasYFlask™, Roskilde, Denmark). Cells were cultured with αMEM culture medium containing 5 % sterile filtered HS (Biowest) and 1 % P/S in Minimum Essential Medium Eagle-Alpha Modification (αMEM) (Gibco by Life Technologies). Culture medium was changed three times a week until cells were plated for experiment.

4.2.2 Human urothelial cells

Human UCs were isolated as described previously (Sartoneva et al., 2011; Southgate et al., 2002) from ureter or renal pelvis tissue pieces, which were received as by-products from elective surgery from child patients. Briefly, tissue pieces were incubated overnight in +4 °C in a stripping solution containing 1 % HEPES (1 M, N′-2-hydroxyethylpiperazine-N′-2-ethanesulphonic acid; Sigma-Aldrich), 0,0001 % aprotin (1 kIU/µl; Sigma-Aldrich), 0.1 % ethylenediaminetetraacetic acid (EDTA; Sigma-Aldrich), 0.01 % P/S (Lonza) in HBSS without Ca^{2+} and Mg^{2+} (Invitrogen). The epithelium layer was separated from the stroma and incubated for 60 min in 0.1 % trypsin (Lonza) in +37 °C water bath with shaker. Tissue pieces were then centrifuged and plated in Epilife growth medium on CellBIND T75 flasks (Sigma-Aldrich). Used hUC cell line donors are presented in Table 2. Corning™ CellBIND™ surface flasks 75 cm^2 (Sigma-Aldrich) were used for expansion hUCs cultured in Epilife medium. Culture medium was changed three times a week until cells were plated for experiment

Table 2 Information on the urothelium tissue donors and hUCs used in this study. General information on the donor and the sample origin are presented. M = used in monoculture, C = used in co-culture.

Donor	Study	Passage	Age	Sex	Anatomical place	Indication
1	II	3 (M) 4 (C)	3 months	Male	Renal pelvis	Pyeloureteral (PU) obstruction
2	II	3 (M) 4 (C)	2 years 7 months	Female	Renal pelvis	PU obstruction
3	II	3	2 years 9 months	Female	Ureter	Vesicoureteral reflux

4.2.3 Human adipose derived stem cells

Human ASCs were isolated as described previously (Haimi et al., 2009; Kyllönen et al., 2013) from fat tissue pieces derived from patients undergoing routine surgical procedures such as breast reduction. Briefly, the donated tissues were cut to small pieces and digested with 1.5 mg/ml collagenase type I (Invitrogen) while incubating for 60 min at +37 °C water bath with shaker. Digested tissues were then centrifuged and filtered and expanded in DMEM/F12 medium. Donor information of hASCs is described in Table 3.

Table 3 Information on the adipose tissue donors and isolated hASCs used in this study. General information on the donor and the sample origin are presented. M = used in monoculture, C = used in co-culture.

Donor	Study	Passage	Age	Sex	Anatomical place
1	II	3 (M) 4 (C)	62 years	Male	Abdomen
2	II	3 (M) 4 (C)	43 years	Female	Subcutaneous
3	II	3	71 years	Female	Subcutaneous

Prior the experiments, the hASCs were thawed and expanded on polystyrene T75 cm^2 flasks (Nunc™ EasYFlask™). Cells were cultured with αMEM culture medium containing 5 % sterile filtered HS (Biowest) and 1 % P/S (Lonza) in αMEM (Gibco by Life Technologies). Culture medium was changed three times a week and then cells were plated for experiment.

4.2.4 Ethical consideration

Cells used in this project were isolated from tissue samples received from Tampere University Hospital. The cells were isolated with the supportive statements of the Ethics Committee of Pirkanmaa Hospital District, Tampere, Finland: R07160 for hUCs, R15161 for hASCs and R15051 for hVSCs. Also written consent was obtained from the patients or parents in case of hUCs.

4.2.5 Phase I: hVSC seeded PLCL membranes

Phase II was carried out with three different hVSC cell lines. Membranes were placed to 24-wellplates and fixed to the bottom of the well with CELLCROWN™ (Scaffdex Oy) and incubated in αMEM medium in +37 °C for 24 hours before cell seeding. Cells were seeded in a concentration of approximately 5 000 cells/well, except for immunocytochemistry staining and Live/Dead® assay with concentration of approximately 7 000 cells/well. The cells were seeded on the membranes in a medium volume of 30 µl to the wells with 1 ml of 5 % HS in αMEM medium.

4.2.6 Phase II: hUC and hASC monocultures and hUC/hASC co-culture

Monocultures were conducted with hUCs and hASCs from three patients. Approximately 150 000 cells were plated on the upper surface of 3D scPLCL scaffolds. Cells were seeded in a medium volume of 50 µl and let to attach for two hours in +37 °C before adding 1 ml of either Epilife for hUCs or 5 % HS in αMEM medium for hASCs. For polystyrene control wells (24-well plate, Nunc, Roskilde, Denmark), 20 000 hUCs or 2 000 of hASCs were plated per well.

Prior to the 3D scaffold co-culture study, different medium compositions were tested with hUC and hASC monocultures to optimize the medium composition for hUC/hASC co-culture. The tested medium compositions are presented in Table 4. The hUCs or hASCs from one donor were seeded on 24 well plate (Corning™ CellBIND™, Sigma-Aldrich) in five different medium compositions. Plating density for hASCs were approximately 2 000 cells/well and for hUCs approximately 20 000 cells/well. Cell viability, proliferation and morphology were

observed with Live/Dead® assay, CyQUANT® assay and light microscope (Nikon eclipse TE2000-S (Nikon, Tokyo, Japan) on d1, d7 and d14. Additionally, the pan-cytokeratin [AE1/AE3] expression of hUCs were determined on d14. The best performing medium was then selected to be used in hUC/hASC co-culture.

The hUC/hASC co-culture was carried out in medium B (Table 4). Study was conducted with two different hASC and hUC cell lines. First, hASC were plated on other side of 3D scaffolds in concentration of 150 000 cells/scaffold. Human ASCs were cultured on scaffolds in 5 % HS in αMEM for five days in order to expand the amount of hASCs before plating hUCs to co-culture. The scaffolds were turned upside down and hUCs plated on other side in concentration of 150 000 cells/scaffold. Simultaneously, the medium was changed to Epilife medium, the medium composition B, for hUC/hASC co-culture study (Table 4).

Table 4 Tested co-culture mediums for hUC/hASC co-culture. Five different mediums including basic hASC medium (A) and hUC medium (B) and different combinations of these two were tested t be used in hUC/hASC co-culture in Phase II.

A	**B**	**C**	**D**	**E**
5 % HS	1 % EDGS	0.35 % P/S	1 % EDGS	1 % HS
1 % P/S	0.1 % $CaCl_2$	in 1:1 EpiLife:αMEM	0.1 % $CaCl_2$	1 % EDGS
in αMEM	0.35 % P/S		0.35 % P/S	0.1 % $CaCl_2$
	in EpiLife		in 1:1 EpiLife:αMEM	0.35 % P/S
				in 1:1 EpiLife:αMEM

4.3 Used assays

4.3.1 Cell morphology and viability (I, II): Live/Dead®

Live/Dead® Viability/Cytotoxicity Kit for mammalian cells (Molecular probes, Invitrogen, Eugene, Oregon, USA) was used to determine the qualitative viability of the cells. Living cells transform calcein acetoxymethyl ester (Ca-AM) into fluorescent calcein intracellularly, staining them green. Ethidium homodimer-1 (EthD-1) can penetrate to dead cells due to their damaged cell membranes, and undergoes a modification when binding with nucleic acids, staining dead cells red in fluorescent imaging. (https://www.thermofisher.com/, 21.10.2018) Dye concentrations were determined by the scaffold used in cell culture. Used dye concentrations are presented in Table 5.

Table 5 Dye concentrations in Live/Dead® assay. Concentrations of EthD-1 and Calcein-AM dyes in Live/Dead® assay vary in different phases of the study according to the used scaffold.

Phase	EthD-1 (µM)	Calcein-AM (µM)
I PLCL membranes	0.3	0.25
II 3D scPLCL scaffolds	$3.75*10^{-5}$	0.5
II co-culture medium optimization	0.25	0.5

Viability of hVSCs (I) was evaluated at d7 and d14 time points and the viability of hUCs and hASCs (II) at d1, d7 and d14 time points. Imaging was performed with Olympus IX51 fluorescent microscope (IX51S8F-2, camera DP71; Olympus, Tokyo, Japan). Pictures were edited by combining colour channels with Adobe Photoshop CS4 (Version 11.0, Adobe Systems, San José, CAL, USA).

4.3.2 Cell proliferation (I, II): CyQUANT®

CyQUANT® Cell Proliferation Assay Kit (Molecular probes, Invitrogen, Eugene, Oregon, USA) was used to determine the proliferation of the cells by quantifying the amount of DNA present. CyQUANT® GR dye in working solution binds nucleic acids in the cells, creating fluorescence proportional to the amount of present DNA. The cell proliferation was evaluated after 1, 7, and 14 days of cell culture. At each time point, cells were first washed with Dulbecco's Phosphate-buffered saline (DPBS; Lonza, BioWhittaker), lysed with 0.1 % Triton

x-100 (4-(1,1,3,3-tetramethylbutyl)phenyl-polyethylene glycol; Sigma Aldrich) and stored in -80 °C until analysed. On the day of the analyse, thawed cell lysates were pipetted onto a 96-MicroWell plate (Nunc, Roskilde, Denmark) 20 µl per well, with 180 µl of CyQUANT® working solution, containing cell lysis buffer (Life Technologies, Eugene, Oregon, USA) and CyQUANT® GR reagent (Life Technologies). The fluorescence in 480/520 nm was measured with Wallac Victor 1420 multilabel counter (PerkinElmer Life and Analytical Sciences, Wallac Oy, Turku, Finland).

4.3.3 Immunocytochemistry (I, II)

The indirect immunocytochemistry (ICC) staining was performed at d14 to visualize the specific antigens in sample. The samples were fixated with 0.2 % Triton x-100 (Sigma Aldrich) in 4 % PFA (paraformaldehyde; Sigma Aldrich) for 15 min in room temperature (RT). Prior to immunostaining, the fixated samples were blocked to avoid any unspecific binding. Samples were incubated for 60 min in +4 °C on a turner in a blocking solution of 1 % BSA (bovine serum albumin; Sigma) in DPBS (Lonza). The sample was treated with specific primary antibody for the selected antigen wanted to be visualized. The primary antibody was diluted in blocking solution and added on sample, incubating overnight in +4 °C on a turner. Next, the sample was treated with fluorescent-labelled secondary antibody, which binds to the primary antibody. Secondary antibody was diluted into blocking solution, and added on sample, incubating 45 min +4 °C on a turner. Cell nuclei were stained with fluorescent DAPI (4',6-diamidino-2-phenylindole), to determine the cell localization. Used primary and secondary antibodies are presented in Table 6. The sample was then visualized with florescent imaging, where the fluorophore bound to secondary antibody and DAPI bound to cell nuclei emit light visualizing the antigen localization in sample. Simplified figure of the method is presented in Figure 12. Samples were imaged with fluorescence microscope (IX51S8F-2, camera DP71; Olympus, Tokyo, Japan). Pictures were edited by combining colour channels with Adobe Photoshop CS4 (Version 11.0, Adobe Systems).

Table 6 Information of used primary and secondary antibodies in immunocytochemistry staining.

Primary antibody	Manufacturer	Reference	Dilution	Secondary antibody	Dilution
αSMA	Abcam	ab7817	1/200	A11029	1/300
COL I	Abcam	ab90395	1/2000	A21121	1/400
DAPI	Invitrogen	D3571	1/2000		
Pan-cytokeratin [AE1/AE3]	Pierce	MA5-13156	1/250	A21121	1/400
Phalloidin	Sigma	P1951	1/500		
UPIIIA	Orbyt	orb248591	1/100	A11037	1/300

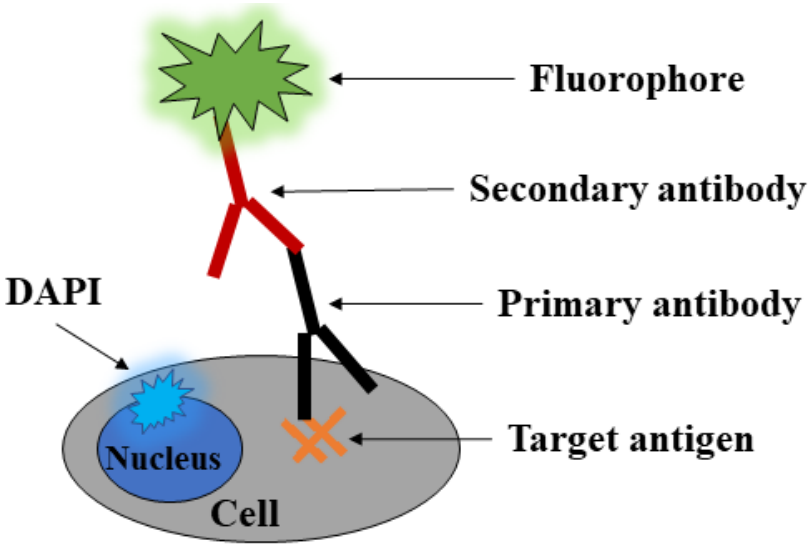

Figure 12 The simplified visualization of indirect ICC detection of target antigens in a cell.

4.3.4 Sircol™ soluble collagen assay (I, II)

The amount of produced collagen was assessed with Sircol™ soluble collagen assay kit (Biocolor, Carrickfergus, United Kingdom) after 14 days of cell culture. The assay measures acid-soluble and pepsin-soluble collagens and newly synthesised collagen (http://www.biocolor.co.uk/, 21.06.2018). Collagen was dyed with Sirius red in 1 % picric acid, and the produced absorbance was quantified with microplate reader. Samples were incubated 4 hours in +4 °C with ice cold 0.1 mg/ml pepsin (Sigma Aldrich) in 0.5 M acetic acid. After incubation, 200 µl from each sample was moved to separate low protein binding Eppendorf tubes (Eppendorf AG, Hamburg, Germany). Collagen standard was prepared by diluting provided Sircol collagen standard with 0.5 M acetic acid to concentrations between 300 µg/ml and 0 µg/ml. Thereafter, 1 ml of Sircol Dye Reagent was added to each sample and standard tube, and incubated 30 min in RT. After incubation, the tubes were centrifuged 12 000 rpm for 10 min, which after the supernatant was removed extra carefully. Thereafter, 750 µl ice-cold Sircol Acid-Salt Wash Reagent was gently added to all tubes, the samples were centrifuged again 12 000 rpm for 10 min and supernatant was carefully removed. Finally, 250 µl Sircol™ Alkali Reagent was added to each tube and vortexed until pellet was completely dissolved. Two parallel 100 µl samples were pipetted to 96 well-plate and measured absorbance with Wallac Victor 1420 multilabel counter (PerkinElmer Life and Analytical Sciences, Wallac Oy, Turku, Finland) with a wavelength 544 nm.

4.3.5 Quantitative real time reverse transcription–polymerase chain reaction (I, II)

The gene expression of specific genes was quantified with two-step quantitative real time reverse transcription–polymerase chain reaction (qRT-PCR). In qPCR the amplification of DNA is monitored simultaneously with the progression of the reaction. First, the RNA is purified from samples and transcripted to complementary DNA (cDNA). The cDNA is then used in the qRT-PCR run. In qRT-PCR, the template sequences of selected primers begin the gene sequence amplification by joining with the complementary target DNA sequences. During the thermal cycles of the run, the DNA strands denaturate at 95 °C and when temperature is lowered to 60 °C, the primers anneal with the target sequences. Then, when temperature is raised again, the polymerase enzyme elongates the sequence onward from the primers. These cycles are repeated to amplify the gene sequence (Figure 13). In real time PCR, the amount of produces DNA is monitored with fluorescent marker that binds to two-stranded DNA.

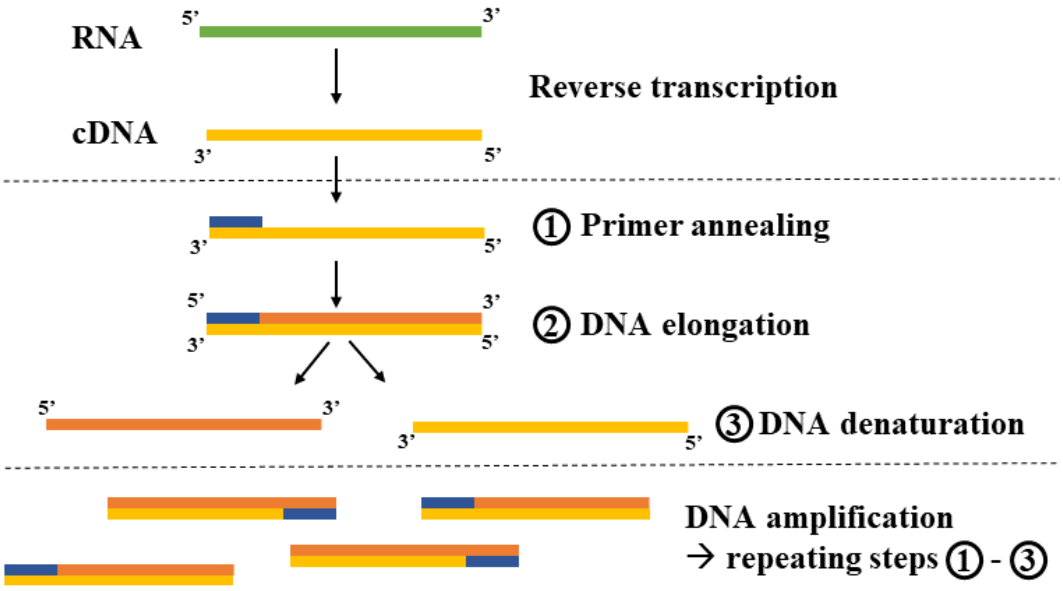

Figure 13 The main steps in qRT-PCR. Isolated sample RNA is first reverse transcripted to cDNA, which is then used in qRT-PCR, where thermal cycles regulate DNA amplification.

To execute qRT-PCR, the RNA was first collected from the samples. The RNA was purified from samples according to Nucleospin® RNA-purification kit and protocol (Macherey-Nagel GmbH & Co. KG, Düren, Germany). Samples were collected on d14 by lysing the cells. Each sample was suspended with solution of 350 µl RA1 lysis buffer and 3.5 µl 2-mercaptoetanol (Sigma). The RNA was purified from the lysate by following the RNA purification protocol (Macherey-Nagel, 06/2015, Rev. 17). The attained RNA amount and quality were then determined with NanoDrop 2000 Spectrophotometer (Thermo Fisher Scientific). Which after, the RNA of the samples was diluted with sterile water (Aqua Sterilisata Braun, B. Braun, Melsungen, Germany) to a concentration of 100 ng/µl, or if the total ng/µl yield was lower, the samples were not diluted at all. Next, the RNA containing samples were transcripted to cDNA using the High-Capacity cDNA Reverse Transcriptase Kit (Applied Biosystems, Life Technologies). The reverse transcription was performed with Eppendorf PCR machine (Eppendorf, Hamburg, Germany) with a run program 25 °C 10 min, 37 °C 2 h, 85 °C 0,05 s.

For qPCR run, the cDNA samples were diluted 1:1 with sterile water (B. Braun). Expression of collagen type I (COL I), collagen type III (COL III), αSMA and elastin for hVSCs (I) and hASCs (II), and expression of cytokeratins CK7, CK8 and CK19, uroplakins UPIa, UPIb and UPIII for hUCs (II) were analyzed. Housekeeping gene RPLP0 (large ribosomal protein P0) was used for the normalization of the results. The sequences of used PCR primers are presented in Table 7.

Table 7 DNA primers used in qRT-PCR. Primers were selected to assay the state of cellular ECM synthesis and cell phenotype. Primer forward (F) and reverse (R) sequences and manufacturer information is presented.

Gene	Forward and reverse sequences	Manufacturer
αSMA	F: 5' – GAC AAT GGC TCT GGG CTC TGA AA – 3' R: 5' – ATG CCA TGT TCT ATC GGG TAC TT – 3'	Metabion Oligomer
CK7	F: 5' – CAT CGA CAT CGC CAC CTA CC – 3' R: 5' – TAT TCA CGG CTC CCA CTC CA – 3'	Metabion
CK8	F: 5' – CCA TGC CTC CAG CTA CAA AAC –3' R: 5' – AGC TGA GGT TTT ATT TTG GGA CC – 3'	Metabion
CK19	F: 5' – ACT ACA CGA CCA TCC AGG AC – 3' R: 5' – GTC GAT CTG CAG GAC AAT CC – 3'	Metabion
COL I	F: 5' – CCA GAA GAA CTG GTA CAT CAG CAA – 3' R: 5' – CGC CAT ACT CGA ACT GGA ATC – 3'	TAG Copenhagen A/S
COL III	F: 5' – CAG CGG TTC TCC AGG CAA GG – 3' R: 5' – CTC CAC TGA TCC CAG CAA TCC C – 3'	Oligomer
Elastin	F: 5' – GGT GCG GTG GTT CCT CAG CCT – 3' R: 5' – GGG CCT TGA GAT ACC CCA – 3'	Metabion
RPLP0	F: 5' – AAT CTC CAG GGG CAC CAT T – 3' R: 5' – CGC TGG CTC CCA CTT TGT – 3'	Oligomer
UPIA	F: 5' – GGC ATC TCC AGT TGT GGT GG – 3' R: 5' – GTC CTC CCA CCCTCT GTT TG – 3'	Metabion
UPIB	F: 5' – AGT CAC CAA AAC CTG GCA CAG – 3' R: 5' – TGA TGG ACC ATT TAC GCC ACA – 3'	Metabion
UPIII	F: 5' – TCA GTG CAA GAC ACC ACC AA – 3' R: 5' – GTC CTC CCA CCC TCT GTT TG – 3'	Metabion

For each measured gene, a standard was diluted with sterile water (B. Braun) to cDNA concentrations of 50 ng/µl, 5 ng/µl, 0.5 ng/µl, 0.05 ng/µl and 0.005 ng/µl to form the standard line. The cell type used to form the standard was selected to be a cell type most relevant for the studied gene. In Phase I, the hVSCs were used as a control for all studied genes. In Phase II, the hASCs were used as a control for RPLP0, COL I, COL III, αSMA, and elastin, and hUCs as a control for uroplakins and cytokeratins. Master mix solution contained Power SYBR Green PCR Master Mix (Thermo Fischer), 10 µM forward primer, 10 µM reverse primer and sterile water (B. Braun). The passive reference 6-carboxy-X-rhodamine (ROX) dye was used in the protocol to internally normalize the data during the reaction. For the qPCR run, 1 µl of standard and 2 µl of sample were pipetted with 14 µl master mix per well. The plastic covered measuring well plate was then run with ABI 7300 Real Time PCR System (Applied Biosystems, Thermo Fischer Scientific, USA). The used run had stages of 95 °C 10 min, 45 x (95 °C 15 s, 60 °C 1 min), 95 °C 15 s, 60 °C 1 min, 95 °C 15 s. Collected data was then normalized to the expression

of housekeeping gene RPLP0. Data was collected with software 7300 System Sequence Detection Software (version 1.4.1, Life Technologies Corporation, Carlsbad, CA, U.S.).

4.3.6 Scanning electron microscope imaging (II)

SEM imaging was performed for one cell line of hUC and hASC monocultures at d1, d7 and d14 time points. Samples were imaged with Scanning Electron Microscope Zeiss ULTRAplus (Zeiss, Oberkochen, Germany) at former Department of Materials Science, Tampere University of Technology (Figure 14).

On the time point, the samples were fixed with 5 % glutaraldehyde (Sigma Aldrich) in 0.1 M phosphate buffer (pH 7.4, Sigma Aldrich) for 48 hours in RT. After fixation, the scaffolds were rinsed with 1 x DPBS (Lonza) and stored in +4 °C in 1 x DPBS (Lonza) until further sample processing. The samples were dehydrated with ascending ethanol (EtOH) series and dried with hexamethyldisilane (HMDS) treatment prior to SEM imaging. Samples were incubated for 15 min at RT in ascending EtOH concentrations 50 %, 60 %, 70 %, 80 %, 90 % and 100 % EtOH. 100 % EtOH incubation was repeated once. After EtOH series, the samples were moved to 1:2 HMDS:100 % EtOH -solution for 20 min. The HMDS concentration was then raised to 2:1 HMDS:100 % EtOH -solution and incubated 20 min. Finally, samples were incubated twice in 100 % HMDS for 20 min before leaving all the HMDS to evaporate. Dried samples were sputtered with carbon coating. (https://research.jcu.edu.au/archive/enabling/aac/cairns-aac/biological-sample-preparation-for-the-sem, 04.12.2018)

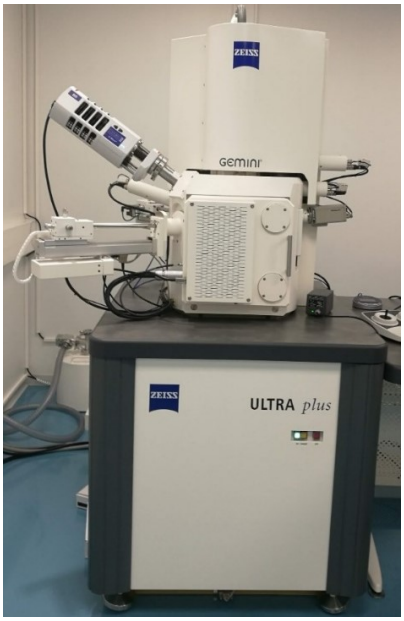

Figure 14 The SEM used for imaging hUC and hASC scPLCL monoculture samples.

4.3.7 Statistical analysis

The achieved quantitative results were analysed with IBM SPSS Statistics version 25 (IBM Corp., Armonk, NY, USA) to establish the statistical significance of the results. The quantitative data was analysed with Mann-Whitney test (two samples) or one-way ANOVA (three or more samples) with Bonferroni post-hoc test. Significance level of $p < 0.05$ was considered as significant and $p < 0.01$ as highly significant.

5 RESULTS

5.1 Phase I: hVSC seeded PLCL membranes

5.1.1 Viability and morphology of hVSCs

The viability of hVSCs on PLCL membranes was determined with Live/Dead® assay on d7 and d14 of cell culture. Live/Dead® staining demonstrates that majority of cells were viable (green fluorescence) cells in all tested materials (Figure 15) and hardly any dead cells (red fluorescence) were detected.

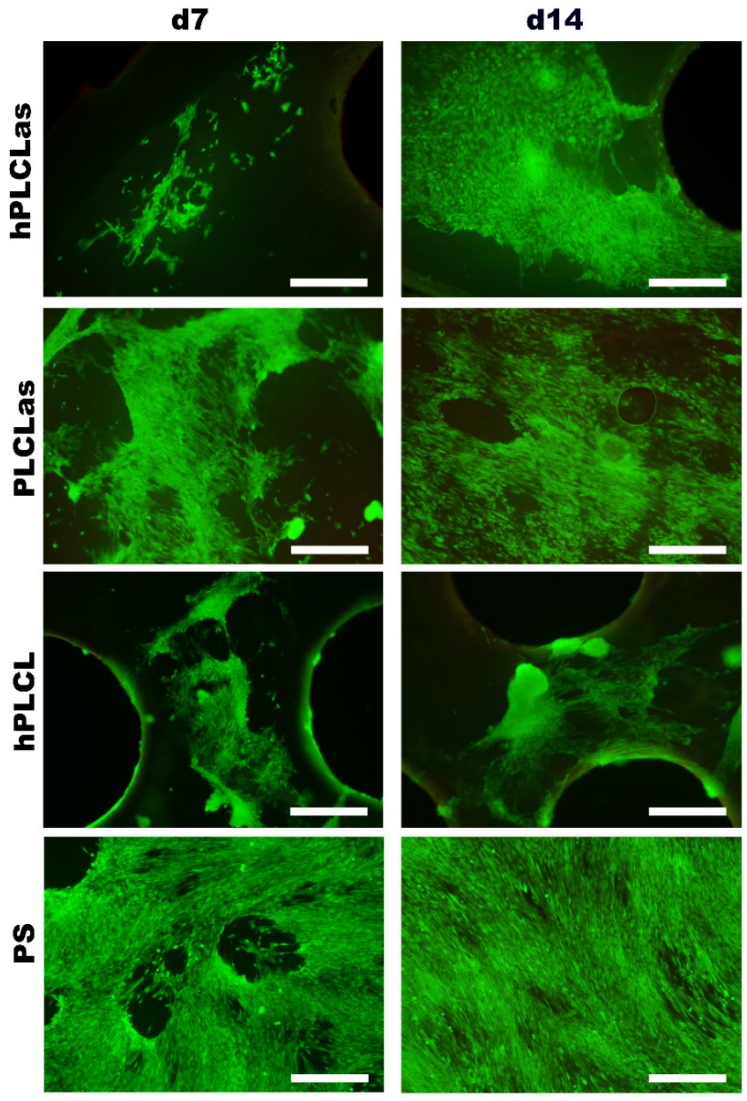

Figure 15 Human VSC Live/Dead® assay. Images of Live/Dead® viability assay performed on d7 and d14 for hVSCs cultured on hPLCLas, PLCLas, hPLCL and control PS. Viable cells are stained green and dead cells red. Some background stain visible from membranes. Scale bar 500 µm.

On PLCLas membranes, the cells mostly appear to form a uniform cell layer with very few cell clusters, and clusters further diminishing from d7 to d14. On plain hPLCL, the cells form cell clusters and small cell layers on both d7 and d14. According to the Live/Dead® staining, the morphology of hVSCs on hPLCLas and PLCLas on d14 seem similar to cells on PS. Human VSCs seem to be more elongated the denser they grow. However, some rounder cells can be seen in areas with sparser cell layer on all materials. Yet, the cell clusters formed on membranes cannot be seen on the PS at all. Qualitatively, the hVSC cell number seems to be higher on hPLCLas and PLCLas -membranes than on hPLCL.

5.1.2 Proliferation of hVSCs

The proliferation of hVSCs was evaluated with quantitative CyQUANT® assay on d1, d7 and d14 time points. The results were normalized to d1 PS samples. The relative DNA contents are presented in Figure 16.

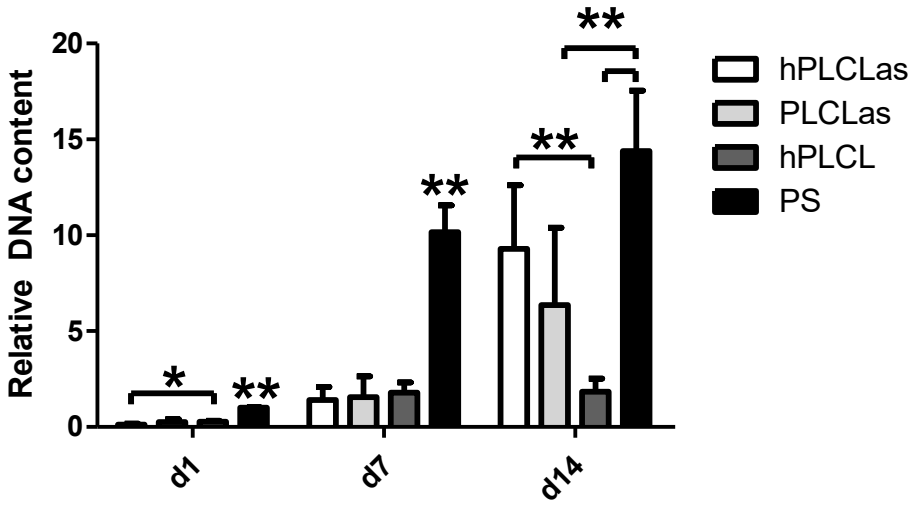

Figure 16 CyQUANT® proliferation assay of hVSCs. Relative DNA content of hVSCs membranes on d1, d7 and d14 of cell culture. * $p < 0.05$ ** $p < 0.01$. N = 6.

On d1, slightly significant difference ($p < 0.05$) in DNA content between hPLCLas and hPLCL is seen. However, DNA content on PS is significantly higher than on any of the biomaterials tested ($p < 0.001$ on d1 and d7, and no statistical differences is detected between biomaterial membranes on d7. On d14, DNA amount on PS is significantly higher than on PLCLas and hPLCL ($p < 0.01$), yet not higher than on hPLCLas ($p = 0.108$). Further, DNA content on d14 is significantly higher on hPLCLas than on hPLCL ($p = 0.008$). DNA amount significantly increased on hPLCLas and PLCLas between d7 and d14, $p < 0.001$ and $p = 0.011$ respectively, whereas no statistical difference could be detected on hPLCL. These proliferation assay results are in line with the qualitative results of viability assay.

5.1.3 Immunocytochemistry of hVSCs

The ICC staining was used to determine the level of hVSC collagen production and myofibroblast differentiation along with the capability to maintain the myofibroblast phenotype on d14 (Figure 17). Immunostaining of COL I was used to visualize the differences in collagen synthesis. The αSMA was used as a marker for determining the myofibroblast in hVSCs cultured on different biomaterials.

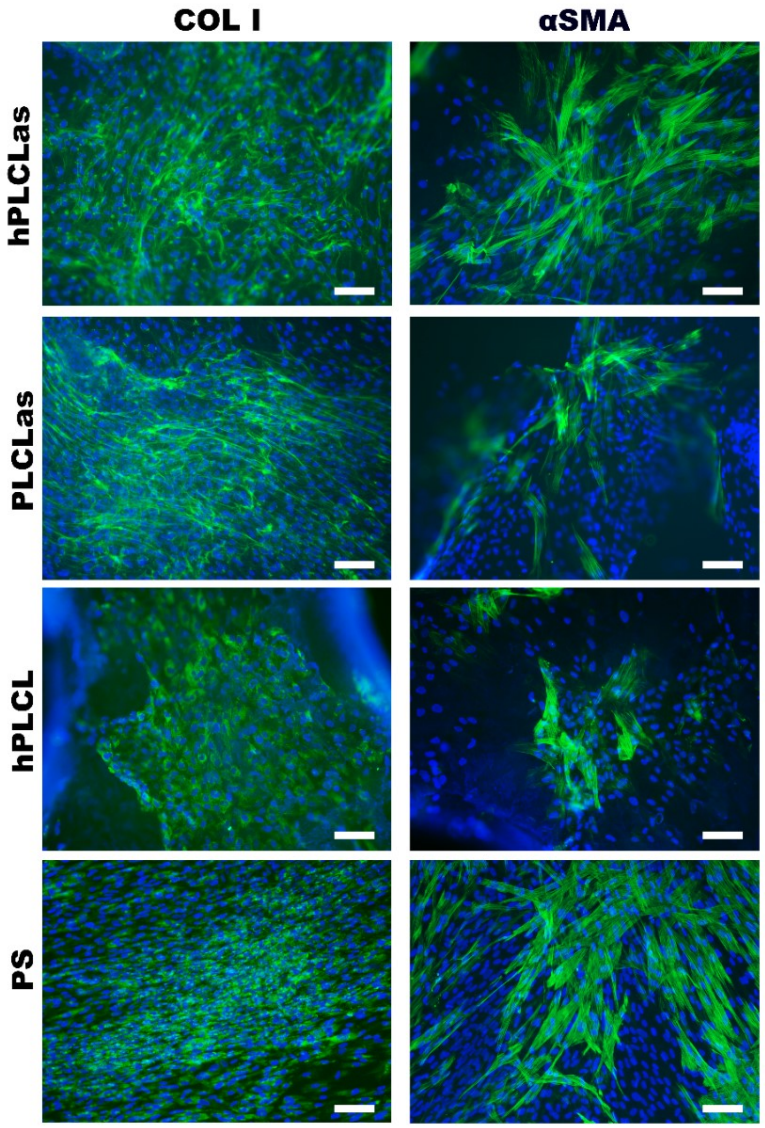

Figure 17 ICC of hVSCs. ICC stain of COL I and αSMA in hVSCs cultured on hPLCLas, PLCLas, hPLCL and PS samples on d14 of cell culture. Scale bar 200 µm.

COL I production appears to be enhanced in PLCLas and hPLCLas membranes compared to hPLCL and PS. According to immunostaining, the hVSCs cultured on hPLCLas and PLCLas membranes secrete COL I fibres outside the cells, forming fibre-rich areas to ECM. The excreted collagen fibres also seem align in some level, especially on PLCLas. Stained COL I

spots are also visible inside the cells, where the collagen is being modified and not secreted yet. In hPLCL sample, the COL I still remains inside the cells going through last-stage modifications before secretion. It is visible how the collagen fills the cell in small grains, but no secreted fibres are visible in ECM. Viability of hVSCs on hPLCL seem very similar to PS control, where the COL I is also inside the cells and not yet matured enough to be secreted. Thus, the collagen maturation and production appear to be increased on hPLCLas and PLCLas compared to PLCL and PS.

In αSMA immunostaining, the form of the actin fibres seems similar between the biomaterials and PS and no specific structural differences can be identified. Human VSCs on all materials maintained the myofibroblast phenotype. According to the qualitative assessment, the amount of αSMA on hPLCLas and PLCLas appears to be greater than on hPLCL, meaning more myofibroblasts are present. The amount of αSMA on hPLCLas seem very similar to PS.

5.1.4 Quantitative analysis of hVSC collagen production

The amount of total acid-soluble and pepsin-soluble collagen was quantified with Sircol™ Soluble Collagen Assay after 14 days of cell culture. The Figure 18 shows the total collagen concentrations in samples (µg/ml).

The amount of produced collagen was significantly higher on hPLCLas and PS than on hPLCL ($p < 0.01$). No statistical significance was detected between PLCLas and hPLCL. However, when statistically analysing only the biomaterials and not taking PS into account, both hPLCLas and PLCLas had higher collagen amounts than hPLCL ($p < 0.01$).

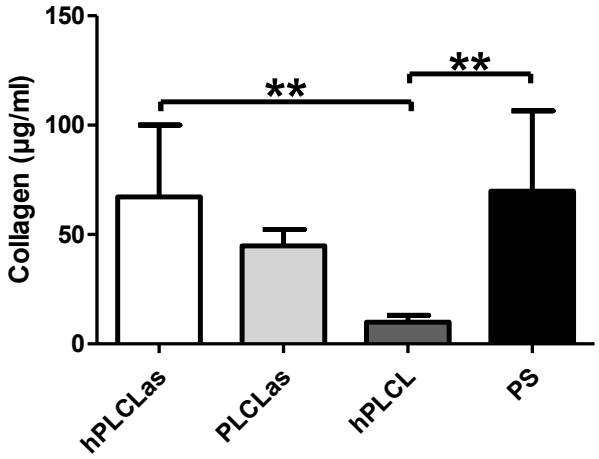

Figure 18 Total amount of acid soluble and pepsin soluble collagen on d14 produced by hVSCs cultured on hPLCLas, PLCLas, hPLCL and PS materials. ** = $p < 0.01$. N = 6.

5.1.5 Gene expression of hVSCs

The relative gene expression of αSMA, COL I, COL III and elastin was evaluated on d14 with qRT-PCR. Results are first normalized to sample's parallel RPLP0 result, which is then further normalized to PS control result individually inside each donor's samples to achieve the relative expression compared to PS control. Averages of relative expression of the three donors' samples are presented in Figure 19. Statistical analysis was not performed as the sample size N = 3 is too small for reliable statistical analysis. Nevertheless, the results show some reference to differences in gene expression between the materials.

The relative expression of αSMA seems to be increased on AAD membranes compared to hPLCL but stay still under the level of PS control. Further, the relative expression of COL I and COL III seems to be increased on AAD membranes, even over the level of PS. This is in line with the results of Sircol™ and ICC results. The deviations in elastin results are quite large, but still it seems like the elastin expression is higher on biomaterials than on PS control. The results display increased elastin expression especially on holed membranes hPLCLas and hPLCL.

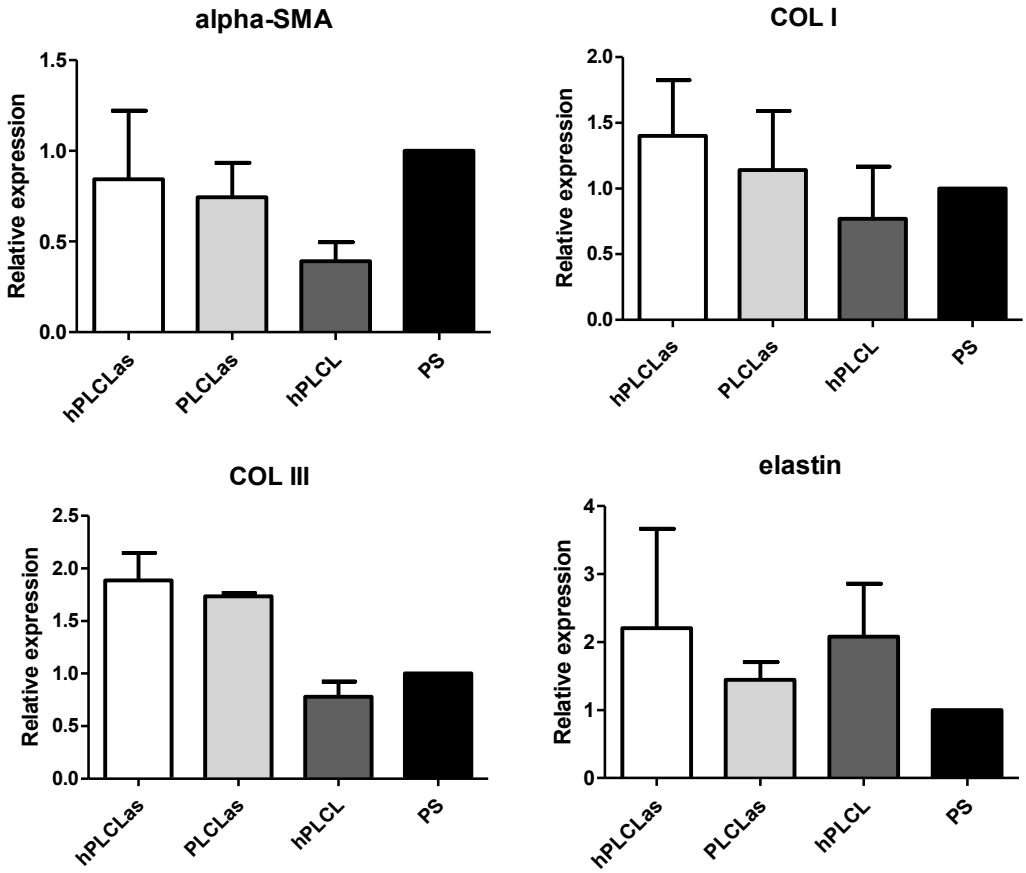

Figure 19 qRT-PCR results of hVSC culture. Relative gene expression of αSMA, COL I, COL III and elastin in hVSCs cultured on hPLCLas-, PLCLas-, hPLCL- membranes and PS control. N = 3.

5.1 Phase II: hUC monoculture on scPLCL scaffolds

5.1.1 The hUC monoculture SEM imaging

The attachment and morphology of hUCs were evaluated with SEM imaging on d1, d7 and d14 of cell culture. 125 times magnification images from all time points and 500 times magnification images on d14 time points are shown in Figure 20.

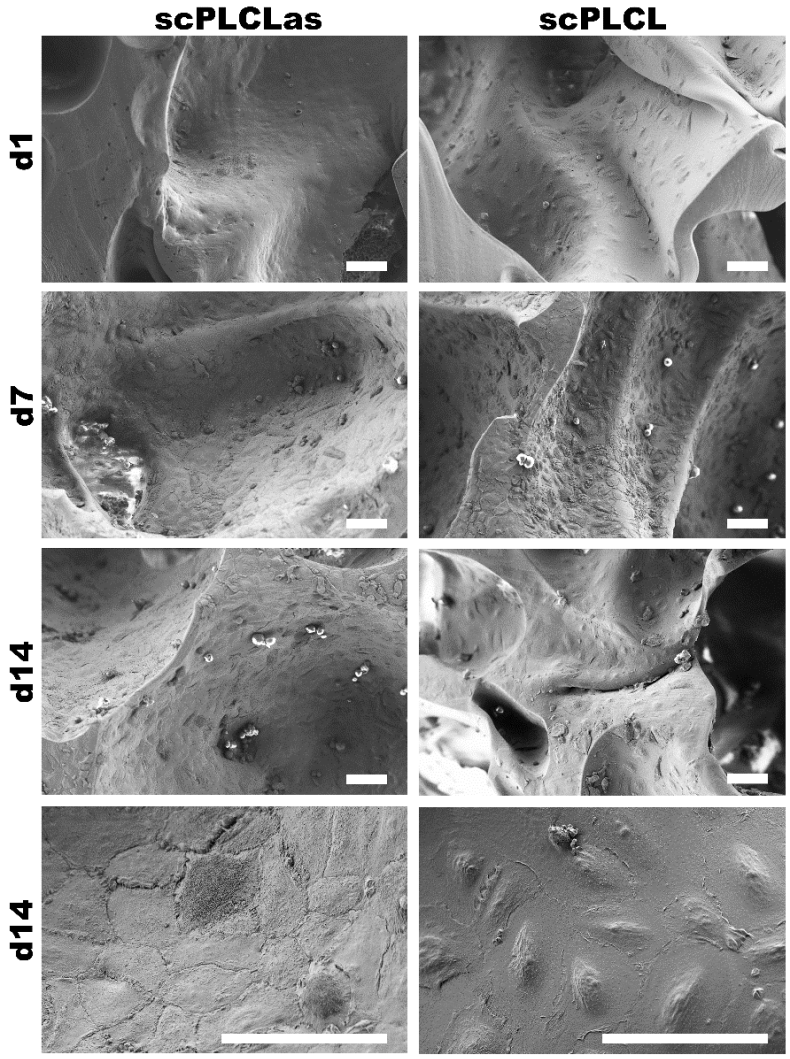

Figure 20 SEM images of hUC monoculture on scPLCLas and scPLCL scaffolds. 125x magnifications from time points d1, d7 and d14 are presented with single 500x magnification images from d14. Scale bar 100 µm.

Cell attachment and morphology on d1 seems similar and well attached on both biomaterials and no striking difference can be seen. The cells are sparse but flattened along the material, preferring the pores of the scaffolds, as also seen in Live/Dead® assay. On d7 the cell number has increased considerably on both studied materials and the material surface seems to be

covered with cells. On scPLCLas, the hUCs surface seem smoother than on scPLCL. Whereas, the cell borders on scPLCL are more evident compared to scPLCL and the individual cells are easily distinguished at d7 and d14 time points. Further, small vesicles can be seen on the cell borders of the scPLCL.

On d14, both biomaterial surfaces are covered with hUCs. When qualitatively evaluated, the cell number in scPLCLas appears higher than on scPLCL. In higher magnification, the hUCs on both scaffolds are cuboidal and flattened representing the morphology of urothelial cells and especially on scPLCLas, the hUCs have highly apparent cell borders. On scPLCL hUCs seem flattened with visible nuclei. In Live/Dead® this difference could not be distinguished. Some round hUCs can be seen on both materials in all time points.

5.1.2 Viability and morphology of hUCs in monoculture

The viability of hUC monocultures on scPLCLas and scPLCL scaffolds was determined with Live/Dead® assay on d1, d7 and d14 of cell culture. Human UCs remained viable on both biomaterials. Qualitatively, the hUCs appeared to increase the cell number during the assessment period. No striking differences in cell number cannot be seen between the biomaterials with qualitatively inspection, and hardly any dead cells were visible (Figure 21).

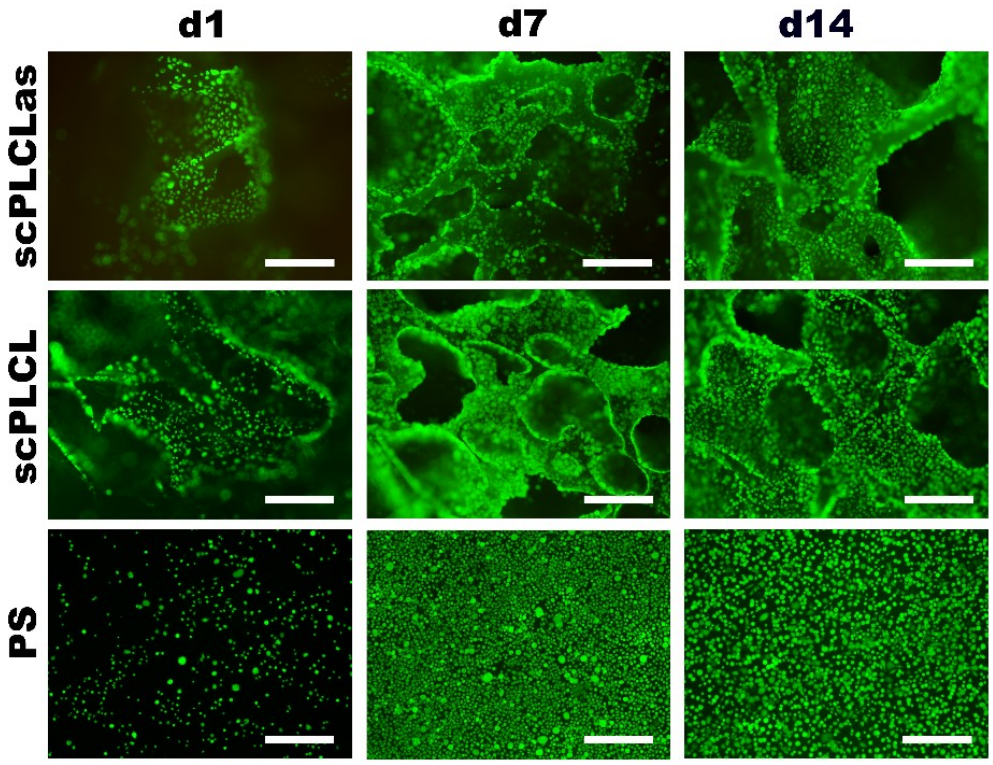

Figure 21 Live/Dead® assay of hUCs in monoculture on scPLCLas, scPLCL scaffolds and PS control on time points d1, d7 and d14 of cell culture. Scale bar 500 µm.

The hUCs preferred to grow in the scaffold pores on both biomaterials as visible in d1 images. However, the cells also seem to spread and grow on the smooth areas of the scaffolds. Based on qualitative evaluation, the cell amount seems to increase during the cell culture. On PS control, the cells are roundish, whereas on the scaffolds hUCs seem to possess more epithelial-like cuboidal morphology. Differences in hUC morphology between scPLCLas and scPLCL are not so evident. On scPLCLas the hUCs seem more elongated along the material surface on d14 with some cobblestone structure typical for epithelium. Whereas on scPLCL, the cells seem smaller and rounder with somewhat irregular appearance on d7 and d14.

5.1.3 Cell proliferation in hUC monocultures

The relative DNA content of hUCs was assessed with CyQUANT® on d1, d7 and d14 of cell culture time points with CyQUANT® assay. The results presented in Figure 22 are relative to scPLCL d1 DNA amounts.

The DNA amount was significantly higher on scPLCL samples than scPLCLas in every time point. The difference was highly significant on d1 and d7 ($p < 0.001$) and significant on d14 ($p < 0.05$). No statistical difference in hUC DNA content between time points on scPLCLas could be detected. On scPLCL no significant difference was detected between d7 and d14, but between d1 and d14, DNA content had significantly increased ($p < 0.001$). The AAD seems to cause hUC proliferation to decrease compared to plain scPLCL.

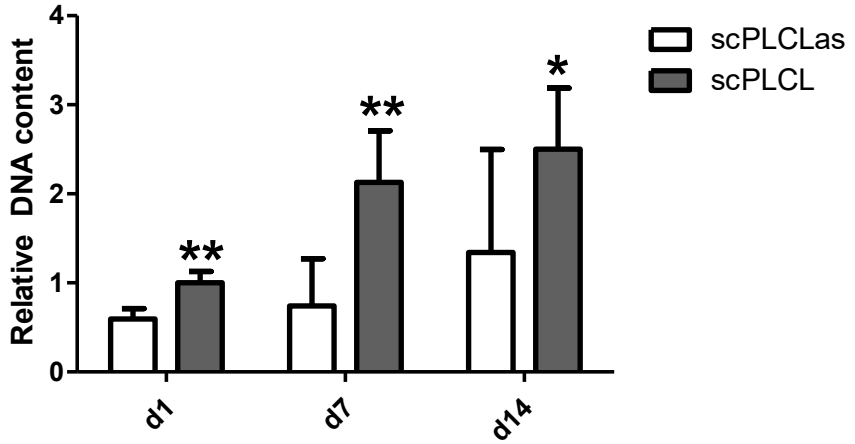

Figure 22 CyQUANT® proliferation assay of hUC monoculture. The DNA amounts of hUC monocultures on scPLCLas and scPLCL relative to d1 scPLCL sample were quantified on d1, d7 and d14 of cell culture. * = $p < 0.05$, ** = $p < 0.01$, N = 9.

5.1.4 Collagen production of hUCs in monoculture

The total amount of produced acid-soluble and pepsin-soluble collagen in hUC monoculture was determined with quantitative Sircol™ collagen assay on d14 time point. Sircol™ assay results are displayed in Figure 23. The amount of produced collagen was significantly higher on scPLCL samples than on scPLCLas ($p < 0.01$).

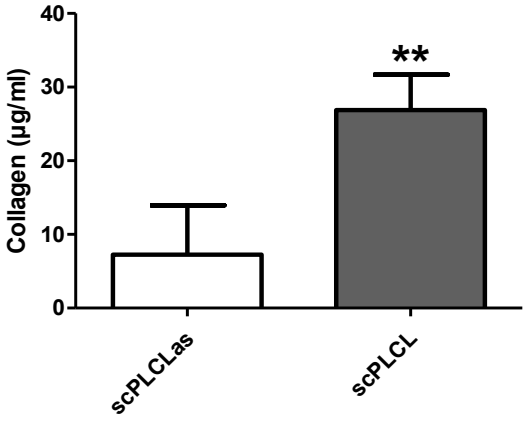

Figure 23 Sircol™ assay results of hUC monoculture. Total amount of acid-soluble and pepsin-soluble collagen in hUC monocultures on scPLCLas and scPLCL scaffolds was measured on d14 time point. ** = $p < 0.01$, N = 9.

5.1.5 Gene expression of hUCs in monoculture

Relative gene expression of urothelial markers CK7, CK8, CK19, UPK1A, UPK1B and UPK3 was quantified with qRT-PCR. Results from tested genes were normalized to sample's parallel RPLP0 result and further to hUCs cultured on PS individually for each donor's cells to achieve the relative expression to samples cultured on PS control. Statistical analysis was not performed as the sample size N = 3 is too small for reliable statistical analysis. Nevertheless, the results can display some tendency of differences in gene expression between samples (Figure 24).

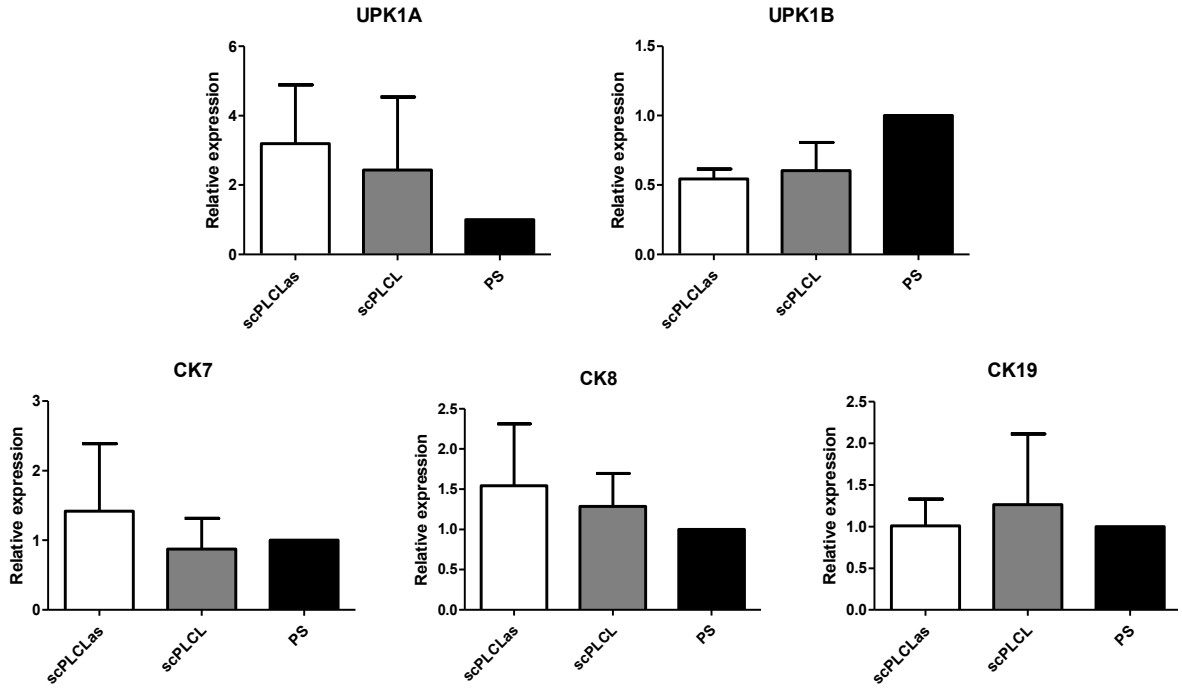

Figure 24 Relative gene expression of CK7, CK8, CK19, UPK1A, UPK1B and UPK3 of hUCs in monoculture on scPLCLas, scPLCL -scaffolds and PS control was determined on d14 time point. N = 3.

The amount of UPKIII was not detected reliably and thus excluded from the results. The standard deviations are large, and no exact conclusions can be made from the results. However, it seems like the CK 7 and CK8 expression is increased on scPLCLas scaffold compared to scPLCL and PS. Also, the relative expression of UPK1A seems to be higher on scPLCLas and scPLCL scaffolds than on PS control. Further, the expression of UPK1B seems decreased on scPLCLas and scPLCL scaffolds compared to PS. No apparent difference between materials is seen in the expression of CK19.

5.2 Phase II: hASC monoculture on scPLCL scaffolds

5.2.1 The SEM imaging of hASC monoculture

The attachment and morphology of hASCs on scPLCLas and scPLCL -scaffolds were evaluated with SEM imaging on d1, d7 and d14. 125 times magnification from each time point is presented in Figure 25 along with single higher 500 times magnification on d14.

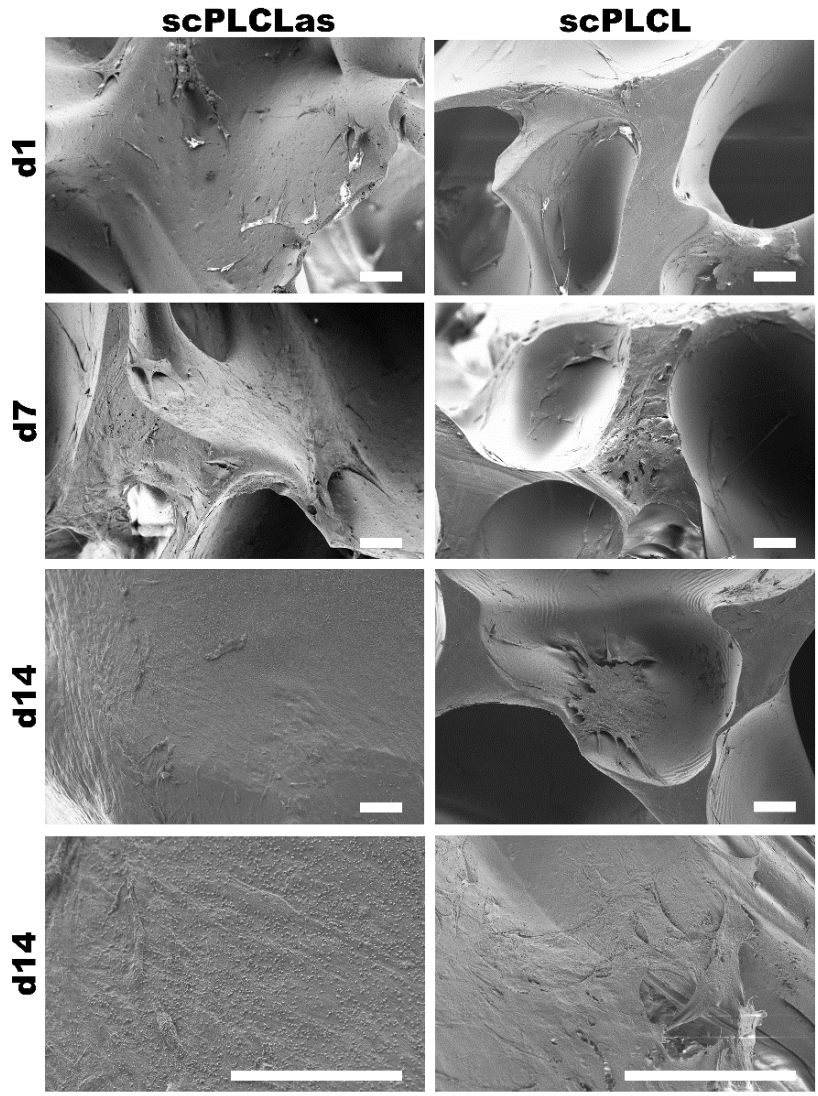

Figure 25 SEM images of hASC monocultures. SEM imaging was performed for hASC monocultures on scPLCLas and scPLCL scaffolds on d1, d7 and d14. 125x magnifications are presented from time points d1, d7 and d14, with additional 500x magnification image from d14 from both materials. Scale bar 100 µm.

On d1, the cells are attached both in pores and smooth scaffold surfaces on both materials and no striking difference in hASC number can be seen. Qualitatively on d7, there seems to be considerably greater amount of hASCs on scPLCLas, where the cells seem begin forming a dense cell sheet, whereas on scPLCL some small cell sheets along with cell clusters can be seen. On d14, the whole surface on scPLCLas is covered with hASC sheet. The sheet is smooth and covers the scaffold pores of the material. Some outlines of the pores can be seen underneath the cell sheet. On scPLCL, the cells seem to form loosely attached smaller sheets, but not as covering as in scPLCLas. Some larger cell clusters can also be seen apart from the cell sheets. In 500 times magnification on d14, the difference between scPLCLas and scPLCL is apparent.

Dense cell sheet is only visible on scPLCLas, yet on scPLCL loosely attached small cell sheets and dense clustered cell regions can be detected.

5.2.2 Viability and morphology of hASCs in monoculture

Viability of hASCs in monoculture on scPLCLas and scPLCL scaffolds was determined with Live/Dead® assay on time points d1, d7 and d14 of cell culture, PS served as a control. Majority of the hASCs remain viable on all materials (Figure 26).

Although hASCs remain viable on all materials and no individual dead cells are visible, striking difference in hASC attachment and morphology can be seen between scPLCLas and scPLCL. Qualitatively inspecting, the cell number keeps increasing on scPLCLas from d1 to d14, forming dense cell sheet over the material, covering the scaffold pores. The increase in cell number between d1 and d7 is highly noticeable. hASCs on scPLCLas seem to have the same morphology as on the PS, but the cells seem to grow more densely.

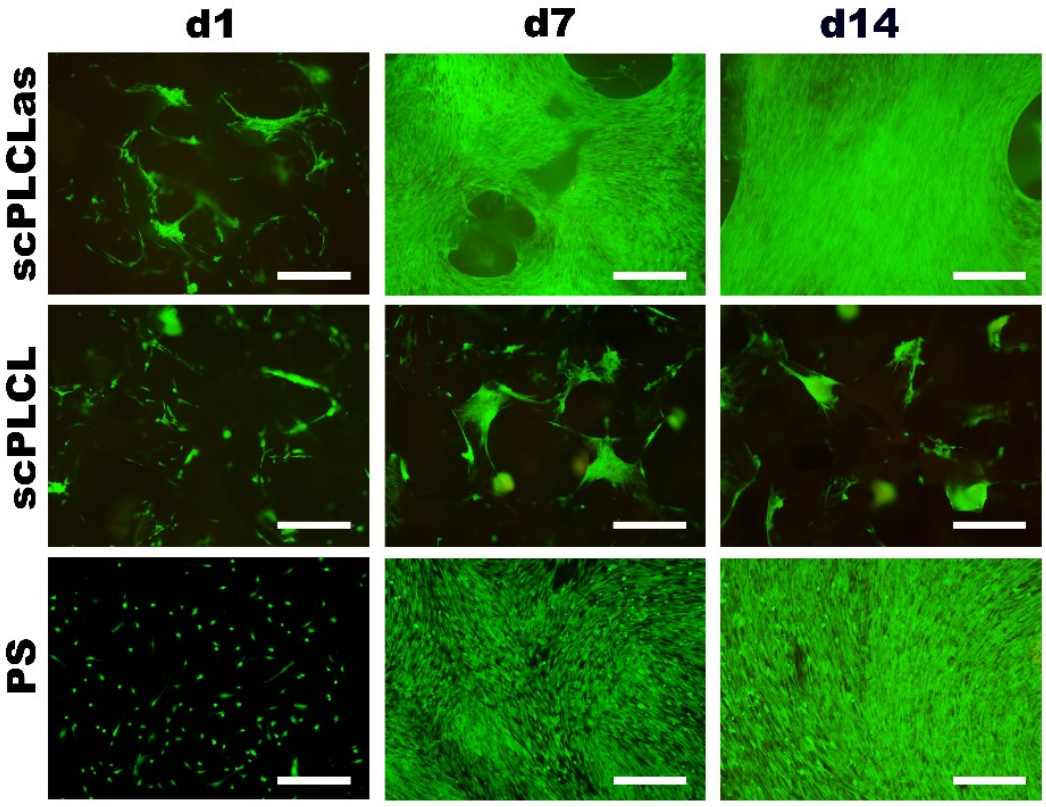

Figure 26 Viability assay images of hASC monoculture. Live/Dead® assay of hASCs in monoculture on scPLCLas, scPLCL scaffolds and PS control on time points d1, d7 and d14 of cell culture. Scale bar 500 µm.

On scPLCL, the cells form clusters and there seems to be some dead cells in the middle of the clusters, since the red hue is seen through the green surface of the hASC clusters. However, the surrounding cells in the clusters are viable. The clusters do not seem to change in appearance between d7 and d14. Morphology of hASCs on scPLCL are very different from the hASCs on PS or scPLCLas.

5.2.3 Cell proliferation of hASCs in monoculture

The proliferation of hASCs in monocultures on scPLCLas and scPLCL scaffolds was assayed with quantification of relative DNA amount with CyQUANT® assay on time points d1, d7 and d14. Results are relative to hASC DNA amount on d1 on scPLCL. Normalized results are presented in Figure 27.

On d1 the DNA contents were similar on both biomaterials and no significant difference was detected. The DNA content was significantly higher ($p < 0.01$) on scPLCLas scaffold on d7 and d14 compared to scPLCL. On scPLCL the DNA amount increased between the d1 and d7 ($p < 0.001$) and d7 and d14 ($p = 0.021$). However, DNA content remained stable on scPLCL and no significant difference was visible between d1 and d7 ($p = 0.180$) or d7 and d14 ($p = 0.962$). Thus, the AAD in scPLCLas increased proliferation rate of hASCs.

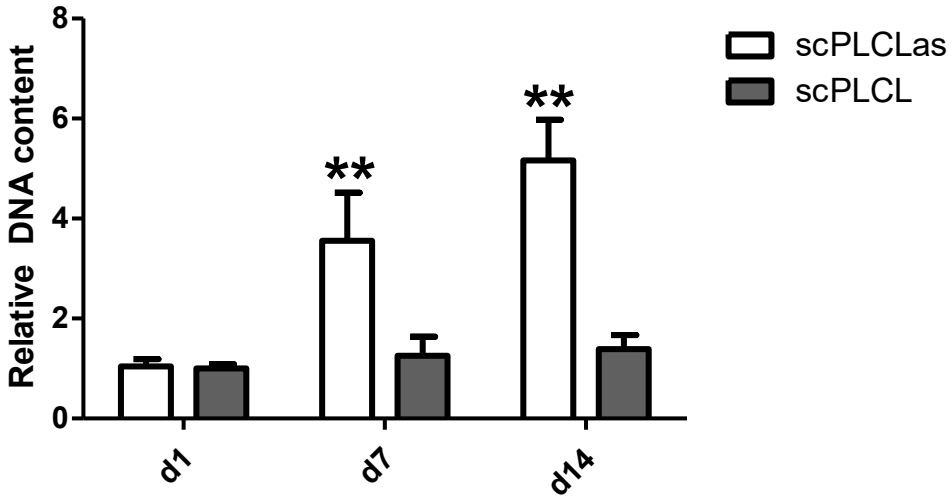

Figure 27 Relative DNA amounts of hASC monocultures. The DNA amounts of hASC monocultures on scPLCLas and scPLCL relative to d1 scPLCL sample were quantified on d1, d7 and d14 of cell culture. * = $p < 0.05$, ** = $p < 0.01$. N = 9.

5.2.4 Collagen production in hASC monoculture

The amount of hASC synthetized acid-soluble and pepsin-soluble collagen was measured with Sircol™ collagen assay on d14 on scPLCLas and scPLCL -scaffolds (Figure 28). The total amount of quantified acid-soluble and pepsin-soluble collagen in hASC monocultures was significantly higher ($p < 0.01$) scPLCLas scaffolds than on plain scPLCL.

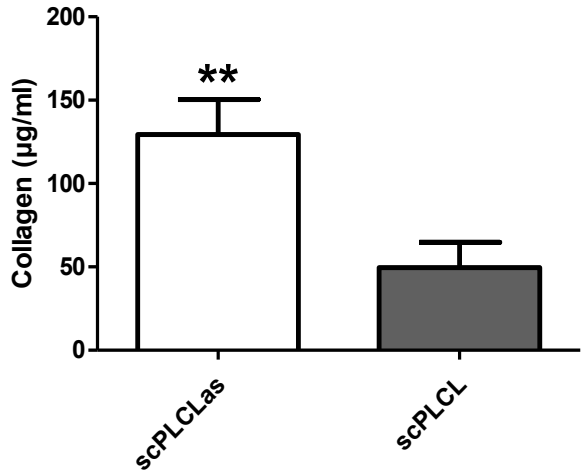

Figure 28 Sircol™ assay of hASC monoculture. Total acid-soluble and pepsin-soluble collagen amount of hASC monocultures on scPLCLas and scPLCL scaffolds measured on d14 time point, ** = $p < 0.01$. N = 9.

5.2.5 Relative gene expression in hASC monocultures

The relative gene expression of αSMA, COL I, COL III and elastin of hASC monocultures on scPLCLas and scPLCL was quantified on d14 with qRT-PCR. Results from tested genes were normalized to sample's parallel RPLP0 result and further to hASCs cultured on PS individually for each donor's cells to achieve the relative expression to samples cultured on PS control. Statistical analysis was not performed as the sample size N = 3 is too small for reliable statistical analysis. Nevertheless, the results can display some degree of differences in gene expression between samples (Figure 29).

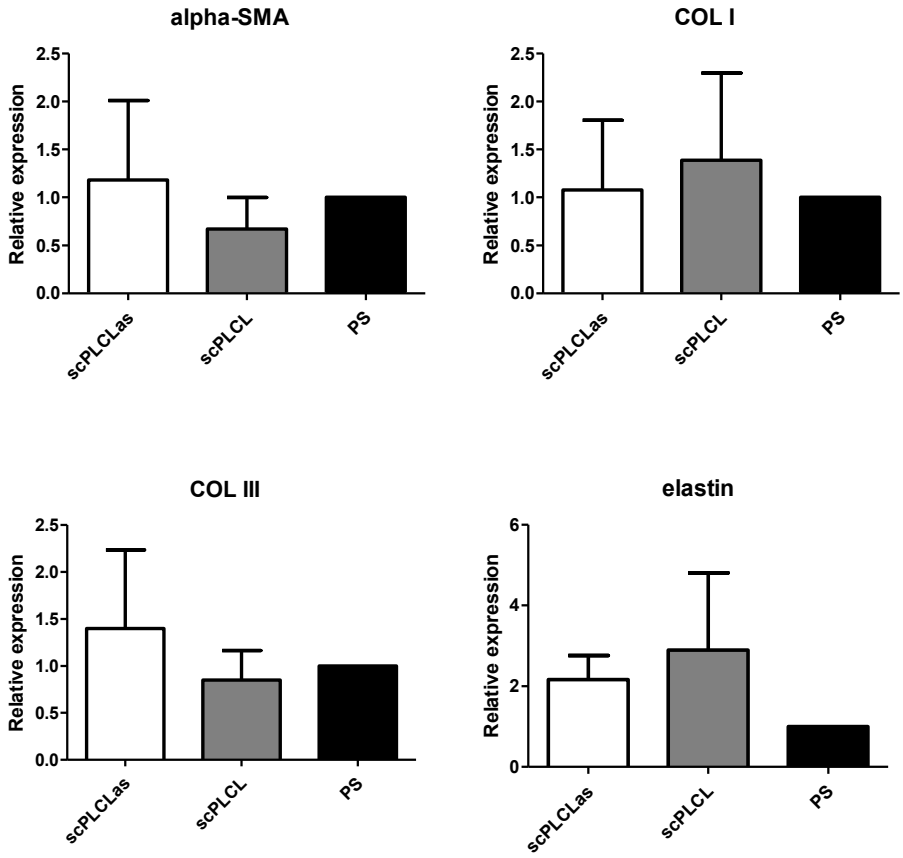

Figure 29 Relative gene expression of αSMA, COL I, COL III and elastin of hASC monocultures cultured on scPLCLas and scPLCL -scaffolds, quantified on d14 of cell culture. Results are normalized to PS results. N = 3.

The donor cell lines were very varying in their gene expression and thus the standard deviations are large. The expression of αSMA seems to be increased in scPLCLas scaffold compared to scPLCL, in which the expression seems decreased compared to PS control. No clear difference can be stated in relative expression of COL I. However, the expression of COL III seems increased on scPLCLas compared to scPLCL and PS. Relative expression of elastin seems higher on biomaterials than PS control, being higher on scPLCL than scPLCLas.

5.3 Phase II: Medium optimization for hUC/hASC co-culture on scPLCL scaffolds

5.3.1 Viability and morphology of hUCs and hASCs

The viability of the hUCs and hASCs were determined with Live/Dead® staining on d7 and d14 time points. The contents of tested mediums are presented in Table 4. Medium A is the basic culture medium for hASCs, and B basic culture medium for hUCs, whereas mediums C, D and E are different combinations of these two.

The viability of hUCs was good in medium compositions B, C and D, but in mediums A and E, the cells were quite sparse, however, no dead cells are visible in any culture medium condition (Figure 30). The hUCs cell number does not seem to qualitatively increase in mediums A and E, the two mediums both with added HS. Mediums B, C and D all have more present hUCs than A and E mediums. However, although the hUCs are viable and proliferating in mediums C and D, the hUC morphology does not resemble the morphology of hUCs in basic medium composition B. Some hUCs in B and D seem to swell and grow larger over cells attached to well bottom.

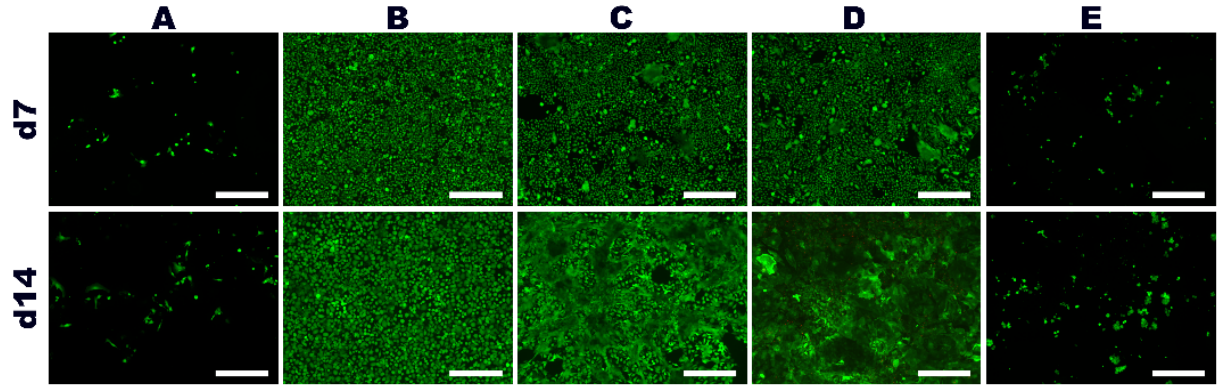

Figure 30 Images from Live/Dead® viability assay performed on d7 and d14 time points for hUC cultured on five different cell culture medium conditions. A being the basic medium for hASCs and B the basic medium for hUCs. Rest mediums are combinations of A and B mediums. Detailed components are presented in Table 4. Green cells represent viable cells and red dead cells. Scale bar 500 µm.

The hASCs remained viable in all medium compositions, but great variety in cell number can be seen (Figure 31). No dead cells are visible in any medium compositions. The basic hASC medium is the composition A, where the cell number seems to increase between d7 and d14. Whereas in mediums B, C and D the cell number seems not to increase noticeably when qualitatively inspecting. In medium composition A, the basic hASC culture medium, cells grow densely elongated. The hASC morphology in B, C and D mediums seem elongated, but cells are sparse. In medium E, the hASCs seem to grow densely but seem larger than in basic medium.

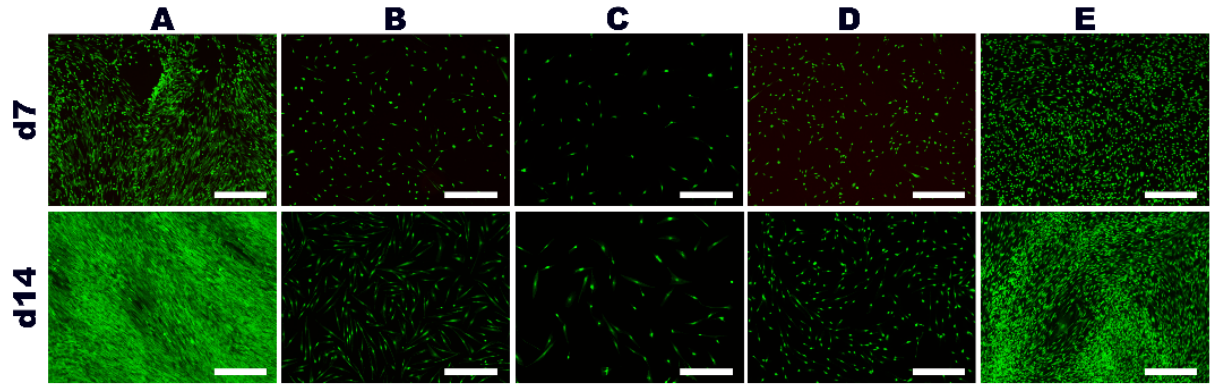

Figure 31 Images from Live/Dead® viability assay performed on d7 and d14 time points for hASCs cultured on five different cell culture medium conditions. A being the basic medium for hASCs and B the basic medium for hUCs. Rest of the mediums are combinations of A and Bs. Detailed components are presented in Table 4. Green cells represent viable cells and red dead cells. Scale bar 500 µm.

As seen in Figures 30 and 31, hUCs and hASCs preferred opposite mediums, yet they remained viable in all medium conditions. However, there is differences is cell morphologies even when the cells seem to proliferate.

5.3.2 The immunostaining of hUC cytokeratin structure

Immunostaining of pan-cytokeratin [AE1/AE3] was performed on hUCs cultured in five different medium compositions (Table 4) on d14 time point, to assess changes in cytokeratin cytoskeleton structure (Figure 32). Medium B is the basic culture medium for hUCs, and A basic culture medium for hASCs, whereas mediums C, D and E are different combinations of these two.

Human UCs in medium B, the basic hUC culture medium, present the normal hUC cytokeratin structure and the morphology of cells is normal to hUCs. The hUCs seem to be noticeably larger in presence of HS, as seen in the medium compositions A and E. In A (5 % HS), hUCs are large and individual keratins are visible. In E (1 % HS), hUCs are large and the keratin staining slightly resembles hUCs in B. However, the hUCs are abnormally large and grow clustered. In the mediums C and D, the cell borders are not detectable, and no individual cells can be distinguished. In majority of the cells in medium C, the pan-cytokeratin signal is not very intense and there are some small brightly stained hUCs among the cells. Qualitatively analysing the number of DAPI-stained nuclei, the cell amount seems to be higher in the medium composition C. Apart from medium B, the hUCs in do not resemble the typical cuboidal hUC morphology in any of the experimented medium compositions.

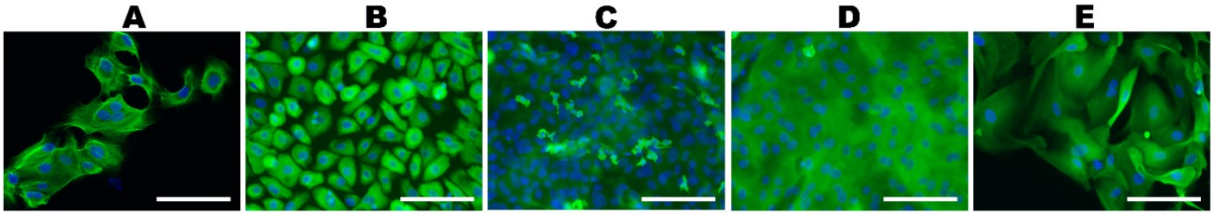

Figure 32 Immunofluorescence images of hUCs cultured in five different medium compositions A-E. A being the basic medium for hASCs and B the basic medium for hUCs. Rest of the mediums are combinations of A and B. Detailed components are presented in Table 4. Pan-cytokeratin [AE1/AE3] marker (green) was used to stain the hUC cytokeratin structure. DAPI was used for nuclei staining (blue). Scale bar 100 µm.

5.3.3 Cell proliferation of hUCs and hASCs

Relative DNA content of hASCs and hUCs cultured in five different medium compositions (Table 4) was evaluated with CyQUANT® assay on d1, d7 and d14. Medium A is the basic culture medium for hASCs, and B basic culture medium for hUCs, whereas mediums C, D and E are different combinations of these two basic mediums. No statistical analysis was performed, because the sample size of N = 3 is too small for reliable statistical testing. The relative DNA contents of hUCs presented in Figure 33 are normalized to d1 hUCs samples cultured in medium B.

The hUCs proliferated most in medium compositions B, C and D, and least in mediums A and E, as also seen in viability assay and in ICC staining. In medium A (5 % HS) the DNA amount seems to decrease during the assessment period, whereas in medium E (1 % HS) the cell number seems to remain steady. In absence of HS in mediums B, C and D, the cells proliferate rapidly in 7 days, but only slight increase is seen between d7 and d14.

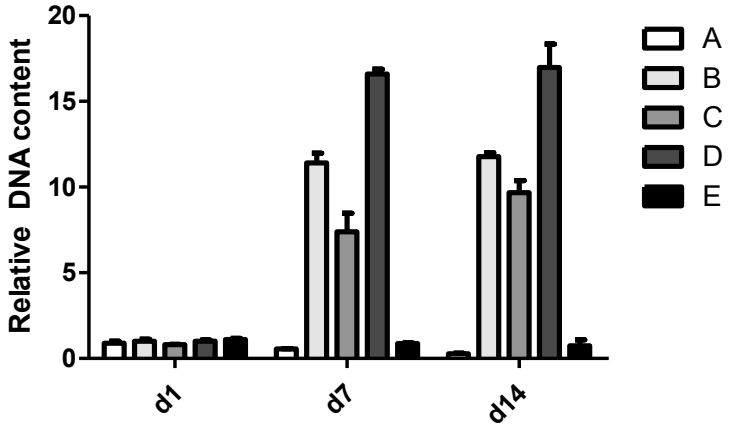

Figure 33 Proliferation assay results of hUCs in medium testing. The relative DNA amount of hUCs cultured on five different medium compositions was quantified with CyQUANT® assay on d1, d7 and d14 of cell culture. N = 3.

The proliferation results were the very opposite for hASCs, where the hASCs were not proliferating in absence of HS. The relative DNA contents of hASCs presented in Figure 34 are normalized to d1 hASCs samples cultured in medium A.

Human ASCs rapidly proliferate in mediums A and E between d1 and d7, and further slightly increase by d14. In mediums B and D, the DNA amount seems to increase slightly between d1 and d7 and remain steady through to d14. In medium composition C, the hASC number does not change at all during the whole assessment period.

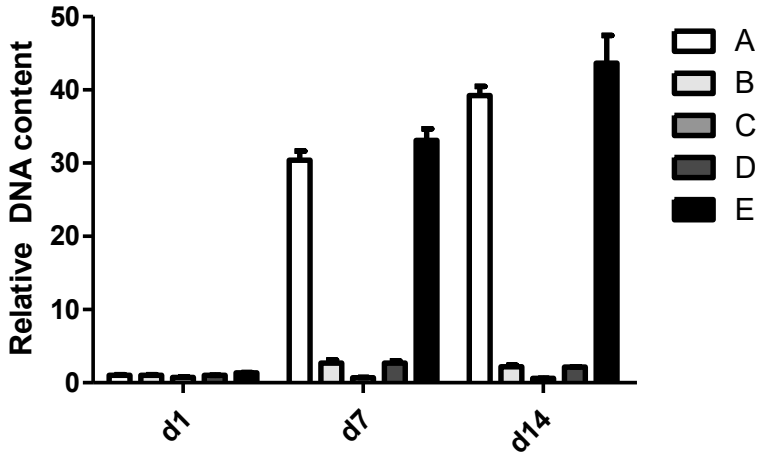

Figure 34 Proliferation assay results of hASCs in medium testing. The relative DNA amount of hASCs cultured on five different medium compositions was quantified with CyQUANT® assay on d1, d7 and d14 of cell culture. N = 3.

When considering the cell proliferation and viability results, medium composition B, the basic hUC culture medium, was selected to be used in further studies of hUC/hASC co-cultures.

5.4 Phase II: hUC/hASC co-culture on scPLCL scaffolds

5.4.1 Viability of cells in hUC/hASC co-culture

Live/Dead® assay was performed for hUC/hASC co-cultures on scPLCLas and scPLCL scaffolds on d1, d7 and d14 time points to assess the viability of the hUCs and hASCs in co-culture. The hASCs remained viable throughout the study on scPLCLas but formed cell clusters on scPLCL with visible dead cells, further diminishing towards d14 of co-culture (Figure 35). Even cell sheet of hASCs is visible on scPLCLas scaffold, but it is not spreading as robustly as seen in hASC monoculture (Figure 26).

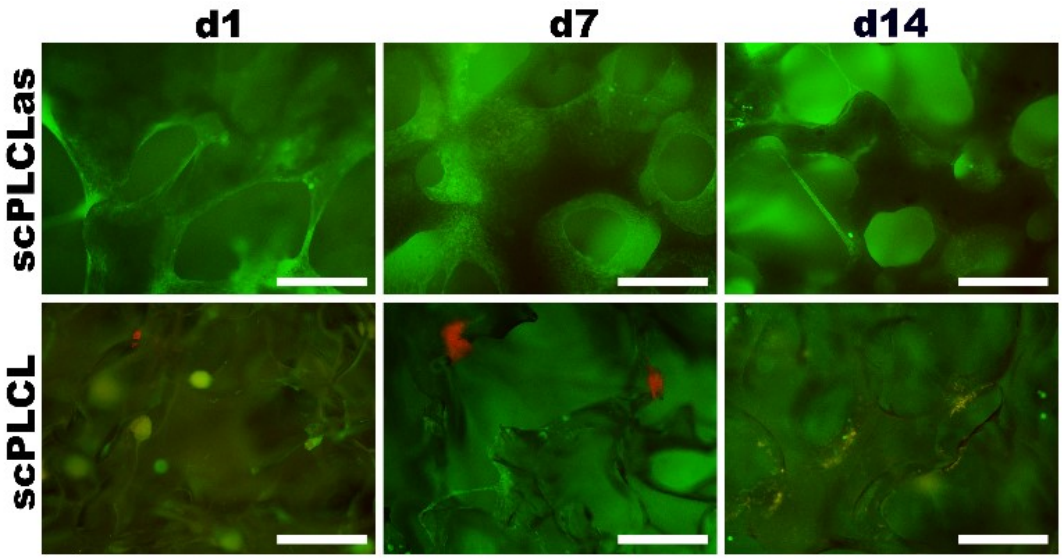

Figure 35 Live/Dead® results of hASCs in co-culture. Viability of hASCs cultured in hUC/hASC co-culture on scPLCLas and scPLCL scaffolds was assayed on time points d1, d7 and d14. Scale bar 500 µm.

Human UCs remained viable throughout the study and seemed to increase cell number on both scPLCLas and scPLCL scaffolds when qualitatively inspecting (Figure 36). No dead cells are visible in any of the samples and the cells seem to prefer growing inside the pores of the scaffold in both biomaterials.

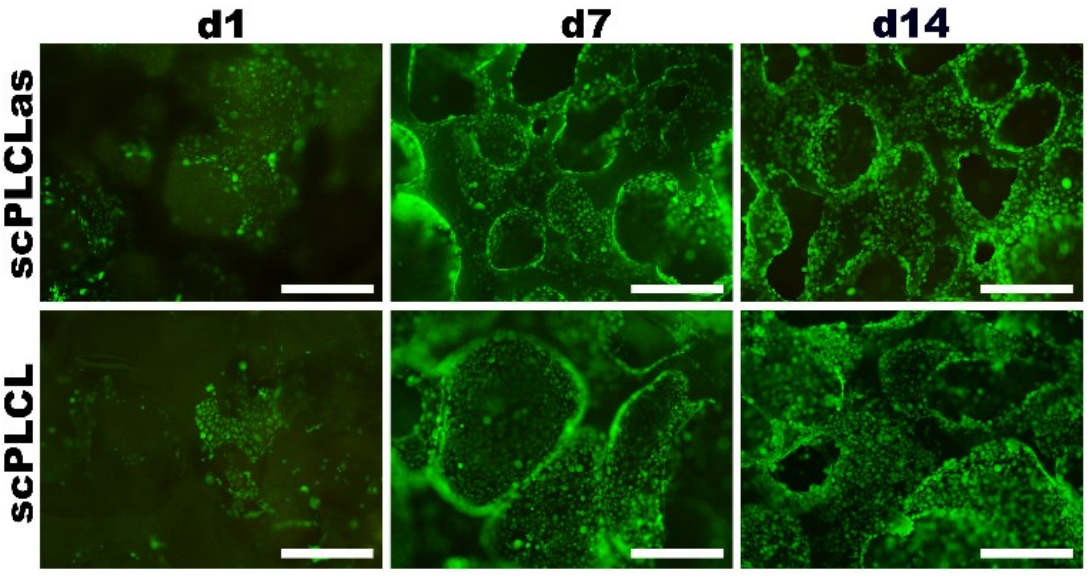

Figure 36 Live/Dead® results of hUCs in co-culture. Viability of hUCs cultured in hUC/hASC co-culture on scPLCLas and scPLCL scaffolds was assayed on time points d1, d7 and d14. Scale bar 500 µm.

Both hASCs and hUCs remained viable in co-culture during the assessment period of 14 days. Human ASCs maintained viable better on scPLCLas scaffold, whereas no difference can be assessed in hUC viability by qualitative inspection.

5.4.2 The immunostaining on hUC/hASC co-cultures

ICC was performed for hUC/hASC co-cultures on scPLCLas and scPLCL scaffolds to determine the cell phenotype maintenance and hUC maturation on d14 time point. Immunostaining was conducted with two co-stainings. Co-staining of immunomarkers αSMA and UPK3A was performed to determine the myogenic capability of hASCs, and late maturation of hUCs, respectively. The immunostaining of αSMA and UPK3A of hASCs in co-culture is presented in Figure 37.

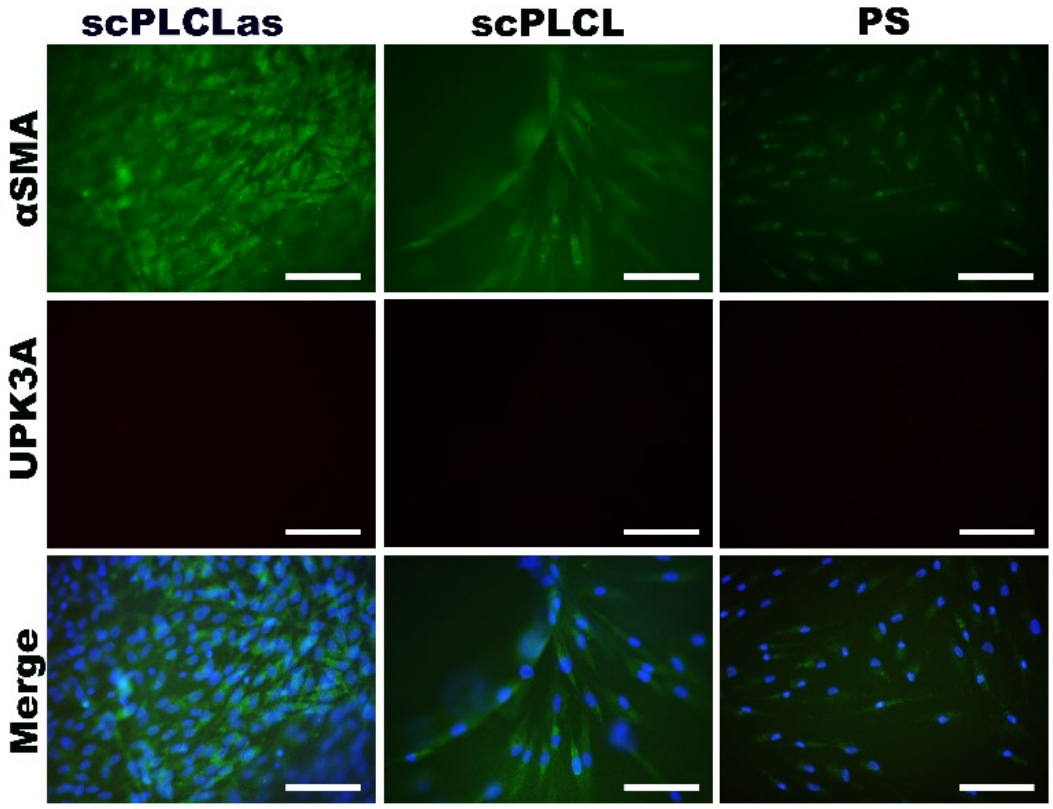

Figure 37 Immunofluorescence images of hASCs cultured in hUC/hASC co-culture on scPLCLas and scPLCL scaffolds and hASCs in PS monoculture. Myogenic marker αSMA (green) and urothelial maturation marker UPK3A (red) was stained on d14 of co-culture. Nuclei were stained with DAPI. Scale bar 200 µm.

Human ASCs did show αSMA on both biomaterials, but the protein was more visible on scPLCLas scaffold than scPLCL scaffold. It seems like the hASCs on scPLCLas showed more αSMA than hASCs on scPLCL scaffold or plain PS. No UPK3Awas detected in hASCs in

hUC/hASC co-culture either on scPLCLas or scPLCL scaffolds, as expected. Immunofluorescence images of co-stain of αSMA and UPK3A in hUCs are presented in Figure 38.

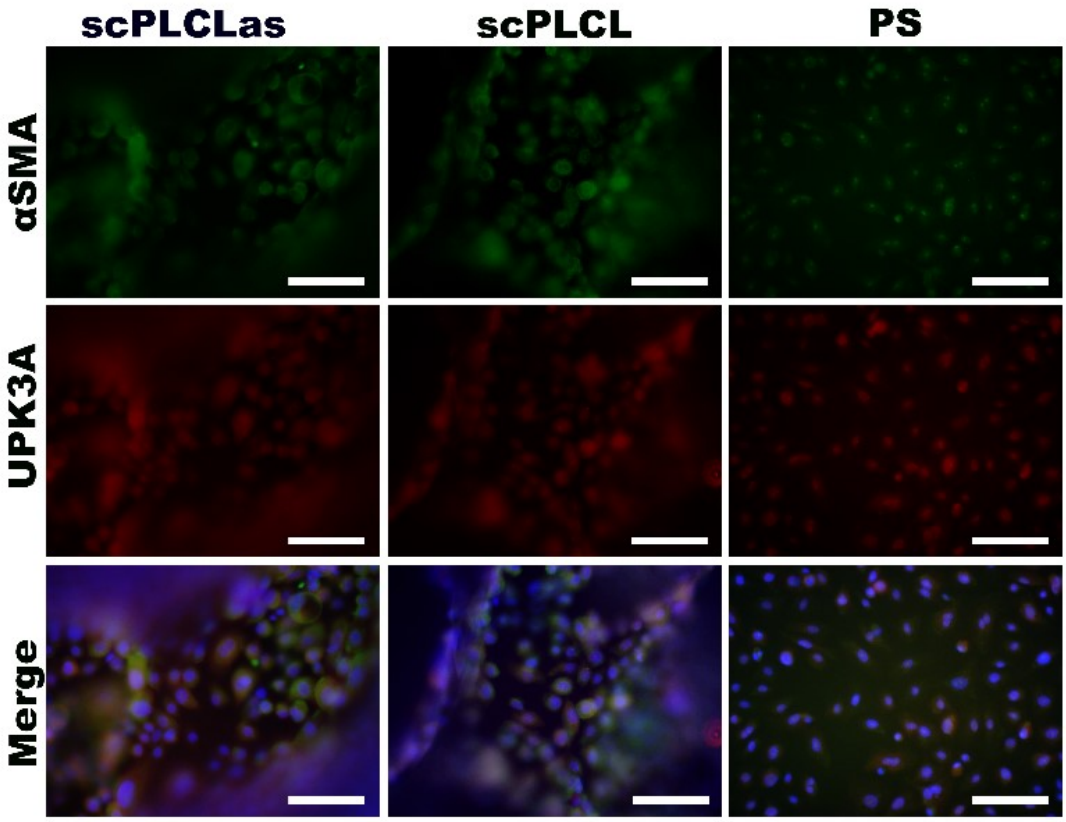

Figure 38 Immunofluorescence images of hUCs cultured in hUC/hASC co-culture on scPLCLas and scPLCL scaffolds and hUC monoculture on PS control. Myogenic marker αSMA (green) and urothelial maturation marker UPK3A (red) was stained on d14 of co-culture. Nuclei were stained with DAPI. Scale bar 100 µm.

The hUCs in hUC/hASC co-culture expressed both αSMA and UPK3A markers. However, no noticeable difference in staining intensity is seen between scPLCLas and scPLCL scaffolds. Yet on plain PS, as a monoculture control, both αSMA and UPK3A signals seem to be weaker.

Co-immunostaining of pan-cytokeratin [AE1/AE3], marker for phenotypic hUC cytokeratin profile, and phalloidin, F-actins of cytoskeleton, was also performed for hUC/hASC co-cultures on scPLCLas and scPLCL scaffolds on d14 time point. No cytokeratins were detected in hASC cells on either of the scaffolds (Figure 39). The hASCs have preserved their structure of actin cytoskeleton. The actins seem more structured and linear on scPLCLas samples, where on scPLCL the cytoskeleton is not as well organized.

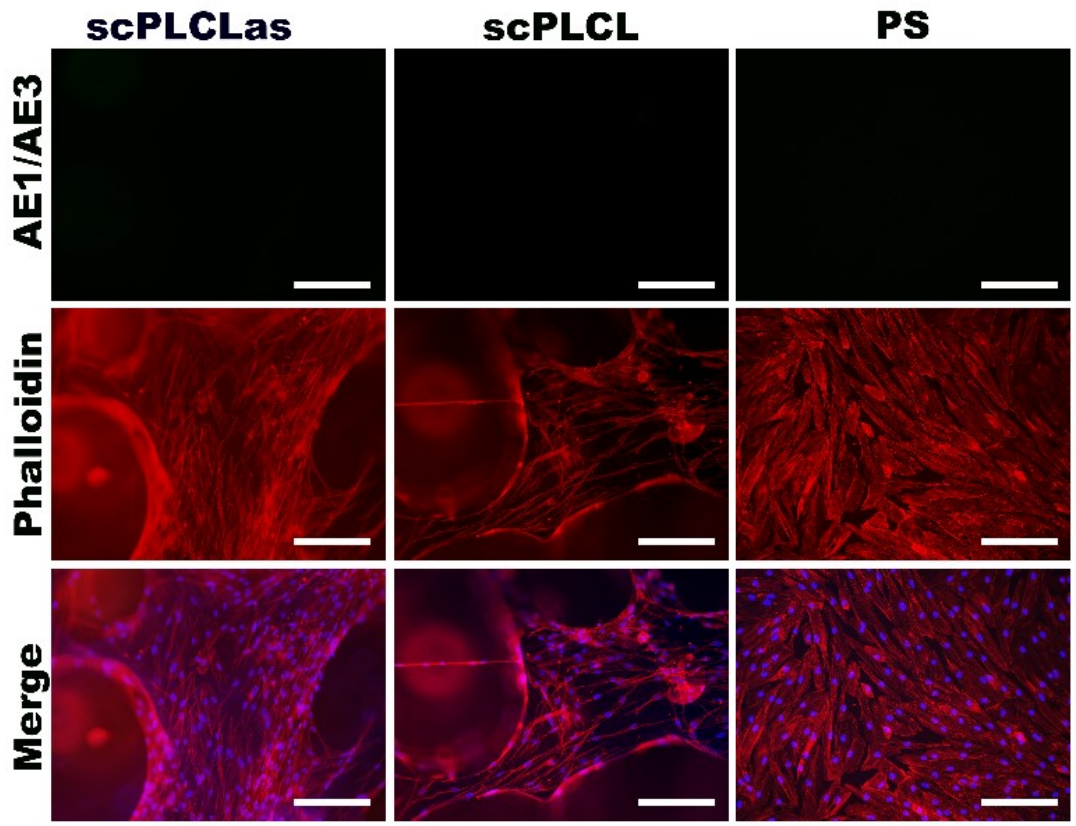

Figure 39 ICC images of pan-cytokeratin [AE1/AE3] and F-actins in hASCs cultured in hUC/hASC co-culture. Pan-cytokeratin [AE1/AE3] (green) and F-actins with phalloidin (red) were stained on d14 of hUC/hASC co-culture on scPLCLas and scPLCL scaffolds and hASC monoculture on PS control. Nuclei were stained with DAPI. Scale bar 200 µm.

The same co-staining of pan-cytokeratin [AE1/AE3] and phalloidin in hUCs showed that hUCs in hUC/hASC co-culture do maintain the hUC phenotype by expressing the hUC cytokeratin profile (Figure 40). Human UCs also have F-actins in their cytoskeleton.

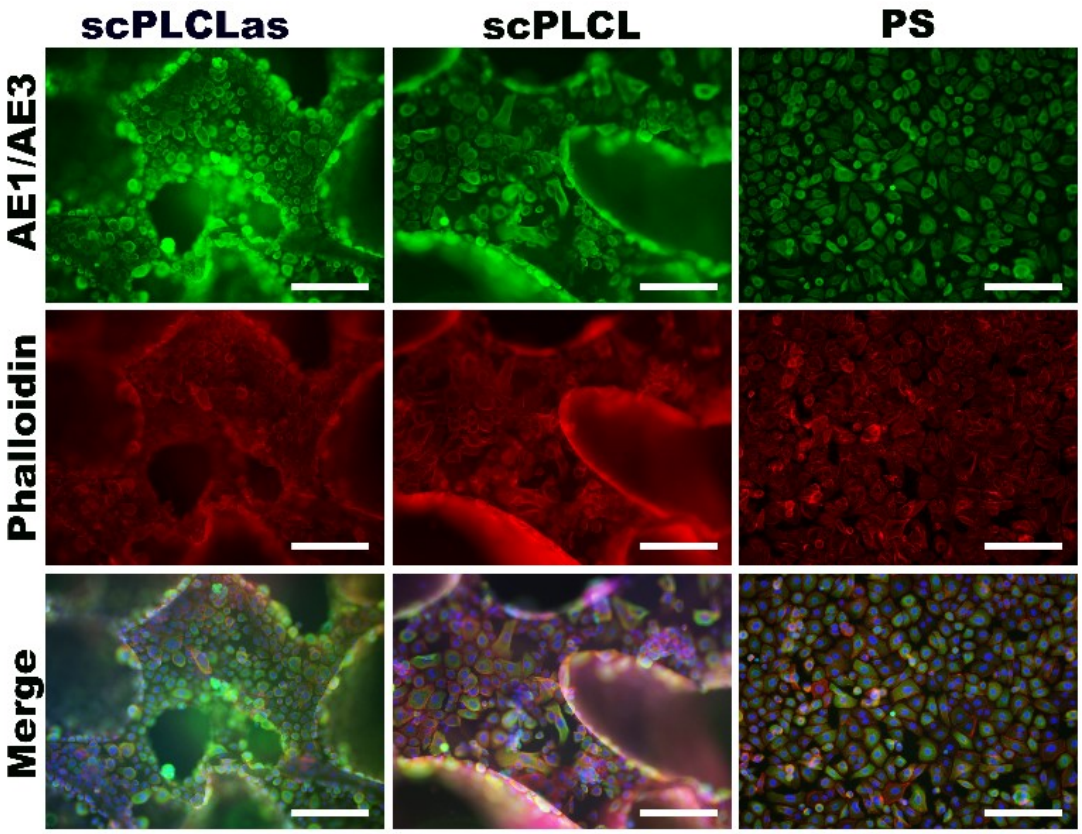

Figure 40 ICC images of pan-cytokeratin [AE1/AE3] and F-actins in hUCs cultured in hUC/hASC co-culture. Expression of pan-cytokeratin [AE1/AE3] (green) and F-actins with phalloidin (red) were stained on d14 of hUC/hASC co-culture on scPLCLas and scPLCL scaffolds and hUC monoculture on PS control. Nuclei were stained with DAPI. Scale bar 200 µm.

No difference in hUC immunostainings of pan-cytokeratin or phalloidin is visible between the biomaterials or even the PS monoculture control. However, it seems like the hUCs on scPLCL seem more elongated and seem to less present the epithelial cuboidal morphology seen on scPLCLas and PS control.

6 DISCUSSION

Pelvic floor and urethra are both elastic tissues that are subjected to various repetitive forces. Therefore, the scaffold material used in these applications needs to be flexible and able to withstand repeated stress. Due to these properties, PLCL has previously been studied for soft tissue engineering applications with promising results (Pangesty et al., 2017; Sartoneva et al., 2018; Wu et al., 2016). Additionally, the permeability of PLCL to various drugs enables the addition various growth factors into the PLCL matrix (Nair & Laurencin, 2007). By embedding PLCL scaffolds with selected growth factors or nutrients, the tissue regeneration *in vivo* could be enhanced. Therefore, PLCL was selected as the scaffold material for this study. The aim of this study was to determine the effect of added AAD in PLCL scaffolds to different cell types. PLCL membranes were studied with hVSCs (I) and scPLCL scaffolds with hUCs and hASCs (II). Additionally, a suitable medium for hUC/hASC co-culture was tested and applied for hUC and hASC co-culture on scPLCL scaffolds (II). Cell viability and morphology was assessed with Live/Dead® assay (I, II) and SEM-imaging (II), cell proliferation quantified with CyQUANT® (I, II), relative gene expression with qRT-PCR (I, II), acid-soluble and pepsin-soluble collagen amount measured with Sircol™ collagen assay, and localization of specific proteins visualized with ICC (I, II).

6.1 Phase I: hVSC seeded PLCL membranes

The ideal material for pelvic floor regeneration is still non-existent. The non-absorbable meshes have substantially high complication rates and therefore development of new biomaterials for reconstructive POP surgery is important (Medel et al., 2015; Osborn et al., 2013; Roman et al., 2015). In this study, hVSCs cultured on PLCL membranes were studied aiming to regeneration of neofascia. The final aim is that the tissue engineered graft would enhance ECM production *in vivo* to restore the strength and support of pelvic floor fascia. This study revealed that the novel PLCLas membrane increased collagen production and supported the myofibroblast phenotype of the vaginal stromal cells.

6.1.1 hVSCs remained viable and their proliferation was enhanced by AAD

As observed with Live/Dead® assay, all studied PLCL membranes supported the cell viability and no dead cells were detected. The membranes with AAD seem to better support the cell attachment, as seen as more spread cell layer and absence of cell clusters. The hVSC attachment

seemed to be less ideal on hPLCL membranes. On hPLCL, cells formed cell clusters and seemed to prefer attachment with each other than the material, additionally, the hVSCs did not spread evenly on the material. Similar cluster forming was observed with hASCs on scPLCL scaffolds. Yet, on hPLCLas and PLCLas membranes, the cells formed large, even cell sheets along the material surface. The cells mainly shared the morphology of control cells, even though in more sparse regions the cells seemed larger and more rounded. Cell number seemed to be higher on hPLCLas and PLCLas membranes compared to hPLCL. This might be due to AAs proliferative effect on cells along with the incapability of the hVSCs to attach and spread on hPLCL. However, as PLCL is hydrophobic biomaterial (Webb et al., 1998), the poor attachment of hVSCs might be due to the PLCL material properties. By embedding hydrophobic PLCL with hydrophilic AAD, the scaffold hydrophilicity might be increased and thus the cell attachment is enhanced on hPLCLas and PLCLas (Webb et al., 1998; Zhao et al., 2014). In addition, the better cell attachment on PLCLas membranes might be due to the different material surface topologies present. Dissolving embedded AAD leaves behind surface irregularities that might in part enhance cell attachment. It was clearly visible that hVSCs prefer PLCLas membranes over plain hPLCL. Therefore, both hPLCLas and hPLCL membranes can be thought as suitable scaffolds for hVSC cell culture.

The relative proliferation of hVSCs were quantified with CyQUANT® assay on d1, d7 and d14 of cell culture. The PS control was the best out of all samples on every time point, yet between the biomaterials, hPLCLas and PLCLas had higher DNA contents than plain hPLCL membrane. The cell proliferation on hPLCLas and PLCLas seemed to speed up after 7 days of cell culture, with approximately fourfold increase in DNA amount on d14. The results are in line with Live/Dead® results. The added AAD thus seems to have significant role in increasing hVSC proliferation. Also, Saitoh *et al.* have showed that additional AA or its derivatives do increase cell proliferation even in senescence human fibroblasts (Saitoh et al., 2013).

However, the hVSC proliferation did not reach the rate of PS control. This might due to the growth area differences. The growth area on biomaterials (~1.1 cm^2) is smaller than the area of PS well (1.9 cm^2), and the holes in holed membranes further increase the difference. Additionally, using CELLCROWN™ to hold the membranes further decreased the cell culture area. The free area for cell growth inside CELLCROWN™ is 0.58 cm^2. So, the free growth area differs between the control and membranes, certainly affecting the proliferation results to some degree. Further, numerous cells escaped during cell seeding from the material surface to the well bottom, and thus were excluded from the performed analysis. Significant difference in

DNA content can be seen on d1 between biomaterials and control. This might be because the cells escaped through the membrane holes or under the CELLCROWN™ to well bottom. Letting cells attach for few hours before adding the medium, instead of seeding cells as droplets in to medium, might have been more appropriate to retain more cells on the membranes. However, this way the cells would not have been spread evenly on the membrane and therefore the droplet seeding method was selected. Alternatively, it might have been possible to include the cells from well bottoms to assays. However, this way the interaction between the cells and the material might not have been as clear. By studying only the hVSCs attached to the membrane, the results of cells interacting directly with the material could be examined.

6.1.2 AAD increases collagen synthesis in hVSCs

The fibroblastic metabolism of hVSCs was visualized with COL I marker, and myofibroblast phenotype with αSMA marker with ICC. The COL I synthesis appears to be enhanced in the presence of AAD in the scaffold. AA is essential in collagen synthesis and no collagen is excreted without AA (Arrigoni & De Tullio, 2002; Fernandes et al., 2009; Pozzer et al., 2017). As the cell culture medium already contains 50 mg/L AA (https://www.thermofisher.com/us/en/home/technical-resources/media-formulation.210.html, 5.3.2019), the hVSCs on all membranes are capable of synthetizing collagen. However, with added AAD in hPLCLas and PLCLas, COL I is produced and secreted more rapidly than on plain hPLCL or PS control, where majority of the COL I is still going through post-translational modifications in ER before secretion. On the hPLCLas and PLCLas membranes, COL I forms large fibril bundles to ECM, with possibly some visible orientation, especially on PLCLas. Fibre alignment is essentially important for pelvic fascia, as it enables the tissue to withstand subjected forces without breaking. With weakened stress threshold, the fascia could break or loosen and lead to development of POP. (Roman et al., 2015; Ruiz-Zapata et al., 2016). However, specialized assays should be used for closer inspection on the collagen orientation and AAD's effect to it. The increased amount of secreted collagen in presence of AAD is also seen in the results of Sircol™ assay.

Amounts of acid-soluble and pepsin-soluble collagen were quantified with Sircol™ collagen assay. The synthesized collagen amount was lowest in hPLCL, supporting the results of COL I ICC assay. Total collagen amount was significantly higher on hPLCLas and PLCLas than on hPLCL ($p < 0.001$ and $p < 0.05$ respectively) when only taking into account the biomaterials in the statistical analysis. With PS control in the statistical analysis, no significant difference

between PLCLas and hPLCL was detected ($p = 0.051$). The lower amount of synthetized collagen on hPLCL is not explained with the presence of less cells, because even when considering the cell number, the amount of produced collagen is the lower on hPLCL (not shown here). However, the differences between novel PLCLas membranes and control were not as prominent in Sircol™ assay as in ICC staining. The Sircol™ assay takes into account all collagen types I-V, whereas in ICC only COL I was stained. Supporting both ICC and Sircol™ analysis, the results from qRT-PCR point towards increased relative gene expression of COL I and more visibly increased relative expression of COL III on hPLCLas and PLCLas membranes compared to hPLCL. Result is in agreement with previous studies, where AA has been shown to enhance collagen gene expression in fibroblasts (Kishimoto et al., 2012). It has also been stated that AA enhances the stability of collagen mRNA, so in addition to increased gene transcription, it might also be that the mRNAs are more stable during the protein synthesis (Arrigoni & De Tullio, 2002; Pinnell, 1985).

All three of the performed assays, qualitative ICC and quantitative Sircol™ and qRT-PCR present results in line with each other showing that AAD in PLCL scaffolds increases collagen production in hVSCs. Further, results are in agreement with previous studies stating that AA increases fibroblast collagen production (Boyera et al., 1998; Mangir et al., 2016; Piersma et al., 2017; Pinnell, 1985). In case of pelvic floor repair, the ratios of synthetized collagen types seem to be important for sufficient support capability and for the hVSCs proliferation. The ratio of COL I and COL III in a copolymer affects the biomechanical properties of the tissue (Peeters et al., 2014; Vashaghian et al., 2018). Increased amount of COL III leads to decreased fibre size and thus to lower strength. In turn, decreased COL III amount causes increased stiffness of the tissue. (Alperin & Moalli, 2006; Peeters et al., 2014; Zhou et al., 2012) Zhou *et al.* observed decrease in quantified COL III amount in POP patients and that the vaginal tissue was stiffer compared to controls, but they did not detect change in COL I amount (Zhou et al., 2012). In a study by Hung *et al*., the cell culture of POP-patient-derived hVSCs with higher COL I/COL III ratios achieved significantly higher cell proliferation rate than those with lower COL I/COL III ratios (Hung et al., 2010). Further, mechanical stimulation of hVSC culture lead to increased COL I/COL III ratio in a study by Vashaghian *et al.* (Vashaghian et al., 2018). Thus, study on the effect of AAD on the collagen types synthetized should be considered and more closely inspected in upcoming studies. Moreover, in further experiments of hPLCLas and PLCLas membranes, the addition of strain would be important to further investigate the effect on the

mechanical properties of the formed fascia, when considering the clinical applications for pelvic floor repair.

However, the relative expression of elastin seems not to be increased with addition of AAD into the scaffold, yet the expression levels are higher on biomaterials than on PS control, being highest on hPLCL. This result is in line with the findings of studies with human keratinocytes and fibroblasts showing that AA increases collagen synthesis but in turn decreases elastin synthesis (Pullar et al., 2017). Yet in aortic smooth muscle cells, AA has been shown to increase elastin expression (Okada et al., 2013). Further, AA has been shown to destabilize elastin mRNA during synthesis (Arrigoni & De Tullio, 2002). However, elastin production is activated later into the ECM remodelling and is rather stable during one's life time (Alperin & Moalli, 2006; Klutke et al., 2008; Ribeiro-Filho & Sievert, 2015) Many cell types have poor capabilities for elastin synthesis (Ribeiro-Filho & Sievert, 2015), though in vaginal tissues the elastin synthesis is important due to the changes subjected from pregnancy and vaginal delivery (Alperin & Moalli, 2006; Klutke et al., 2008). It might be that the assessment period of two weeks is not enough to see the induced changes in elastin synthesis. Increased elastin synthesis would be the desired outcome when considering pelvic floor applications, as abnormal elastin metabolism is associated with POP and UI (Alperin & Moalli, 2006; Chapple et al., 2015; Klutke et al., 2008; Ribeiro-Filho & Sievert, 2015).

Human VSC myofibroblastic phenotype was assayed by ICC staining of αSMA marker (Jones & Ehrlich, 2011; Piersma et al., 2017). Plenty of αSMA was visible on hPLCLas and PLCLas membranes, along with the PS control. Some αSMA was also present on plain hPLCL. However, as seen also in viability and proliferation assays, the cell number on hPLCL is significantly lower, and thus the decreased presence of myofibroblasts might also be due to a lower number of cells compared to other biomaterials, and not solely as a result of the effect of AAD. However, qRT-PCR results of αSMA expression show slight increase on hPLCLas and PLCLas membranes, pointing towards the effect of AAD in the membranes. Fibroblast differentiation to myofibroblasts is controlled by TGF-β1 (Hinz et al., 2001; Ruiz-Zapata et al., 2016; Sun et al., 2016). AA appears to increase TGF-β1 production and thus induce higher rate of myofibroblast differentiation (Lee et al., 2013; Piersma et al., 2017). Fibroblasts have been shown to transiently differentiate to myofibroblasts when ECM needs to be repaired or reorganized (Ruiz-Zapata et al., 2016). Thus, enhancing presence of myofibroblasts could lead to more effective ECM regeneration *in vivo.* In future, gentle strain could be added for the

hVSC *in vitro* culture, as it has been shown to increase ECM remodelling and accumulation (Gray et al., 2005; Roman et al., 2014; Vashaghian et al., 2018).

The findings of this study are valuable for fascial tissue engineering, as women suffering from POP have significantly reduced collagen content in their endopelvic fascia when compared to healthy women (Alperin & Moalli, 2006; Mangir et al., 2016; Zhou et al., 2012) and also altered elastin synthesis (Alperin & Moalli, 2006; Chapple et al., 2015; Klutke et al., 2008). By being able to induce increased collagen and elastin production, the generation of neofascia could be enhanced. However, as AA seems to increase collagen production and myofibroblasts differentiation, excessive amount of AA could lead to harmful fibrosis, rather that tissue regeneration on site (Piersma et al., 2017). Therefore, the rate of ECM synthesis should be increased only to the rate where it stays under control and does not lead to excessive fibrosis.

6.2 Phase II: hUC and hASC monocultures on scPLCL scaffolds

The first aim of the Phase II was to determine the effect of AAD in scPLCL scaffolds to hASCs and hUCs in monocultures. Human UCs are tested to determine the suitability of the scPLCLas and scPLCL scaffolds for regenerating mature urothelium, and hASCs to enhance to regeneration of vasculature and SMC layers of the urethra. The effect of AAD on cell viability, morphology, collagen synthesis and cell proliferation were investigated by performing Live/Dead®, CyQUANT®, Sircol™ and qRT-PCR analyses along with SEM-imaging. No PS could be used as control for scPLCL scaffolds since, the two-dimensional PS well bottom is not the ideal control material for 3D biomaterial studies. Therefore, PS control was excluded from the quantitative analyses performed for scPLCL scaffolds.

6.2.1 Effect of AAD to hUC and hASC viability, morphology and proliferation

Viability of hUCs and hASCs in monocultures were evaluated with Live/Dead® assay. Human UCs remained viable on all materials. The hUCs seem to be more rounded and smaller, with some grainy appearance on scPLCL compared to scPLCLas, as also seen in the higher magnification image in Figure 41. On scPLCLas some elongated well-attached hUCs can be seen.

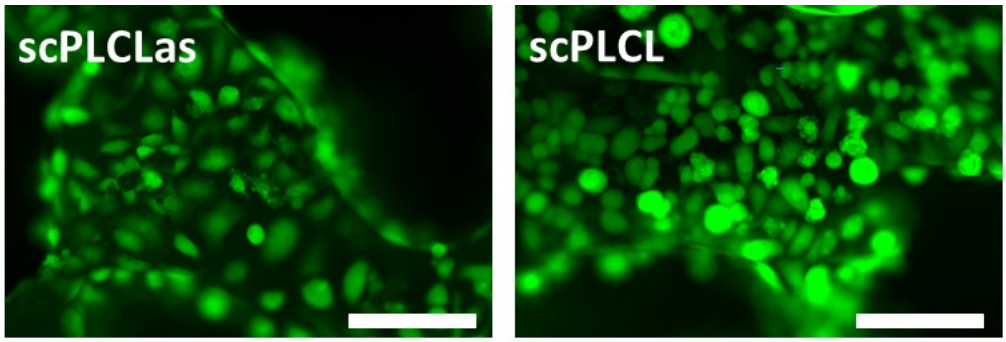

Figure 41 Higher magnification of the hUC monoculture Live/Dead® assay on d14 on scPLCLas and scPLCL scaffolds. More flattened and elongated cells could be seen on scPLCLas scaffolds, whereas on scPLCL there were smaller cells with some vesicle-like particles. Scale bar 200 µm.

Qualitatively, no distinct difference in cell number could be seen. However, in CyQUANT® proliferation assay, it is visible that hUCs proliferated significantly more on scPLCL scaffold. Such a difference in cell number was not strikingly visible in Live/Dead® assay or SEM imaging. It seems like the presence of AAD reduces hUC proliferation, but enhances the proliferation of fibroblastic cells, shown with hVSCs. This reduction in hUC cell proliferation might be due to the fact that AA can be inhibiting cell growth in excessive concentrations in the cell culture medium (Choi et al., 2008). The AA concentration in plasma is kept at 50 µM, and 1-10 mM inside cells (D'Aniello et al., 2017). The human AA intake from nutrition mainly takes place in small intestine enterocytes and renal cells (Du et al., 2012). The AAD released from scPLCLas scaffold could possibly raise the AAD concentration in the culture medium to too high levels for hUCs to withstand, which could then lead to decreased proliferation rate.

SEM-imaging was performed for closer inspection of the hUC morphology. The hUCs formed even cell layer along the material surface on both materials. Human UCs on both biomaterials on d7 seem to have visible cell borders. On d14 the cells on scPLCLas seem to maintain similar morphology to d7, whereas on scPLCL the apparent cell borders diminish between d7 and d14 and hUCs seem very flat on d14. When inspecting the 500 times magnification images, the hUCs on scPLCLas seem almost hexagonal with some vesicles on the cell borders. Hexagonal shape is seen in mature urothelium also (Cattan et al., 2011; Khandelwal et al., 2009). Some cells seem to have acquired more irregular cell surface, appearing as darker cells in the images. This might be due to the presence of microvilli or microridges on the hUC apical membrane, which could be a sign of maturation and presence of AUMs (Cattan et al., 2011). According to SEM-images, the hUCs are able to maintain their morphology during the assessment period on both scaffolds, however, on scPLCL the morphology seems flatter and smoother compared to

scPLCLas. However, no consistent differences between biomaterials visible in both Live/Dead® and SEM can be stated. Nevertheless, the AAD seems to have effect on the hUC morphology but defining the exact change would need closer inspection and further research on the matter.

For hASCs the AAD was strikingly effective. The high cell proliferation on scPLCLas was visible in CyQUANT® assay, Live/Dead® assay and SEM images. Proliferation assay results show increase in hASC proliferation on scPLCLas scaffold compared to scPLCL. With added AAD, hASCs significantly proliferated between each time point, whereas DNA amount on plain scPLCL remained stable during the assessment period. Additionally, both SEM and viability images (Live/Dead® assay) strongly support the results of the quantitative assessment. Even cell sheet is formed over the pores of the scaffolds on scPLCLas, whereas on scPLCL the hASC seem not to be able to attach properly and form cell clusters, similar to those seen with hVSCs in Phase I. On scPLCLas scaffold, hASCs are growing densely and have elongated morphology. Whereas on plain PLCL the hASCs remain relatively large, not stretching along the scaffold surface. Similarly, as in Phase I, the AAD embedded in PLCL might enable better cell attachment by increasing scaffold hydrophilicity. Additionally, the pores left behind from the dissolving AAD might further support the attachment of hASCs, forming irregularities to material surface. Obtained results are in line with existing literature; AA and its derivatives have been proven to increase hMSC proliferation rate in numerous studies (Choi et al., 2008; Fernandes et al., 2009; Saitoh et al., 2013; Weiser et al., 2009). Fernandes *et al*. showed that proliferation of hMSCs was impaired without endogenous collagen synthesis resulting from absence of AA (Fernandes et al., 2009). So, while increasing collagen production, AA simultaneously enhances hMSC cell proliferation. In a study by Lee *et al*. they showed that ASCs efficiently utilized supplemented AA. The serum concentrations of AA decreased in the presence of ASCs transplanted into mice. (Lee et al., 2013) ASCs therefore seem to be effective in AA uptake and utilizing, and thus have rapid effects in their cellular function. However, the proliferation rate cannot be indefinitely increased by increasing AA concentrations. Concentrations over 500 mM are shown to decrease proliferation rate of hMSCs (Choi et al., 2008; Saitoh et al., 2013; Sato et al., 2017). The hASCs visibly preferred scPLCLas scaffold over scPLCL scaffold, and the released AAD significantly increased their proliferation.

6.2.2 AAD enhances hASC collagen synthesis, but decreases it in hUCs

Collagen production in hUC and hASC monocultures on scPLCLas and scPLCL scaffolds was quantified with Sircol™ assay. Human UC collagen production was significantly lower on scPLCLas scaffold than on scPLCL. As collagen is mainly produced by fibroblastic cells, no high collagen amounts were expected from hUC cells. However, presence of AAD further decreased the collagen synthesis in hUCs.

In turn, collagen synthesis of hASCs was significantly increased on scPLCLas scaffolds compared to plain scPLCL. Increased hASC collagen synthesis with addition of AA derivate has also been shown in earlier studies (D'Aniello et al., 2017; Yu et al., 2014). However, the qRT-PCR results for COL I and COL III, show only slight differences between the biomaterials. Expression of COL I on scPLCLas seems to be slightly lower, whereas COL III expression seems higher than on scPLCL. However, as the standard deviations are so large, no clear conclusions can be made about the effect of AAD on COL I or COL III relative expressions. Similar observation can be made from the results of relative expression of αSMA and elastin. Expression of αSMA seems to be slightly increased on scPLCLas and expression of elastin seems higher on biomaterials than PS control, but because of the high standard deviations no certain conclusion can be made. Previously, elastin production has been enhanced by AA in muscle cells (Okada et al., 2013).

The qRT-PCR results for hUCs show that cells on both biomaterials express CK7, CK8 and CK19, the cytokeratins expressed in all urothelium cell layers (Khandelwal et al., 2009; Southgate et al., 1999). Further, the qRT-PCR results show slight increase in relative expression of UPK1A, with large standard deviations, and slight decrease in UPK1B expression on both biomaterials compared to PS. The UPK1B is critical for AUM plaque formations. Cuaresma *et al.* showed that in UPK1B knock-out mice, no functional formation of AUMs was detected (Cuaresma et al., 2015). Therefore, observed decrease of UPK1B expression would decrease the maturation of hUCs. Further, no UPKIII expression was detected but only in the strongest concentration of qRT-PCR run standard (not shown here), and thus the results were discarded from further analysis.

6.3 Phase II: hUC/hASC co-culture on scPLCL scaffolds

Human UC/hASC co-cultures on scPLCL scaffolds were performed aiming to regenerate functional urothelium and SMC layer differentiated from hASCs on opposite sides of 3D

scaffold, to mimic the urethral histological layers. Cell viability and phenotype were determined by Live/Dead® assay and immunological staining. In addition to hASCs capability to differentiate into myogenic lineage, MSCs secrete growth factors and cytokines on site, regulating tissue regeneration and injury repair. Human ASCs participate into tissue healing *in vivo* by recruiting endogenous stem cells and regulating their differentiation, along with secreting antioxidants and immunosuppressive molecules. Furthermore, hASCs produce cytokines inducing vasculature formation, guiding the formation of neovasculature to regenerating tissue. (Sterodimas et al., 2010) Therefore, in addition to providing alternative cell source for SMCs, hASCs would mediate inflammation and tissue healing *in vivo*, enhancing urethral regeneration (Gimble et al., 2007).

6.3.1 hUC/hASC co-culture medium optimization

The appropriate co-culture medium composition was tested individually for hUC and hASC monocultures prior to co-culture. Cells were cultured in five different medium compositions for two weeks, and their viability and proliferation were evaluated. Additionally, hUCs were stained with pan-cytokeratin [AE1/AE3] to assess medium's effect on hUC cytokeratin structure. The hUCs and hASCs preferred almost strictly the opposite mediums tested. Human UCs could not withstand any HS in the medium and diminished even with 1 % HS concentration in medium composition E. The normal UC culture medium contains growth supplements and hormones for maintaining epithelial phenotype. However, the hUCs proliferated even without any supplements at all in medium composition C, which only contained 1:1 EpiLife and αMEM basal mediums, so HS seems to be inhibiting hUC proliferation. This could be due to the fact that hUC are not supposed to be in contact with blood serum *in situ*, but to filtrate components from diffusing from urea to blood circulation. Therefore, coming into contact with HS might disturb hUC proliferation. Similar results were found with lung epithelial cells by Lau *et al.,* where HS induced apoptosis of the epithelial cells but no such response was observed when in contact with fetal bovine serum (FBS) (Lau et al., 2006).

When further inspecting the effects of tested medium compositions to hUC cytokeratin phenotype by ICC, the results are consistent with the viability assay results. No normal hUC morphology was achieved in any of the tested medium compositions apart from medium B, the basic hUC culture medium.

According to Live/Dead® results, hASCs suffered clearly without HS in the medium as is seen in the Live/Dead© results of medium compositions B, C and D. The cells have remained viable,

but the cell number seems not noticeably increased. However very slight increase can be detected in B and D mediums, both with epithelial growth supplements. The less suitable medium compositions for hASCs therefore seems to be medium C, which only contains basal mediums without additives. It seems like even concentration of 1 % HS maintains hASC proliferation, but slight increase is also possible with epithelial supporting supplements.

In previous UC/SMC co-culture studies, medium has been composed of 1:1 keratinocyte serum-free medium:DMEM medium (Liu et al., 2009; Wu et al., 2011). However, the 1:1 Epilife:αMEM culture mediums containing medium composition D was not sufficient for both hUCs and hASC in this performed co-culture medium test. The priority for hUC/hASC co-culture was set to achieve viable and phenotypic hUCs, so the co-culture medium was selected to be the basic hUC medium, the medium composition B. Human ASC cells also remained viable in medium composition B and appeared to slightly increase in number during the assessment period. Therefore, medium composition B was selected for the further experiments.

6.3.2 Cells remain viable in hUC/hASC co-culture on scPLCL scaffolds

The viability of cells was determined with Live/Dead® assay. Both cells remained viable in co-culture. The viability assay results seem very similar to those seen in monoculture studies, especially in case of hUCs. Human UCs remain viable on both scaffolds and preferred to grow on the pores of the scaffold. It also seems like the cells on scPLCL are smaller than the hUCs on scPLCLas, similarly as in hUC monoculture. However, the hASCs did not form large cell sheet over the scPLCLas scaffold as they did in hASC monoculture. Human ASCs on scPLCLas did not seem to increase in cell number after the co-culture was initiated, but also did not die during the assessment period. Further, the hASCs on scPLCL initially form cell clusters like those seen in monoculture. Yet, during the 14-day co-culture period, the cell clusters seem to disappear and barely anything is visible on d14. It seems like the hASCs need the AAD in the scaffold to survive in the tested co-culture medium. Even though AA and its derivatives are shown to increase hMSC proliferation (Choi et al., 2008; Fernandes et al., 2009; Saitoh et al., 2013; Weiser et al., 2009), it seems likely that the selected medium is not ideal for supporting hASC growth in hUC/hASC co-culture. Further medium optimization is therefore needed for upcoming experiments.

In fluorescence imaging assays of Live/Dead® and ICC, the hUCs stained more intensively than hASCs, which interfered with imaging of hASCs, even though the cells were on opposite sides of the scaffold. Human ASC sheets spreading over scaffold pores were somewhat visible

on the microscope, but as the staining was so dim it was difficult to capture. Dead hASCs are much more visible than the live cells, as the EthD-1 signal was more intense than the Ca-AM in viable cells. The imaging could have been easier if the scaffold was halved for imaging. However, this would be very difficult to perform without seriously damaging the cells on the scaffold surfaces. Some other method should be considered for further experiments.

6.3.3 Cell phenotypes in hUC/hASC co-culture

State of hUC and hASC phenotypes was determined by ICC staining of specific markers. Co-staining of αSMA and UPK3A was performed to assess the hASC myogenic capability and late maturation status of hUCs. Human ASCs did express SMC marker αSMA on both biomaterials, as revealed by ICC staining, illustrating their potential to differentiate towards SMCs (Lee et al., 2006). The amount of αSMA seems to be higher on scPLCLas than on plain scPLCL. Yet, as seen in Live/Dead® assay, the number of hASCs is lower on scPLCL, and therefore the difference seems likely to be due to the reduced number of cells. However, addition of β-mercaptoethanol and AA to hASC culture has been shown to slightly increase αSMA expression (Lee et al., 2006). No UPK3A expression was detected in hASCs, which was expected, as it is a late UC maturation marker (Khandelwal et al., 2009).

Surprisingly, αSMA was also visible in hUCs along with expression of UPK3A. Alpha SMA is a mesenchymal marker and is not therefore expected to be found in epithelial cells. UCs have been shown to express αSMA when going through epithelial-mesenchymal transition (EMT) (Foreman et al., 2015; Islam et al., 2013). TGF-β1 has been stated as one EMT inducer (Islam et al., 2013; Kasai et al., 2005). Lee *et al.* showed that AA upregulated TGF-β1 production in muscle cells (Lee et al., 2013). As a speculation, AA could affect similarly to ASCs and increase their TGF-β1 production, which then could possibly induce EMT in UCs in the co-culture. However, the exact phenotype of isolated primary hUCs has not been assayed, so it might be that amongst the achieved cells might be urothelial progenitor cells capable for differentiating to various cell types. These urothelial stem cells have been suggested to reside amongst the basal cells of the urothelium (Hickling et al., 2015; Ho et al., 2012). It might be that the early SMC marker αSMA could be slightly expressed in these cells in some point before committing to epithelial lineage. To determine whether or not hUCs are undergoing EMT in future hUC/hASC co-cultures, changes to epithelial markers such as claudins and tight junctions (Khandelwal et al., 2009), and additional mesenchymal markers in addition to αSMA, should be assessed to determine whether or not the epithelial phenotype is changing in hUCs.

Simultaneous expression of mesenchymal marker and hUC late-maturation marker UPK3A seems unlikely, but currently the explanation for achieving result like this remains unspecified and needs further studies on the matter. Staining could be done for histological urothelium sample to determine whether the used αSMA antibody would be expressed in mature urothelium. This would reveal the possible unspecific binding of the antibody. Similar test could be also performed for UPK3A. Alternatively, other antibodies binding to different region of the αSMA or UPK3A protein could be tested to confirm the positive result.

The second co-staining of pan-cytokeratin [AE1/AE3] and phalloidin was conducted to determine whether hASCs have preserved their F-actin cytoskeleton and if the hUCs still express the hUC cytokeratin profile. Human ASCs did not express any of the cytokeratins in hUCs' cytokeratin profile but seem to have maintained their actin cytoskeleton, with more normal organization visible on scPLCLas scaffold. On scPLCL, the hASC actin cytoskeleton seem more disorganized. Human ASCs do not maintain their normal morphology as also seen in viability assay both in co-culture and monoculture, and therefore the cytoskeleton is expected to be altered. Pan-cytokeratin was expressed in hUCs on both biomaterials, showing that they have maintained their hUC phenotype. Human UCs also stained for F-actins on the cell borders, staining the cortical actin cytoskeleton (Khandelwal et al., 2009).

As the aim of the hUC/hASC co-culture was also to evaluate how the cells maturate and maintain their phenotype in co-culture conditions. This study showed that hASCs maintained their potential to myogenic differentiation, so in future experiments it is essential to optimize the hASC niche to guide differentiation towards SMC phenotype *in vitro* and *in vivo*. The scPLCLas seems promising material for performing hUC/hASC co-cultures for urethral tissue engineering, but the used co-culture conditions still need to be optimized to maintain phenotypes and viability in both cell types.

7 CONCLUSION

Aim of this study was to analyse the effect of AAD embedded in PLCL scaffolds on hVSCs, hUCs and hASCs and hUC/hASC co-culture. AAD seems the enhance ECM production and proliferation of mesenchymal cells but does not affect similarly on hUCs. The main conclusions obtained from this research are:

I. AAD significantly increased hVSC proliferation and collagen production. Gene expression of COL I and COL III also seem increased in PLCL membranes embedded with AAD, however, no increase in elastin expression was detected. In AAD embedded membranes, more myofibroblasts were present in ICC assay of αSMA marker, along with increased gene expression of αSMA. Obtained results show that added AAD is beneficial for hVSCs and that both hPLCLas and PLCLas show promising results considering pelvic floor tissue engineering applications.

II. AAD significantly increased hASC proliferation and collagen production, but in turn significantly decreased them in hUCs. Relative expression of αSMA and COL III were enhanced with addition of AAD into scaffold. ScPLCLas scaffold thus seems beneficial for hASC culture for soft tissue engineering applications. Human UCs maintained their viability and morphology on both scPLCLas and scPLCL scaffolds.

In hUC/hASC co-culture, both cell types remained viable on scPLCLas, whereas on plain scPLCL hASCs diminished. Myogenic phenotype of hASCs was also maintained in the co-culture on both scaffolds. Thus, AAD seems to be able to maintain hASCs in co-culture with used design. Co-culture medium still needs optimization, to be able to maintain good viability, proliferation capability and phenotype in both cell types.

ScPLCLas scaffold appeared as promising scaffold for urethral tissue engineering applications, but some further optimizations for co-culture design should be considered.

8 REFERENCES

Abbas, T. O., Mahdi, E., Hasan, A., AlAnsari, A. & Pennisi, C. P. (2018). Current Status of Tissue Engineering in the Management of Severe Hypospadias. *Frontiers in Pediatrics*, *5*, 283.

Aboushwareb, T., Mckenzie, P., Wezel, F., Southgate, J. & Badlani, G. (2011). Is Tissue Engineering and Biomaterials the Future for Lower Urinary Tract Dysfunction (LUTD)/Pelvic Organ Prolapse (POP)? *Neurourol Urodyn.*, *30*, 775–782.

Alperin, M. & Moalli, P. A. (2006). Remodeling of vaginal connective tissue in patients with prolapse. *Current Opinion in Obstetrics and Gynecology*, *18*(5), 544–550.

Arrigoni, O. & De Tullio, M. C. (2002). Ascorbic acid: much more than just an antioxidant. *Biochimica et Biophysica Acta*, *1569*, 1–9.

Ashton-Miller, J. A. & DeLancey, J. O. L. (2007). Functional anatomy of the female pelvic floor. *Annals of the New York Academy of Sciences*, *1101*, 266–296.

Atala, A., Bauer, S. B., Soker, S., Yoo, J. J. & Retik, A. B. (2006). Tissue-engineered autologous bladders for patients needing cystoplasty. *Lancet*, *367*(9518), 1241–1246.

Atala, A., Danilevskiy, M., Lyundup, A., Glybochko, P., Butnaru, D., Vinarov, A. & Yoo, J. J. (2017). The potential role of tissue-engineered urethral substitution: clinical and preclinical studies. *Journal of Tissue Engineering and Regenerative Medicine*, *11*(1), 3–19.

Barber, M. D. (2016). Pelvic organ prolapse. *BMJ*, *354*, i3853.

Barber, M. D. & Maher, C. (2013). Epidemiology and outcome assessment of pelvic organ prolapse. *International Urogynecology Journal and Pelvic Floor Dysfunction*, *24*(11), 1783–1790.

Bhargava, S., Chapple, C. R., Bullock, A. J., Layton, C. & Macneil, S. (2004). Tissue-engineered buccal mucosa for substitution urethroplasty. *BJU International*, *93*, 807–811.

Bhargava, S., Patterson, J. M., Inman, R. D., MacNeil, S. & Chapple, C. R. (2008). Tissue-Engineered Buccal Mucosa Urethroplasty-Clinical Outcomes. *European Urology*, *53*(6), 1263–1271.

Boyera, N., Galey, I. & Bernard, B. A. (1998). Effect of vitamin C and its derivatives on collagen synthesis and cross- linking by normal human fibroblasts. *International Journal of Cosmetic Science*, *20*(3), 151–158.

Cattan, V., Bernard, G., Rousseau, A., Bouhout, S., Chabaud, S., Auger, F. A. & Bolduc, S. (2011). Mechanical stimuli-induced urothelial differentiation in a human tissue-engineered tubular genitourinary graft. *European Urology*, *60*(6), 1291–1298.

Chapple, C. R., Osman, N. I., Mangera, A., Hillary, C., Roman, S., Bullock, A. & Macneil, S. (2015). Application of Tissue Engineering to Pelvic Organ Prolapse and Stress Urinary Incontinence. *LUTS: Lower Urinary Tract Symptoms*, *7*(2), 63–70.

Chen, B., Wen, Y. & Polan, M. L. (2004). Elastolytic Activity in Women with Stress Urinary Incontinence and Pelvic Organ Prolapse. *Neurourology and Urodynamics*, *23*(2), 119–126.

Choi, K.-M., Seo, Y.-K., Yoon, H.-H., Song, K.-Y., Kwon, S.-Y., Lee, H.-S. & Park, J.-K. (2008). Effect of ascorbic acid on bone marrow-derived mesenchymal stem cell proliferation and differentiation. *Journal of Bioscience and Bioengineering*, *105*(6), 586–

594.

Cuaranta-Monroy, I., Simandi, Z., Kolostyak, Z., Doan-Xuan, Q.-M., Poliska, S., Horvath, A., … Nagy, L. (2014). Highly efficient differentiation of embryonic stem cells into adipocytes by ascorbic acid. *Stem Cell Research*, *13*, 88–97.

Cuaresma, E. J., Hains, D. S., Chen, X., Ching, C. B., Becknell, M. B., McHugh, K. M. & Carpenter, A. R. (2015). Uroplakin 1b is critical in urinary tract development and urothelial differentiation and homeostasis. *Kidney International*, *89*(3), 612–624.

D'Aniello, C., Cermola, F., Patriarca, E. J. & Minchiotti, G. (2017). Vitamin C in Stem Cell Biology: Impact on Extracellular Matrix Homeostasis and Epigenetics. *Stem Cells International*, 8936156.

Davis, N. F., Callanan, A., McGuire, B. B., Flood, H. D. & McGloughlin, T. M. (2011). Evaluation of viability and proliferative activity of human urothelial cells cultured onto xenogenic tissue-engineered extracellular matrices. *Urology*, *77*(4), 1007.e1–1007.e7.

Davis, N. F., Cunnane, E. M., O'Brien, F. J., Mulvihill, J. J. & Walsh, M. T. (2018). Tissue engineered extracellular matrices (ECMs) in urology: Evolution and future directions. *Surgeon*, *16*(1), 55–65.

De Filippo, R. E., Kornitzer, B. S., Yoo, J. J. & Atala, A. (2015). Penile urethra replacement with autologous cell-seeded tubularized collagen matrices. *Journal of Tissue Engineering and Regenerative Medicine*, *9*(3), 257–264.

De Filippo, R. E., Yoo, J. J. & Atala, A. (2002). Urethral Replacement Using Cell Seeded Tubularized Collagen Matrices. *The Journal of Urology*, *168*(4), 1789–1793.

de Graaf, P., van der Linde, E. M., Rosier, P. F. W. M., Izeta, A., Sievert, K.-D., Bosch, J. L. H. R. & de Kort, L. M. O. (2017). Systematic Review to Compare Urothelium Differentiation with Urethral Epithelium Differentiation in Fetal Development, as a Basis for Tissue Engineering of the Male Urethra. *Tissue Engineering Part B: Reviews*, *23*(3), 257–267.

de Kemp, V., de Graaf, P., Fledderus, J. O., Ruud Bosch, J. L. H. & de Kort, L. M. O. (2015). Tissue Engineering for Human Urethral Reconstruction: Systematic Review of Recent Literature. *Plos One*, *10*(2), e0118653.

De Lancey, J. O. L. (2016). What's new in the functional anatomy of pelvic organ prolapse? *Current Opinion in Obstetrics and Gynecology*, *28*(5), 420–429.

Denstedt, J. & Atala, A. (2009). *Biomaterials and Tissue Engineering in Urology* (1st ed.). Woodhead Publishing.

Dorati, R., Colonna, C., Tomasi, C., Genta, I., Bruni, G. & Conti, B. (2014). Design of 3D scaffolds for tissue engineering testing a tough polylactide-based graft copolymer. *Materials Science and Engineering C*, *34*(1), 130–139.

Dorin, R. P., Pohl, H. G., De Filippo, R. E., Yoo, J. J. & Atala, A. (2008). Tubularized urethral replacement with unseeded matrices: What is the maximum distance for normal tissue regeneration? *World Journal of Urology*, *26*(4), 323–326.

Drake, R. L., Vogl, A. W. & Adam, W. M. (2015). *Gray's anatomy for students* (3rd ed.). Philadelphia: Churchill Livingstone Elsevier.

Du, J., Cullen, J. J. & Buettner, G. R. (2012). Ascorbic acid: Chemistry, biology and the treatment of cancer. *Biochimica et Biophysica Acta - Reviews on Cancer*, *1826*(2), 443–457.

Elsawy, M. M. & de Mel, A. (2017). Biofabrication and biomaterials for urinary tract reconstruction. *Research and Reports in Urology*, *9*, 79–92.

Esteban, M. A., Wang, T., Qin, B., Yang, J., Qin, D., Cai, J., … Pei, D. (2010). Vitamin C Enhances the Generation of Mouse and Human Induced Pluripotent Stem Cells. *Cell Stem Cell*, *6*(1), 71–79.

Faiena, I., Koprowski, C. & Tunuguntla, H. (2016). Female Urethral Reconstruction. *Journal of Urology*, *195*(3), 557–567.

FDA. (2011). Food and Drug Administration. FDA safety communication: Urogynecologic Surgical Mesh : Update on the Safety and Effectiveness of Transvaginal Placement for Pelvic Organ Prolapse. *Review Literature And Arts Of The Americas*, (July), Available at: http://www.fda.gov/downloads/medical.

Fernandes, H., Mentink, Anoukde Boer, J., Bank, R., Stoop, R. & van Blitterswijk, C. (2009). Endogenous Collagen Influences Differentiation of Human Multipotent Mesenchymal Stromal Cells. *Tissue Engineering Part A*, *16*(5), 1693–1702.

Ferraro, G. A., Mizuno, H. & Pallua, N. (2016). Adipose stem cells: From bench to bedside. *Stem Cells International*, *2016*(6), 572–585.

Foreman, K. E., Flanigan, R. C., Greco, K. A., Franzen, C. A., Todorovic, V., Gupta, G. N., … Blackwell, R. H. (2015). Urothelial cells undergo epithelial-to-mesenchymal transition after exposure to muscle invasive bladder cancer exosomes. *Oncogenesis*, *4*(8), e163–e163.

Fossum, M., Gustafson, C. J., Nordenskjöld, A. & Kratz, G. (2003). Isolation and in vitro cultivation of human urothelial cells from bladder washings of adult patients and children. *Scandinavian Journal of Plastic and Reconstructive Surgery and Hand Surgery*, *37*(1), 41–45.

Fossum, M., Svensson, J., Kratz, G. & Nordenskjöld, A. (2007). Autologous in vitro cultured urothelium in hypospadias repair. *Journal of Pediatric Urology*, *3*(1), 10–18.

Fraser, M., Thomas, D. F. M., Pitt, E., Harnden, P., Trejdosiewicz, L. & Southgate, J. (2004). A surgical model of composite cystoplasty with cultured urothelial cells: a controlled study of gross outcome and urothelial phenotype. *BJU International*, *93*, 609–616.

Fu, Q., Deng, C. L., Liu, W. & Cao, Y. L. (2007). Urethral replacement using epidermal cell-seeded tubular acellular bladder collagen matrix. *BJU International*, *99*(5), 1162–1165.

Fu, W., Liu, Z., Feng, B., Hu, R., He, X., Wang, H., … Wang, W. (2014). Electrospun gelatin/PCL and collagen/PLCL scaffolds for vascular tissue engineering. *International Journal of Nanomedicine*, *9*, 2335–2344.

Garkhal, K., Verma, S., Jonnalagadda, S. & Kumar, N. (2007). Fast degradable poly(L-lactide-co-ε-caprolactone) microspheres for tissue engineering: Synthesis, characterization, and degradation behavior. *Journal of Polymer Science, Part A: Polymer Chemistry*, *45*(13), 2755–2764.

Garriboli, M., Radford, A. & Southgate, J. (2014). Regenerative medicine in urology. [Review]. *European Journal of Pediatric Surgery*, *24*(3), 227–236.

Gimble, J. M., Katz, A. J. & Bunnell, B. A. (2007). AdiposeDerived Stem Cells for Regenerative Medicine. *Circ Res*, *100*, 12491260.

Gray, S. D., Tresco, P. A., Hitchcock, R. W., Smeal, R. M., Li, W. & Webb, K. (2005). Cyclic strain increases fibroblast proliferation, matrix accumulation, and elastic modulus of fibroblast-seeded polyurethane constructs. *Journal of Biomechanics*, *39*(6), 1136–1144.

Greenwell, T. & Cutner, A. (2018). The anatomy and an illustrated description of a technique for combined laparoscopic and vaginal total removal of an obturator mid urethral tape. *Translational Andrology and Urology*, *7*(6), 978–981.

Haimi, S., Suuriniemi, N., Haaparanta, A.-M., Ellä, V., Lindroos, B., Huhtala, H., … Suuronen, R. (2009). Growth and Osteogenic Differentiation of Adipose Stem Cells on PLA/Bioactive Glass and PLA/β-TCP Scaffolds. *Tissue Engineering Part A*, *15*(7), 1473–1480.

Herschorn, S. (2004). Female Pelvic Floor Anatomy: The Pelvic Floor, Supporting Structures, and Pelvic Organs. *Reviews in Urology*, *6*(S5), S2–S10.

Hickling, D. R., Sun, T.-T. & Wu, X.-R. (2015). Anatomy and Physiology of the Urinary Tract: Relation to Host Anatomy and Physiology of the Urinary Tract: Relation to Host Defense and Microbial Infection Urinary Tract: Relation to Host Defense and Microbial Infection. *Microbiology Spectrum*, *3*(4), UTI-0016-2012.

Hinz, B., Celetta, G., Tomasek, J. J., Gabbiani, G. & Chaponnier, C. (2001). Alpha-Smooth Muscle Actin Expression Upregulates Fibroblast Contractile Activity. *Molecular Biology of the Cell*, *12*(9), 2730–2741.

Ho, P. L., Kurtova, A. & Chan, K. S. (2012). Normal and neoplastic urothelial stem cells: Getting to the root of the problem. *Nature Reviews Urology*, *9*(10), 583–594.

Horiguchi, A. (2017). Substitution urethroplasty using oral mucosa graft for male anterior urethral stricture disease: Current topics and reviews. *International Journal of Urology*, *24*(7), 493–503.

Hung, M. J., Wen, M. C., Hung, C. N., Ho, E. S. C., Chen, G. Den & Yang, V. C. (2010). Tissue-engineered fascia from vaginal fibroblasts for patients needing reconstructive pelvic surgery. *International Urogynecology Journal*, *21*, 1085–1093.

Islam, S. S., Mokhtari, R. B., El Hout, Y., Azadi, M. A.Yeger, H., Alauddin, M. & Farhat, W. A. (2013). TGF-β1 induces EMT reprogramming of porcine bladder urothelial cells into collagen producing fibroblasts-like cells in a Smad2/Smad3-dependent manner. *Journal of Cell Communication and Signaling*, *8*(1), 39–58.

Jelovsek, J. E., Maher, C. & Barber, M. D. (2007). Pelvic Organ Prolapse. *Lancet*, *369*, 1027–1038.

Jeong, S. I., Kim, B. S., Kang, S. W., Kwon, J. H., Lee, Y. M., Kim, S. H. & Kim, Y. H. (2004). In vivo biocompatibilty and degradation behavior of elastic poly(L-lactide-co-ε-caprolactone) scaffolds. *Biomaterials*, *25*(28), 5939–5946.

Jones, C. & Ehrlich, H. P. (2011). Fibroblast expression of β-smooth muscle actin, β2β1 integrin and βvβ3 integrin: Influence of surface rigidity. *Experimental and Molecular Pathology*, *91*(1), 394–399.

Kasai, H., Allen, J. T., Mason, R. M., Kamimura, T. & Zhang, Z. (2005). TGF-β1 induces human alveolar epithelial to mesenchymal cell transition (EMT). *Respiratory Research*, *6*, 1–15.

Kątnik-Prastowska, I., Lis, J. & Matejuk, A. (2014). Glycosylation of uroplakins. Implications for bladder physiopathology. *Glycoconjugate Journal*, *31*(9), 623–636.

Keays, M. A. & Dave, S. (2017). Current hypospadias management: Diagnosis, surgical management, and long-term patient-centred outcomes. *Canadian Urological Association Journal*, *11*(1–2S),

Khandelwal, P., Abraham, S. N. & Apodaca, G. (2009). Cell biology and physiology of the uroepithelium. *American Journal of Physiology-Renal Physiology*, *297*(6), F1477–F1501.

Kiilholma, P. & Nieminen, K. (2009). Gynekologiset laskeumat. *Duodecim*, *125*, 199–206.

Kim, B.-S., Baez, C. E. & Atala, A. (2000). Biomaterials for Tissue Engineering. *World Journal of Urology*, *18*, 2–9.

Kim, B. S. & Mooney, D. J. (1998). Development of biocompatible synthetic extracellular matrices for tissue engineering. *Trends in Biotechnology*, *16*(5), 224–229.

Kim, S. H. S. H., Jung, Y. & Kim, S. H. S. H. (2013). A Biocompatible Tissue Scaffold Produced by Supercritical Fluid Processing for Cartilage Tissue Engineering. *Tissue Engineering Part C: Methods*, *19*(3), 181–188.

Kishimoto, Y., Saito, N., Kurita, K., Shimokado, K., Maruyama, N. & Ishigami, A. (2012). Ascorbic acid enhances the expression of type 1 and type 4 collagen and SVCT2 in cultured human skin fibroblasts. *Biochemical and Biophysical Research Communications*, *430*(2), 579–584.

Klutke, J., Ji, Q., Campeau, J., Starcher, B., Felix, J. C., Stanczyk, F. Z. & Klutke, C. (2008). Decreased endopelvic fascia elastin content in uterine prolapse. *Acta Obstetricia et Gynecologica Scandinavica*, *87*(1), 111–115.

Kreft, M. E., Sterle, M., Veranic, P. & Jezernik, K. (2005). Urothelial injuries and the early wounds healing response: tight junctions and urothelial cytodifferentiation. *Histochemistry and Cell Biology*, *123*(4–5), 529–539.

Kyllönen, L., Haimi, S., Mannerström, B., Huhtala, H., Rajala, K. M., Skottman, H., … Miettinen, S. (2013). Effects of different serum conditions on osteogenic differentiation of human adipose stem cells in vitro. *Stem Cell Research & Therapy*, *4*(1), 17.

Lau, Y. E., Bowdish, D. M. E., Cosseau, C., Hancock, R. E. W. & Davidson, D. J. (2006). Apoptosis of airway epithelial cells: Human serum sensitive induction by the cathelicidin LL-37. *American Journal of Respiratory Cell and Molecular Biology*, *34*(4), 399–409.

Laurent, C. P., Vaquette, C., Liu, X., Schmitt, J.-F. & Rahouadj, R. (2018). Suitability of a PLCL fibrous scaffold for soft tissue engineering applications: A combined biological and mechanical characterisation. *Journal of Biomaterials Applications*, *32*(9), 1276–1288.

Lee, C. H., Moioli, E. K. & Mao, J. J. (2006). Fibroblastic differentiation of human mesenchymal stem cells using connective tissue growth factor. *Annual International Conference of the IEEE Engineering in Medicine and Biology - Proceedings*, *1*, 775–778.

Lee, E.-M., Ishigami, A., Hong, I.-H., Kim, A.-Y., Park, J.-K., Min, C.-W., … Tremblay, J. P. (2013). Effects of Vitamin C on Cytotherapy-Mediated Muscle Regeneration. *Cell Transplantation*, *22*(10), 1845–1858.

Lee, G. (2011). Uroplakins in the lower urinary tract. *International Neurourology Journal*, *15*(1), 4–12.

Lee, W. C. C., Rubin, J. P. & Marra, K. G. (2006). Regulation of α-smooth muscle actin protein expression in adipose-derived stem cells. *Cells Tissues Organs*, *183*(2), 80–86.

Li, C. L., Liao, W. B., Yang, S. X., Song, C., Li, Y. W., Xiong, Y. H. & Chen, L. (2013). Urethral reconstruction using bone marrow mesenchymal stem cell- and smooth muscle cell-seeded bladder acellular matrix. *Transplantation Proceedings*, *45*(9), 3402–3407.

Li, H., Xu, Y., Xie, H., Li, C., Song, L., Feng, C., … Lv, X. (2014). Epithelial-Differentiated

Adipose-Derived Stem Cells Seeded Bladder Acellular Matrix Grafts for Urethral Reconstruction: An Animal Model. *Tissue Engineering Part A*, *20*(3–4), 778–784.

Lindroos, B., Suuronen, R. & Miettinen, S. (2011). The Potential of Adipose Stem Cells in Regenerative Medicine. *Stem Cell Reviews and Reports*, *7*(2), 269–291.

Liu, J., Huang, J., Lin, T., Zhang, C. & Yin, X. (2009). Cell-to-cell contact induces human adipose tissue-derived stromal cells to differentiate into urothelium-like cells in vitro. *Biochemical and Biophysical Research Communications*, *390*(3), 931–936.

Liu, Y., Bharadwaj, S., Lee, S. J., Atala, A. & Zhang, Y. (2009). Optimization of a natural collagen scaffold to aid cell-matrix penetration for urologic tissue engineering. *Biomaterials*, *30*(23–24), 3865–3873. h

Lobo, R. A., Gershenson, D. M., Lentz, G. M. & Valea, F. A. (2017). *Comprehensive Gynecology*. (R. A. Lobo, D. M. Gershenson, G. M. Lentz & F. A. Valea, Eds.), *Comprehensive Gynecology* (7th ed.). Philadelphia: Elsevier Inc.

Mangera, A., Bullock, A. J., Roman, S., Chapple, C. R. & Macneil, S. (2013). Comparison of candidate scaffolds for tissue engineering for stress urinary incontinence and pelvic organ prolapse repair. *BJU International*, *112*(5), 674–685.

Mangir, N., Bullock, A. J., Roman, S., Osman, N., Chapple, C. & MacNeil, S. (2016). Production of ascorbic acid releasing biomaterials for pelvic floor repair. *Acta Biomaterialia*, *29*, 188–197.

Maya, H., Madduri, S., Rita, G., Tullio, S., Hall, H. & Eberli, D. (2010). Scaffolds for the Engineering of Functional Bladder Tissues. In D. Eberli (Ed.), *Tissue Engineering* (pp. 119–141). InTech. Retrieved from https://www.intechopen.com/books/tissue-engineering/scaffolds-for-the-engineering-of-functional-bladder-tissues

Medel, S., Alarab, M., Kufaishi, H., Drutz, H. & Shynlova, O. (2015). attachment of Primary Vaginal Fibroblasts to Absorbable and Nonabsorbable Implant Materials Coated With Platelet-Rich Plasma: Potential Application in Pelvic Organ Prolapse Surgery. *Female Pelvic Medicine & Reconstructive Surgery*, *21*(4), 190–197.

Nair, L. S. & Laurencin, C. T. (2007). Biodegradable polymers as biomaterials. *Progress in Polymer Science (Oxford)*, *32*(8–9), 762–798.

Norton, P. & Brubaker, L. (2006). Urinary Incontinence in Women. *Lancet*, *367*, 57–67.

Okada, K., Hasegawa, T., Yu, J., Okita, Y., Tanaka, A., Tabata, Y., … Bao, W. (2013). Controlled release of ascorbic acid from gelatin hydrogel attenuates abdominal aortic aneurysm formation in rat experimental abdominal aortic aneurysm model. *Journal of Vascular Surgery*, *60*(3), 749–758.

Olsburgh, J., Harnden, P., Weeks, R., Smith, B., Joyce, A., Hall, G., … Southgate, J. (2003). Uroplakin gene expression in normal human tissues and locally advanced bladder cancer. *The Journal of Pathology*, *199*(1), 41–49.

Orabi, H., Aboushwareb, T., Zhang, Y., Yoo, J. J. & Atala, A. (2013). Cell-seeded tubularized scaffolds for reconstruction of long urethral defects: A preclinical study. *European Urology*, *63*(3), 531–538.

Orabi, H., Bouhout, S., Morissette, A., Rousseau, A., Chabaud, S. & Bolduc, S. (2013). Tissue engineering of urinary bladder and urethra: Advances from bench to patients. *The Scientific World Journal*, *2013*, Article ID 154564, 13 pages.

Osborn, D. J., Reynolds, W. S. & Dmochowski, R. (2013). Vaginal approaches to pelvic organ

prolapse repair. *Current Opinion in Urology*, *23*(4), 299–305.

Pangesty, A. I., Arahira, T. & Todo, M. (2017). Development and characterization of hybrid tubular structure of PLCL porous scaffold with hMSCs/ECs cell sheet. *Journal of Materials Science: Materials in Medicine*, *28*(10), 164.

Peeters, E., De Hertogh, G., Junge, K., Klinge, U. & Miserez, M. (2014). Skin as marker for collagen type I/III ratio in abdominal wall fascia. *Hernia*, *18*(4), 519–525.

Piersma, B., Wouters, O. Y., de Rond, S., Boersema, M., Gjaltema, R. A. F. & Bank, R. A. (2017). Ascorbic acid promotes a TGFβ1-induced myofibroblast phenotype switch. *Physiological Reports*, *5*(17), e13324.

Pinnagoda, K., Larsson, H. M., Vythilingam, G., Vardar, E., Engelhardt, E. M., Thambidorai, R. C., … Frey, P. (2016). Engineered acellular collagen scaffold for endogenous cell guidance, a novel approach in urethral regeneration. *Acta Biomaterialia*, *43*, 208–217.

Pinnell, S. R. (1985). Regulation of collagen biosynthesis by ascorbic acid: A review. *Yale Journal of Biology and Medicine*, *58*(6), 553–559.

Pozzer, D., Favellato, M., Bolis, M., Invernizzi, R. W., Solagna, F., Blaauw, B. & Zito, E. (2017). Endoplasmic Reticulum Oxidative Stress Triggers Tgf-Beta-Dependent Muscle Dysfunction by Accelerating Ascorbic Acid Turnover. *Scientific Reports*, *7*(1), 40993.

Prabhakaran, M. P., Venugopal, J. R. & Ramakrishna, S. (2009). Mesenchymal stem cell differentiation to neuronal cells on electrospun nanofibrous substrates for nerve tissue engineering. *Biomaterials*, *30*(28), 4996–5003.

Pullar, J. M., Carr, A. C. & Vissers, M. C. M. (2017). The roles of vitamin C in skin health. *Nutrients*, *9*(8), 866.

Raya-Rivera, A., Esquiliano, D. R., Yoo, J. J., Lopez-Bayghen, E., Soker, S. & Atala, A. (2011). Tissue-engineered autologous urethras for patients who need reconstruction: An observational study. *The Lancet*, *377*(9772), 1175–1182.

Ribeiro-Filho, L. A. & Sievert, K. D. (2015). Acellular matrix in urethral reconstruction. *Advanced Drug Delivery Reviews*, *82*, 38–46.

Rodríguez, L. V., Lee, M., Zhang, R., Xu, Y., Jack, G. S. & Wu, B. M. (2009). Urinary bladder smooth muscle engineered from adipose stem cells and a three dimensional synthetic composite. *Biomaterials*, *30*(19), 3259–3270.

Rodriguez, L. V, Alfonso, Z., Zhang, R., Leung, J., Wu, B., Ignarro, L. J., … Ignarro, L. J. (2006). Clonogenic multipotent stem cells in human adipose tissue differentiate into functional smooth muscle cells. *Proceedings of the National Academy of Sciences of the United States of America*, *103*(32), 12167–12172.

Roman, S., Mangera, A., Osman, N. I., Bullock, A. J., Chapple, C. R. & MacNeil, S. (2014). Developing a Tissue Engineered Repair Material for Treatment of Stress Urinary Incontinence and Pelvic Organ Prolapse—Which Cell Source? *Neurology and Urodynamics*, *33*, 531–537.

Roman, S., Mangir, N., Bissoli, J., Chapple, C. R. & MacNeil, S. (2015). Biodegradable scaffolds designed to mimic fascia-like properties for the treatment of pelvic organ prolapse and stress urinary incontinence. *Journal of Biomaterials Applications*, *30*(10), 1578–1588.

Ross, M. H. & Pawlina, W. (2011). *Histology - A Text and Atlas* (6th ed.). Philadelphia: Wolters Kluwer Health/Lippincott Williams & Wilkins cop. 2011.

Ruiz-Zapata, A. M., Kerkhof, M. H., Ghazanfari, S., Zandieh-Doulabi, B., Stoop, R., Smit, T. H. & Helder, M. N. (2016). Vaginal Fibroblastic Cells from Women with Pelvic Organ Prolapse Produce Matrices with Increased Stiffness and Collagen Content. *Scientific Reports*, *6*, 22971.

Saitoh, Y., Morishita, A., Mito, S., Tsujiya, T. & Miwa, N. (2013). Senescence-induced increases in intracellular oxidative stress and enhancement of the need for ascorbic acid in human fibroblasts. *Molecular and Cellular Biochemistry*, *380*(1–2), 129–141.

Salerno, A., Saurina, J. & Domingo, C. (2015). Supercritical CO2 foamed polycaprolactone scaffolds for controlled delivery of 5-fluorouracil, nicotinamide and triflusal. *International Journal of Pharmaceutics*, *496*, 654–663.

Sartoneva, R., Haaparanta, A. M., Lahdes-Vasama, T., Mannerström, B., Kellomäki, M., Salomäki, M., … Haimi, S. (2012). Characterizing and optimizing poly-L-lactide-co-1-caprolactone membranes for urothelial tissue engineering. *Journal of the Royal Society Interface*, *9*(77), 3444–3454.

Sartoneva, R., Haimi, S., Miettinen, S., Mannerström, B., Haaparanta, A. M., Sándor, G. K., … Lahdes-Vasama, T. (2011). Comparison of a poly-L-lactide-co-ε-caprolactone and human amniotic membrane for urothelium tissue engineering applications. *Journal of the Royal Society Interface*, *8*(58), 671–677.

Sartoneva, R., Kuismanen, K., Juntunen, M., Karjalainen, S., Hannula, M., Kyllönen, L., … Miettinen, S. (2018). Porous (poly-L-lactide-co-epsilon-caprolactone) scaffold: a novel biomaterial for vaginal tissue engineering. *Royal Society Open Science*, *5*(8), 180811.

Sato, Y., Mera, H., Takahashi, D., Majima, T., Iwasaki, N., Wakitani, S. & Takagi, M. (2017). Synergistic effect of ascorbic acid and collagen addition on the increase in type 2 collagen accumulation in cartilage-like MSC sheet. *Cytotechnology*, *69*(3), 405–416.

Shafiq, M., Jung, Y. & Kim, S. H. (2015). In situ vascular regeneration using substance P-immobilised poly(L-Lactide-co-ε-caprolactone) scaffolds: Stem cell recruitment, angiogenesis, and tissue regeneration. *European Cells and Materials*, *30*, 282–302.

Shakhssalim, N., Soleimani, M., Dehghan, M. M., Rasouli, J., Taghizadeh-Jahed, M., Torbati, P. M. & Naji, M. (2017). Bladder smooth muscle cells on electrospun poly(ε-caprolactone)/poly(L-lactic acid) scaffold promote bladder regeneration in a canine model. *Materials Science and Engineering C*, *75*, 877–884.

Shi, J.-G., Fu, W.-J., Wang, X.-X., Xy, Y.-D., Li, G., Hong, B.-F., … Zhang, X. (2012). Transdifferentiation of human adipose-derived stem cells into urothelial cells: potential for urinary tract tissue engineering. *Cell and Tissue Research*, *347*(3), 737–746.

Singh, A., Bivalacqua, T. J. & Sopko, N. (2018). Urinary Tissue Engineering: Challenges and Opportunities. *Sexual Medicine Reviews*, *6*(1), 35–44.

Southgate, J., Harnden, P. & Trejdosiewicz, L. (1999). Cytokeratin expression patterns in normal and malignant urothelium.pdf. *Histol Histopathol*, *14*, 657–664.

Southgate, J., Masters, J. & Trejdosiewicz, L. (2002). Culture of human urothelium. In R. I. Freshney & FreshneyG (Eds.), *Culture of Epithelial Cells* (2nd ed., Vol. 8, p. 2397). Wiley-Liss, Inc.

Spilotros, M., Venn, S., Anderson, P. & Greenwell, T. (2018). Penile urethral stricture disease. *Journal of Clinical Urology*, *12*(2), 145–157.

Sterodimas, A., De Faria, J., Nicaretta, B. & Pitanguy, I. (2010). Tissue engineering with

adipose-derived stem cells (ADSCs): Current and future applications. *Journal of Plastic, Reconstructive and Aesthetic Surgery*, *63*(11), 1886–1892.

Sun, K.-H., Chang, Y., Reed, N. I. & Sheppard, D. (2016). α-Smooth muscle actin is an inconsistent marker of fibroblasts responsible for force-dependent TGFβ activation or collagen production across multiple models of organ fibrosis. *American Journal of Physiology - Lung Cellular and Molecular Physiology*, *310*(9), 824–836.

Tian, B., Song, L., Liang, T., Li, Z., Ye, X., Fu, Q. & Li, Y. (2018). Repair of urethral defects by an adipose mesenchymal stem cell-porous silk fibroin material. *Molecular Medicine Reports*, *18*(1), 209–215.

Ullah, I., Subbarao, R. B. & Rho, G. J. (2015). Human mesenchymal stem cells - current trends and future prospective. *Bioscience Reports*, *35*(2), 1–18.

Vashaghian, M., Roovers, J. P., Smit, T. H., Diedrich, C. M., Werner, A. & Zandieh-Doulabi, B. (2018). Gentle cyclic straining of human fibroblasts on electrospun scaffolds enhances their regenerative potential. *Acta Biomaterialia*, *84*, 159–168.

Vergeldt, T. F. M., Weemhoff, M., IntHout, J. & Kluivers, K. B. (2015). Risk factors for pelvic organ prolapse and its recurrence: a systematic review. *International Urogynecology Journal*, *26*, 1559–1573.

Versteegden, L. R. M., de Jonge, P. K. J. D., IntHout, J., van Kuppevelt, T. H., Oosterwijk, E., Feitz, W. F. J., … Daamen, W. F. (2017). Tissue Engineering of the Urethra: A Systematic Review and Meta-analysis of Preclinical and Clinical Studies [Figure presented]. *European Urology*, *72*(4),594–606.

Webb, K., Hlady, V. & Tresco, P. A. (1998). Relative importance of surface wettability and charged functional groups on NIH 3T3 fibroblast attachment, spreading, and cytoskeletal organization. *Journal of Biomedical Materials Research*, *41*(3), 422–430.

Weiser, B., Sommer, F., Neubauer, M., Seitz, A., Tessmar, J., Goepferich, A. & Blunk, T. (2009). Ascorbic acid enhances adipogenesis of bone marrow-derived mesenchymal stromal cells. *Cells Tissues Organs*, *189*(6), 373–381.

Wu, S., Liu, Y., Bharadwaj, S., Atala, A. & Zhang, Y. (2011). Human urine-derived stem cells seeded in a modified 3D porous small intestinal submucosa scaffold for urethral tissue engineering. *Biomaterials*, *32*(5), 1317–1326.

Wu, X.-R. R., Kong, X.-P. P., Pellicer, A., Kreibich, G. & Sun, T.-T. T. (2009). Uroplakins in urothelial biology, function, and disease. *Kidney International*, *75*(11), 1153–1165.

Wu, X., Wang, Y., Zhu, C., Tong, X., Yang, M., Yang, L., … He, H. (2016). Preclinical animal study and human clinical trial data of co-electrospun poly(L-lactide-co-caprolactone) and fibrinogen mesh for anterior pelvic floor reconstruction. *International Journal of Nanomedicine*, *11*, 389.

Wünsch, L., Ehlers, E. M. & Russlies, M. (2005). Matrix testing for urothelial tissue engineering. *European Journal of Pediatric Surgery*, *15*(3), 164–169.

Xu, Y., Fu, W., Wang, Z., Li, G. & Zhang, X. (2015). A tissue-specific scaffold for tissue engineering-based ureteral reconstruction. *PLoS ONE*, *10*(3), 1–11.

Yamzon, J., Perin, L. & Koh, C. J. (2008). Current status of tissue engineering in pediatric urology. *Current Opinion in Urology*, *18*(4), 404–407.

Yao, Q., Zhang, W., Hu, Y., Chen, J., Shao, C., Fan, X. & Fu, Y. (2017). Electrospun collagen/poly(L-lactic acid-co-ε-caprolactone) scaffolds for conjunctival tissue

engineering. *Experimental and Therapeutic Medicine*, *14*(5), 4141–4147.

Yu, J., Tu, Y. K., Tang, Y. B. & Cheng, N. C. (2014). Stemness and transdifferentiation of adipose-derived stem cells using l-ascorbic acid 2-phosphate-induced cell sheet formation. *Biomaterials*, *35*(11), 3516–3526.

Zhang, C., Murphy, S. V. & Atala, A. (2014). Regenerative medicine in urology. *European Journal of Pediatric Surgery*, *23*, 106–111.

Zhang, K., Fu, Q., Yoo, J., Chen, X., Chandra, P., Mo, X., … Zhao, W. (2017). 3D bioprinting of urethra with PCL/PLCL blend and dual autologous cells in fibrin hydrogel: An in vitro evaluation of biomimetic mechanical property and cell growth environment. *Acta Biomaterialia*, *50*, 154–164.

Zhang, M., Peng, Y., Zhou, Z., Zhou, J., Wang, Z. & Lu, M. (2013). Differentiation of human adipose-derived stem cells Co-cultured with urothelium cell line toward a urothelium-like phenotype in a nude murine model. *Urology*, *81*(2), 465.e15-465.e22.

Zhao, X., Lui, Y. S., Toh, P. W. J. & Loo, S. C. J. (2014). Sustained release of hydrophilic L-ascorbic acid 2-phosphate magnesium from electrospun polycaprolactone scaffold-A study across blend, coaxial, and emulsion electrospinning techniques. *Materials*, *7*, 7398–7408.

Zhao, Z., Yu, H., Xiao, F., Wang, X., Yang, S. & Li, S. (2012). Differentiation of adipose-derived stem cells promotes regeneration of smooth muscle for ureteral tissue engineering. *Journal of Surgical Research*, *178*, 55–62.

Zhou, L., Lee, J. H., Wen, Y., Constantinou, C., Yoshinobu, M., Omata, S. & Chen, B. (2012). Biomechanical properties and associated collagen composition in vaginal tissue of women with pelvic organ prolapse. *Journal of Urology*, *188*(3), 875–880.

Zhou, S., Yang, R., Zou, Q., Zhang, K., Yin, T., Zhao, W., … Fu, Q. (2017). Fabrication of tissue-engineered bionic urethra using cell sheet technology and labeling by ultrasmall superparamagnetic iron oxide for full-thickness urethral reconstruction. *Theranostics*, *7*(9), 2509–2523.